12-14-2015

Preparation and Characterization of PT-RU Bimetallic Catalysts Using Electroless Deposition Methods and Mechanistic Study of RE and CS Promoters for AG-Based, High Selectivity Ethylene Oxide Catalysts

Weijian Diao
University of South Carolina - Columbia

PREPARATION AND CHARACTERIZATION OF PT-RU BIMETALLIC CATALYSTS USING ELECTROLESS DEPOSITION METHODS AND MECHANISTIC STUDY OF RE AND CS PROMOTERS FOR AG-BASED, HIGH SELECTIVITY ETHYLENE OXIDE CATALYSTS

by

Weijian Diao

Bachelor of Science
Jilin University, 2010

Submitted in Partial Fulfillment of the Requirements

For the Degree of Doctor of Philosophy in

Chemical Engineering

College of Engineering and Computing

University of South Carolina

2015

Accepted by:

John R. Monnier, Major Professor

Donna A. Chen, Committee Member

John R. Regalbuto, Committee Member

Christopher T. Williams, Committee Member

John W. Weidner, Committee Member

Lacy Ford, Senior Vice Provost and Dean of Graduate Studies

DEDICATION

I dedicate this work to my wife Yunya Zhang, for her love, support, help, and company through my graduate studies. You mean more to me than anything in the whole world.

I dedicate this work to my parents Shengnian Diao and Youmei Wang for their unconditional love and support.

ACKNOWLEDGEMENTS

First I want to give my greatest acknowledgment to my advisor Dr. John R. Monnier, thank you for giving me the opportunity to study in the group and teaching me the 'sweet science' of catalysis. I can't imagine how I could finish my graduate school without your guidance and help. Thank you for teaching me so much about designing, improving, and repairing equipment. I have learned so many things I didn't expect to learn when I came to graduate school. Also, thank you for taking the time to introduce me to your industrial contacts. I believe that I will have the chance to use what I have learned from you in industrial R&D in the near future. You taught me more than science, also how to be a good man. I will remember all the 'bonus knowledges' from you, such as super bowl bracket and fishing skills. You have worried about me like a father; thank you very much for your genuine concern.

I also want to acknowledge my PhD committee, Dr. Donna A. Chen, Dr. John R. Regalbuto, Dr. Christopher T. Williams, for your precious time dedicated to teach me. Thanks Dr. Chen for teaching me surface science which brings me to a new world of science. Your circumspect and serous attitude to science impressed me as what a successful scientist should be. Thanks Dr. Williams for all your discussion and guidance in my study. I still remember the first time I met you in Jilin. Thank you for being so friendly and helpful during these years. Thanks Dr. Regalbuto for teaching me SEA and all the useful suggestions. I enjoyed a lot working with you and your students. Thank you so much for offering me the opportunity to work here at USC after my graduation.

In addition, I want to thank the chemical engineering department staffs, Marcia Rowen, Loretta Hardcastle, Kay Dorrell, Vernon Dorrell and Brian Loggans, for their assistance and excellent work on providing a friendly and nice working environment. I also want to give the special thanks to Carol Stork for her generous help on experimental work.

I also want to thank Dr. Christopher DiGiulio, Dr. Shuai Tan, Dr. Xiaojing Sun, Dr. Hyeran Cho, Dr. Abraham Rodriguez, Dr. Randima Galhenage, who has already left USC but taught me a lot on experiments setup and data analysis. I would like to thank my group members and colleagues, John Tengco, Kerry O'Connell, Shuo Cao, Kangmin Xie, Qiuli Liu, Jose Contreras, I am happy to work with you and learn from each other. I want to express my sincere gratitude to my dearest friends, Long Cai, Xiaojing Sun, Fan Wu, Shuai Tan, Qiang Gao, Jingjie Wu, Fusheng Ke, Jingyi Huo, Tingting Yang, Hong Liu, Fang Fang, Kejian Yao, Yiling Dai, Zhiyong Wang, Tianyuan Xie, Yating Mao, Qiuli Liu, Zhuonan Song, Chao Wang, Lei Wang. With all of you, I have spent one of the happiest time of my life in USC.

ABSTRACT

Pt-Ru bimetallic catalysts are widely used for direct methanol fuel cells, biomass upgrading and hydrocarbon refining and offer unique properties compared to Pt or Ru monometallic catalysts due to ensemble effects, electronic effects, and/or bifunctional effects. To achieve better performance, strong metal-metal interactions and true bimetallic surface are needed. Electroless deposition (ED) methods are used in our laboratory to synthesize such bimetallic catalysts. In this study, two series of Ru@Pt/C (Pt deposited on Ru surfaces) and Pt@Ru/C (Ru deposited on Pt surfaces) catalysts have been synthesized. Characterization data from temperature programmed reduction (TPR), selective chemisorption, X-ray photoelectron spectroscopy (XPS), and scanning transmission electron microscopy (STEM) are presented to confirm formation of Pt-Ru bimetallic surfaces with strong metal-metal interactions.

The second part of this study describes the roles of high-valent Re oxyanions and alkali metal promoters for high selectivity ethylene epoxidation catalysts. The world-wide production of ethylene oxide (EO) currently exceeds 25 Mt/yr, placing the synthesis of this oxygenated organic chemical high on the list of the world's most commonly produced chemicals and the highest volume chemical produced by catalytic oxidation. Ag, Cs, Re are the main components for current generation EO catalysts. Even though the first patent describing Re-promoted EO catalysts appeared in 1984 only three peer-reviewed publications had appeared in the literature (prior to our work) addressing the mechanism of Re and co-promoters for improved EO selectivity. We have prepared

extensive series of Cs-Ag, Re-Ag, Cs-Re-Ag and Cs-Re-Mo-Ag catalysts, all supported on a commercial α-Al_2O_3 carrier; they have been evaluated for ethylene epoxidation at industrially-relevant conditions (high pressure and 200-1000 hrs on-line) to determine the mechanism of EO selectivity enhancement from high-valent Re oxyanions and other co-promoters. Analyses by XPS and SEM suggest the origin of both Re and Cs promotions are electronic. A reaction scheme detailing the mechanism of EO formation over Re-modified, Cs-promoted Ag catalysts is presented.

TABLE OF CONTENTS

LIST OF TABLES

LIST OF FIGURES

CHAPTER 1:

INTRODUCTION AND LITERATURE REVIEW

1.1 Catalysis and Bimetallic Catalysts

Catalysts were first used in industrial processes for production of sulfuric acid in 1746; however they were not studied and understood until the late 1800's [1,2]. In 1895 Ostwald realized catalysis as a common phenomenon and defined a catalyst as "a substance which accelerates a chemical reaction without affecting the position of the equilibrium" in terms of the laws of physical chemistry [2]. From petroleum refining to pharmaceuticals to automobile emission control, catalysts are widely used in industrial processes and daily life. Recent studies have shown that catalysts are used for synthesis of over 75% of all chemical products [3]. Catalysts can be arbitrarily be divided into three groups-metals, metal oxides, and acid-base catalysts.

There are two main types of metal catalysts – homogeneous and heterogeneous. Homogeneous catalysis is a sequence of reactions that involve a catalyst in the same phase as the reactants. Most commonly, a homogeneous catalyst is co-dissolved in a solvent with the reactants. This dissertation focuses only on heterogeneous catalysts in which the phase of the catalyst differs from that of the reactants. The great majority of practical heterogeneous catalysts are solids and the great majority of reactants are gases or liquids [4]. A typical solid catalyst is a transition metal which is the active phase maintained on an inert solid support that provides critical surface area and stability for the supported metal(s). Alumina, silica, and carbon are often used as supports for deposition of metal salts. Catalytic activity, selectivity, lifetime, surface area, thermal and mechanical strength are general parameters for evaluation of metal catalysts.

Bimetallic catalysts have been studied since the 1940's [5], since bimetallic catalysts often offer enhanced selectivity, stability, and/or activity compared to their corresponding monometallic components due to concepts referred to as ensemble effects,

electronic effects, and/or bifunctional effects between the two different metallic components [6,7]. Ensemble effects occur when one of the surface components is catalytically-inactive and serves only to dilute the active metal component into discrete aggregates, or ensembles, of atoms. Desirable effects result when the ensemble size permits only certain (desirable) reactions to occur, but prohibit unwanted and non-selective reactions due to larger ensemble requirements for the unwanted reaction. One example of an ensemble effect is the selective hydrogenation of acetylene to form ethylene in the presence of excess ethylene in our recent work for Ag-Pd catalysts [8]. Electronic effects take place when there is electron transfer between the two metal components. For some reactions, e-density changes can modify performance of catalytic reactions. Electronic effects can occur along with ensemble effects, so it can be difficult to isolate effects as being due to only changes in e^--density of the active catalytic component. Bifunctional effects offer the greatest potential for changes in catalyst performance and occur when both metallic components are active for a catalytic reaction. This takes place for bimetallic surfaces where both metallic components are uniformly distributed on the surface to form discrete bimetallic site geometries, such as site pairs. In one application, a site pair of M_a-M_b can activate different atoms of a reactive substrate molecule to alter reaction rates or pathways, such as in the selective oxidation of glycerol over Au-Pd catalysts in work recently published from our group [9]. In other cases, each metal can activate different molecules of a bimetallic reaction to give more favorable reaction kinetics, such as the oxidation of CO using O_2 using Ag-Ir catalysts, again recently published from the Williams and Monnier groups [10]. In this instance,

contiguous Ag and Ir sites selectively adsorb O_2 and CO, respectively, to form CO_2 at higher reaction rates because of more favorable surface kinetics.

1.2 Preparation Methods of Bimetallic Catalysts

Various methods have been developed for bimetallic [11]. The composition and subsequent catalytic performance of bimetallic catalysts are often related to the methods of catalyst preparation. For example, a slight change in parameters (metal salt precursor, pH, temperature, etc.) can significantly change catalyst properties and performance. Only a few methods are used for chemical industry because of the cost of raw materials, limited methods of production, storage and transportation, and potential for scale-up. Impregnation [12], deposition-precipitation [13], strong electrostatic adsorption [14,15] and redox reactions [16] are the most commonly-used methods.

Impregnation

The most widely used method of catalyst preparation is impregnation, either by incipient wetness (dry impregnation) or wet impregnation of the active components (metal salts) on supports [17]. These methods are always followed by drying, calcination and/or reduction of the impregnated support. The most attractive advantage of this method is its simplicity in practical operation at both laboratory and industry levels.

Dry impregnation is a process where an impregnation solution containing the active metal salt component is added to the dry support. The volume of the impregnation solution is equal to or slightly greater than the pore volume of the support. The procedure occurs rapidly, and the active components are transported by convection and capillary action into the pores of the support.

The second common procedure is wet impregnation in which the support is immersed in an excess volume of solution containing the metal salt precursor. It is a slow process because the active component dissolved in solution has to diffuse into the pores of the support. It can take several hours to reach equilibrium between the solution in the bulk and in the pores of the support. The excess solution can be removed by decanting and/or evaporation. If removed by evaporation alone, uneven distribution of the metal salt on the support typically results.

There are two commonly-used methods for impregnation of salts for preparation of bimetallic catalysts: co-impregnation and successive impregnation. Co-impregnation is simultaneous impregnation of both active metal precursor components in a single solution onto the support. Successive impregnation is a two-step process in which impregnation of first metal salt on a support is followed by impregnation of second metal on the monometallic catalyst. Typically, after the first metal salt is impregnated, it is calcined or reduced to render it insoluble for the second impregnation step. Figure 1.1 shows the processes for co-impregnation and successive impregnation.

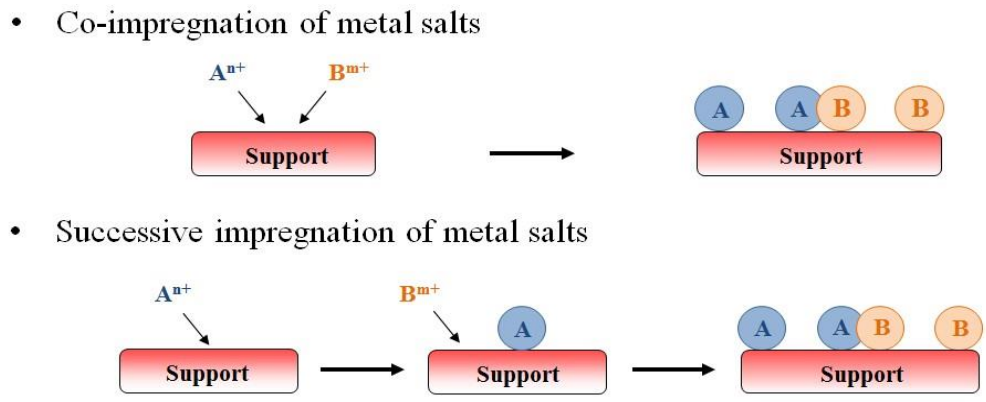

Figure 1.1 Processes of co-impregnation and successive impregnation.

Although impregnation methods are easy to scale-up and are low cost production methods, they are not good pathways for preparation of bimetallic catalysts. The disadvantage of co-impregnation and successive impregnation is that both form monometallic particles, as well as bimetallic particles with variable compositions. Therefore, they are not true bimetallic catalysts, but a wide range of materials with a rather random distribution of monometallic and bimetallic particles. When these catalysts are evaluated, correlation of catalyst composition with performance is highly questionable.

Deposition-Precipitation

The deposition-precipitation method involves the conversion of a highly soluble metal salt precursor into a less soluble substance which precipitates only on the support and not in solution [18]. Typically, this process is achieved by a change in solution pH, addition of a precipitation agent, addition of a reducing agent, or change in the concentration of a complexation agent. There are two main conditions which must be fulfilled to make sure that the precipitation occurs only on the support instead of in solution: a strong interaction between the soluble metal precursor and the surface of the support and controlled concentrations of the precursor in solution to avoid spontaneous precipitation. Usually in the presence of the support, the solubility limit shifts to lower concentrations compared to the solubility limit in solution to favor deposition on the support. The concentration of the metal salt should be maintained between the solubility point and the super-solubility (SS) point in solution to prevent precipitation in the liquid. The super-solubility curve is the boundary of the metastable zone and labile zone (liquid and precipitate).

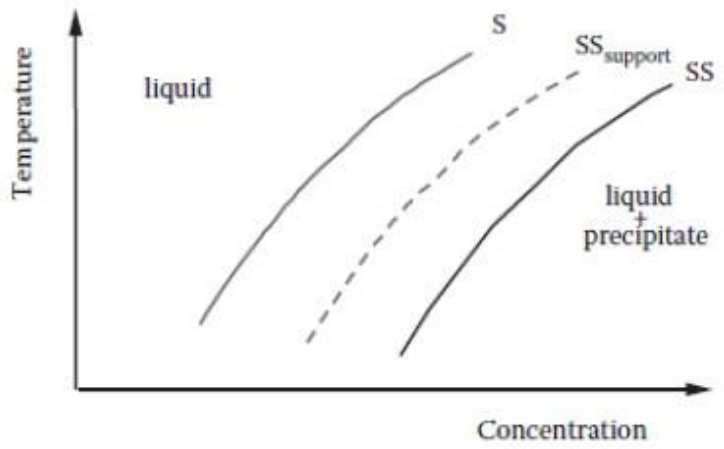

Figure 1.2 Phase diagram for a precipitate in equilibrium with its solution and in the presence of a support [18].

An explanation of deposition-precipitation mechanism is shown above in Figure 1.2. For successful deposition-precipitation, the precipitation agent must be added gradually to keep the local concentration below the super-solubility point to avoid the precipitation in solution [18].

In practice, the support is slurried in the solution containing the soluble precursor. The suspension is thoroughly stirred, and then the precipitating agent is gradually added. Afterwards, the supported solid sample is washed, dried and activated. For preparation of bimetallic catalysts, two metal salts can be precipitated simultaneously or sequentially on the support. However, again this method has poor control of metal distribution and surface composition, which also makes it difficult to prepare true bimetallic catalysts with controlled compositions.

Strong Electrostatic Adsorption (SEA)

Another preparation method has been developed for preparation of monometallic and bimetallic catalysts is strong electrostatic adsorption (SEA) method. In this method,

strong electrostatic interaction between the charged metal complex and the support is used to synthesize supported catalysts [19-23].

The mechanism for catalyst preparation using SEA method has been developed and refined by Regalbuto [14,15,24]. Hydroxyl groups on the surface of an oxide can be protonated or deprotonated depending on the pH of the contacting solution. The pH at which the hydroxyl groups are neutral and no precursor-support interaction occurs is termed the point of zero charge (PZC) [25]. As shown in Figure 1.3, above the PZC, the hydroxyl groups de-protonate and become negatively charged, and the cations such as $[(NH_3)_4Pt]^{2+}$ can be strongly adsorbed. Below the PZC, the hydroxyl groups protonate and become positively charged, and the surface can adsorb anionic metal complexes such as $[PtCl_6]^{2-}$. In both cases, the metal complex deposit onto the surface via SEA [24].

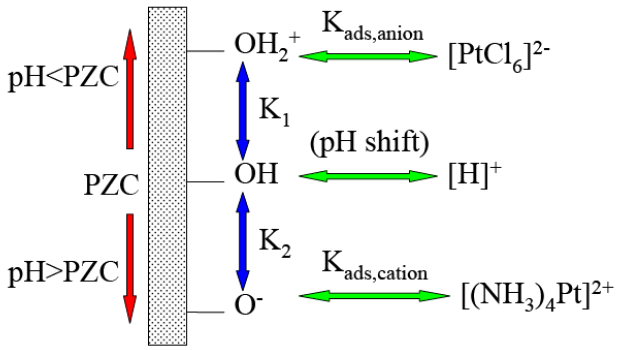

Figure 1.3 Electrostatic adsorption mechanism [24].

By using different metal ion sources (both cations and anions) on different supports (different PZC values), a variety of bimetallic catalysts can be prepared using simultaneous SEA (co-SEA) or sequential SEA. With the different adsorption abilities of different precursors, targeted weight loadings of two metals can be achieved by controlling metal ion concentrations in the solution and solution pH values. SEA method

offers the ability to synthesize monometallic and bimetallic catalysts with highly dispersed and well distributed metal particles.

Redox Methods

Another preparation method that has been developed for preparation of bimetallic catalysts is based on reduction-oxidation (redox) reactions. The main goal of bimetallic catalyst synthesis is to create metal particles having close interactions between the two metallic components to provide unique properties for the catalyst. Intuitively, the maximum bimetallic interaction occurs when two metal components form bimetallic surfaces where both metals are in intimate or proximal contact rather than existing as separate particles. Compared to impregnation and deposition-precipitation, the redox method offers the best opportunity to form close metal interactions. Redox procedures typically begin with a monometallic (primary metal) catalyst to which controlled amounts of a secondary metal are added. The four major classes of redox methods which have been developed for preparation of bimetallic catalysts are (1), direct redox reaction, (2), redox reaction of adsorbed reductant, (3), underpotential deposition, and (4), catalytic reduction [26].

In the direct redox process, also called galvanic displacement, the primary metal is oxidized by reaction with the oxidized form of the secondary metal to reduce the secondary metal. The requirement for the direct redox process is that the secondary metal must have a higher standard electrochemical potential than the primary metal. The difference in their respective equilibrium potentials is the driving force for galvanic displacement. The secondary metal can also be selectively deposited on specific sites (such as corners and edges) of the primary metal surface if the difference between the

equilibrium potentials of the two metal components is small [1,26]. In practice, the direct redox process can be used to deposit a noble metal with higher standard electrochemical potential onto a non-noble metal with lower standard electrochemical potential, e.g., deposition of Pd^{2+} on Ag^{o} [27]. This method provides the ability to prepare true bimetallic catalyst with strong metal interactions; however, the mechanism also limits the application of this method. One serious limitation is that this method is not applicable for the bimetallic systems in which the electrochemical potential of the secondary metal is lower than that of primary metal. A second limitation is that the maximum amount of the second metal that can be added is controlled by the stoichiometry of the redox reaction. In the case of Pd^{2+} deposition on a Ag^{o} surface, only 0.5 monolayer (ML) of Pd can be deposited ($2Ag^{o} + Pd^{2+} \rightarrow 2Ag^{+} + Pd^{o}$).

In the adsorbed reductant method, a primary metal with a selectively pre-adsorbed reducing agent, typically dissociatively-adsorbed H_2, is generated by bubbling H_2 through a solution. The second metal is deposited by reduction of a metal salt with the pre-adsorbed hydrogen on the primary metal. One limitation is that the primary metal (Pt, Pd, Rh, Ru, Ir, etc.) be able to dissociatively chemisorb H_2 and to then add a secondary metal salt (Cu, Re, Ir, Rh, Pd, Pt, Au, etc.) that is reducible by adsorbed hydrogen. Many bimetallic catalysts with a combination of above metals have been prepared by this method. However, only a limited amount of secondary metal may be deposited due to limitations of adsorbed hydrogen. Further, this method is not applicable if the primary metal cannot dissociatively adsorb H_2. Metals such as Ag, Au, Cu, and are unable to dissociatively adsorb H_2 and even metals such as Ru, Co, and Ni exhibit limited ability to dissociatively adsorb H_2 at ambient conditions in the solution phase. If the secondary

metal has a higher standard electrochemical potential than the primary metal, the overall reaction will be complicated since it will involve not only a redox reaction by adsorbed reductant but also a direct redox reaction [1,26].

Underpotential deposition (UPD) refers to a process in which a single layer of atoms can be electrochemically deposited on a primary metal. It is different from the other deposition methods because it does not result in three-dimensional deposition, but rather in the formation of a single monolayer deposition. UPD occurs when the potential of a noble, primary metal is higher than the standard potential necessary for bulk deposition of the secondary metal [28,29]. Modification of the standard potential of the primary metal can be achieved by electrochemical methods for conductive supports such as carbon or by using a supplementary redox system for non-conductive supports such as silica. A hydrogen redox system is used as a supplementary system in solution to adjust the primary metal potential. Hydrogen redox can be controlled by changing the solution pH. Although underpotential deposition can provide controlled coverage of the second metal, the materials and surfaces may be unstable due to diffusion and rearrangement of atoms on the surface, especially at the high temperatures commonly used for most catalytic reactions [26].

Finally, bimetallic catalysts may also be synthesized by the catalytic reduction of a reducible metal salt on a primary metal with an organic, water-soluble reducing agent. This method of bimetallic catalyst preparation is often referred to as electroless deposition (ED). The reducing agent is activated on the primary metal surface to form an active reducing agent (typically assumed to be a hydride-like species) which serves as the site for reduction of a secondary metal salt. Thus, the secondary metal is deposited only

on the primary metal to form a bimetallic surface. After the deposition of secondary metal, the freshly-deposited second metal may also serve as a site for activation of the reducing agent, resulting in three dimensional deposition of the secondary metal occurs on the base catalyst. This type of catalytic reduction (ED) can be applied to a very wide range of combinations of primary metal and secondary metal salts, since the selection of the proper organic reducing agent provides activation on virtually all metal surfaces; this is not the case for adsorption of molecular H_2, which also requires adequate solubility of H_2 in the aqueous solution for activation on the primary metal surface. Hydrogen solubilities are typically quite low at ambient pressures in aqueous solutions. Thus, electroless deposition provides a way to prepare bimetallic catalysts with variable and controlled levels of coverage of the second metal on the first to better explore possibilities of enhanced activities, selectivities and lifetimes for a wide range of catalytic applications. It is discussed in more detail in the following Section.

1.3 Electroless Deposition Method

The electroless deposition method (ED) is a catalytic method in which a metal is deposited on a pre-existing metal substrate in a controlled manner. The ED method was first mentioned by von Liebig in 1835 when he deposited a Ag (I) salt on Ag metal [30]. There was little significant development in the ED method until 1946 when Brenner and Riddell successfully used electroless deposition for deposition of Ni to give smooth Ni films [30]. They defined electroless deposition as an autocatalytic process in which a metal (Ni, in their case) was deposited on just-deposited metal (again, Ni) without using an external electrical current [31]. They first named this process "electroless plating"

since the goal was to produce continuous metal films. This initial definition was used to distinguish from electro-deposition. Technically, electroless plating is a broad area which can be divided into three different types of deposition processes: displacement deposition or galvanic displacement [32], contact or substrate-catalyzed deposition [30], and catalytic/autocatalytic deposition.

Displacement deposition, which has been discussed in section 1.2, involves a process in which a secondary metal ion with higher standard potentials is reduced and deposited at the surfaces of an active metal, as a result of dissolution (oxidation) of the active metal [32]. Potential difference between secondary and primary metal is the driving force for displacement deposition, so this method cannot be used for any bimetallic system in which secondary metal has a lower electrochemical potential, which limits the application of this method.

In the contact deposition process, an auxiliary metal is used as an anode and then is dissolved (oxidized), and another metal acts as the cathode. The electrons transferred between two metals which are physically and/or electrically connected are then used for reduction of a third metal from solution onto the cathodic metal. Similar to galvanic displacement, the amount of metal deposition is limited. As the concentration of dissolved auxiliary metal increases, the solution usually becomes unstable; thus, practical applications for contact deposition are very limited.

The ED method in this study will focus on both catalytic and autocatalytic depositions. In catalytic deposition, a soluble metal salt in solution is selectively deposited on a metal substrate with a reducing agent which has been activated by an organic reducing agent. Since the freshly-deposited secondary metal may also activate the

reducing agent, the remaining metal salt can also be reduced on freshly-deposited secondary metal and this process is called autocatalytic deposition. Electroless deposition always begins with catalytic deposition, and at some point catalytic deposition and autocatalytic deposition occur simultaneously, or successively, depending on the selection of the reducing agent and catalytic properties of the primary and secondary metals. If only catalytic deposition takes place, a mono-dispersed monolayer of the secondary metal will be deposited on the surface of the primary metal. On the other hand, three-dimensional deposition of the secondary metal can result if autocatalytic deposition becomes dominant at some point during the reduction process. If autocatalytic deposition occurs only after the primary metal surface is covered, then a core-shell bimetallic particle is formed, as in the case of Co core-Pt shell and Pd core-Pt shell structures [33,34]. The most attractive advantage of electroless deposition is that most of the metals that can be deposited by electrodeposition can also be deposited electrolessly when proper deposition conditions are used. Many bimetallic catalysts with different metal compositions have been synthesized by deposition of metal salts, including Co, Ni, Cu, Ru, Rh, Pd, Ag, Ir, Pt, Au, etc [8-10, 33-40].

Studies of the stabilities and activities of bath compositions are key to the development of electroless deposition processes for preparation of bimetallic catalysts. Figure 1.4 shows a typical electroless deposition bath. It is typically an aqueous bath maintained at a predetermined pH containing a secondary metal ion salt, a reducing agent, an optional complexing/stabilizing agent [30]. A supported monometallic catalyst is always used as the primary or base catalyst for preparation of bimetallic catalysts. A successful electroless deposition bath must be thermodynamically unstable, yet

kinetically stable (in the absence of a catalytic surface) at deposition conditions. Development of bath compositions will be discussed at a later point in this dissertation.

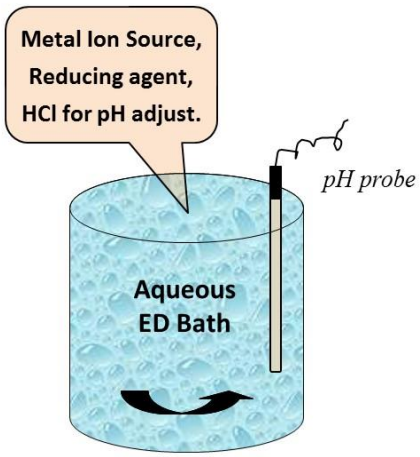

Figure 1.4 Configuration of a typical electroless deposition bath.

Metal Ion Source

Water-soluble and stable (with respect to precipitation) salts are two basic requirements for metal ion sources in an electroless deposition bath. Furthermore, thermodynamic/kinetic and pH stabilities, solubility, and environment concerns should also be considered for choosing metal ion salt. Soluble metal salts, such as sulfates, chlorides, acetates, cyanides and etc., can be used as secondary metal sources. Table 1.1 lists common metal salts used in electroless deposition [41].

Table 1.1 Common metal ion sources for electroless deposition.

Metal	Metal Precursors
Ni	$NiSO_4$, $NiCl_2$, $Ni(H_2PO_2)_2$, $Ni(CH_3COO)_2$
Co	$CoSO_4$, $CoCl_2$
Au	$KAu(CN)_2$, $KAuCl_4$, $Na_3Au(SO_3)_2$
Ag	$AgNO_3$, $NaAg(CN)_2$
Pd	$PdCl_2$, $Pd(NH_3)_4Cl_2$
Pt	$Na_2Pt(OH)_6$, $(NH_3)_2Pt(NO_2)_2$, Na_2PtCl_6
Cu	$CuSO_4$, $KCu(CN)_2$

Reducing Agent

The reducing agent provides the electrons to reduce the secondary metal salts in solution, so selection of reducing agent is very important. The reducing agent must have a favorable oxidation potential to thermodynamically reduce the metal ion, but not be so strong that thermally reduction metal occurs in solution before activation on a primary metal surface. Thus, strong reducing agents such as BH_4^- are typically not used in ED because it will lead to thermal reduction before catalytic activation on the primary metal surface. Hydrazine (N_2H_4), formaldehyde (HCHO), hypophosphite ($H_2PO_2^-$), and dimethylamine borane (DMAB) are commonly used reducing agents [42]. A more negative standard redox potential for reducing agent than the secondary metal is required for the ED method. The catalytic activity of different metals (Au, Pd, Pt, Ag, Ni, Co and Cu) for activation of the above reducing agents was measured and compared by Ohno et al. [42]. Figure 1.5 shows comparison of the anodic oxidation potential of these reducing agents for different metal electrodes at a reference current density. If the reducing agent is more active on the secondary metal surface, autocatalytic deposition will become the

dominated process in ED. Conversely, if reducing agent activity on the primary metal surface is higher, deposition of the second metal on the first metal (i.e., catalytic deposition) will be favored over autocatalytic deposition. Usually, catalytic deposition is desired, since the goal is to form bimetallic surfaces. For example, to deposit Au on Pd, DMAB and hydrazine are good candidates, since higher activity for these reducing agents on Pd surface will favor catalytic deposition. For synthesis of Pd on Au, hypophosphite anion and formaldehyde would be used.

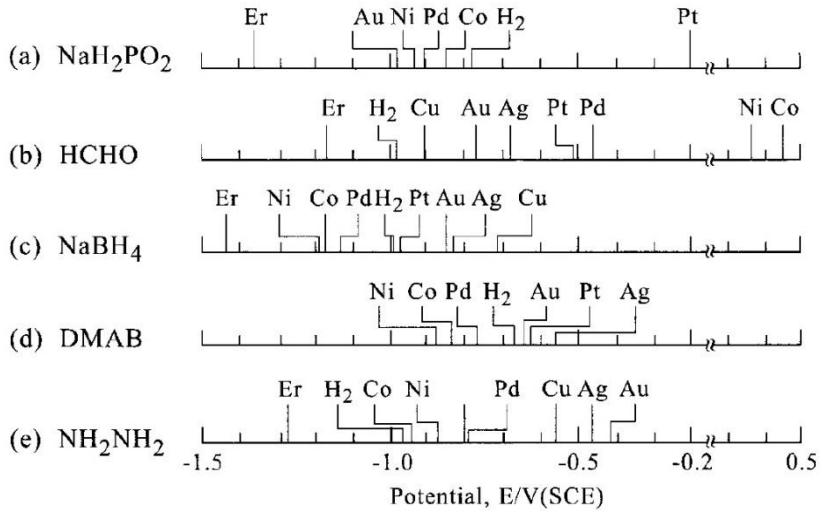

Figure 1.5 Catalytic activities of metals for anodic oxidation of different reductants [42].

Complexing Agent

A complexing agent is a coordinating and electron donating group that displaces hydrated water molecules to occupy metal ion coordination sites in aqueous solutions [43]. Complexing agents are used in electroless deposition to prevent precipitation of hydroxides and metal salts if the ED bath is basic. It also increases the kinetic stability of the ED bath [30], since the coordination reaction between ion and complexing agent lowers the "free" metal ion concentration in solution. In addition, the complexing agent may act as a pH buffer in solution. Generally, these complexing agents are organic acids

(or salts of organic acids), including glycolic, citric, succinic, and tartaric acids (or their salts) [30]. Table 1.2 is a summary of typical complexing agents used for some transition metal ions [44].

Table 1.2 Complexing agents used in the electroless deposition for common metals [44].

Metal	Complexing agents
Ni, Co	propionate, succinate, hydroxyacetate, citrate, EDTA, tartarate
Cu	glycolic acid, EDTA, tartarate, triethyl amine, cyanide
Au	cyanide, sulfate, citrate, chloride, ethanolamine
Ag	cyanide, Ammonium
Pd, Pt, Ru	ethylenediamine, citrate, succinate, acetate, ammonium

Stabilizers

Stabilizing agents are sometimes used during ED process for reasons similar to those of complexing agents. They help prevent precipitation of the metal salts in solution to increase thermal stability and lifetime of the ED bath [30]. The stabilizer effectively shields the solution from active nuclei without having negative impact on the deposited material or causing compatibility problems with other bath components [43,45]. Stabilizers can also be used to optimize the deposition rate by changing the concentration of free ions. The commonly used stabilizing agents for some metals are listed in Table 1.3 [30].

Table 1.3 Stablizing agents used in the electroless deposition for common metals [30].

Metal	Stabilizing agents
Ni	metals (S, Se, Te), oxyanions (AsO_2^-, IO_3^-, MoO_4^{-2}), metal cations, organic acids
Cu	thiourea, cyanide, mercury compounds, butyrol, propionitrile
Au	nitrilotriacetic acid, mercaptosuccinic acid
Ag	metal ions (Cu^{+2}, Ni^{+2}, Zn^{+2}), NaSCN, cystine, mercapto-propane sulfonate
Pd	mercaptoformazon compounds

Agitation, pH and Temperature

Apart from the bath compositions discussed above, operating conditions such as agitation, pH and temperature also have significant effects on deposition results. Increasing bath agitation may increase the rate of deposition by decreasing external mass transfer limitations. For external mass transfer limitations to be operative, the rate of diffusion must be slower than the rate of deposition. This is not necessarily detrimental, but often increasing the stirring rate minimizes diffusion [35]. On the other hand, excessive agitation can attrite the base catalyst to the fine powder which is difficult for filtration and may cause pressure drop in flow reactors during any subsequent evaluation process. A more effective approach is to lower the deposition temperature which lowers the rate of deposition more than lowering the rate of external mass transfer. A recent study has indicated ultrasonic agitation can increase the deposition rate by 15 times [35].

The effect of pH is another important factor in ED method, since stability of some metal salts in solution varies with pH. In some cases, high OH^- concentrations cause precipitation of metal ions as insoluble hydroxides or oxides. Thus, a particular range of pH should be maintained during the ED process. A second reason is that bath pH can

have a large impact on the standard potential of the reducing agent. For example, the standard potentials for oxidation of both formaldehyde and hydrazine can change by ~1 V due to pH changes [30,45]. Thus, changes in pH can cause changes in the rate of deposition. Finally, the effect of temperature has also been studied for electroless deposition [43], since temperature is exponentially related (Arrhenius factor) to the rate of deposition regardless of which reducing agent is used. However, ED baths can also become unstable at high temperatures. Therefore, choosing an appropriate temperature with the balance of bath stability and deposition rate is one of the important parameters in ED bath development process. Further, since a controlled rate of deposition is desired during formation of bimetallic catalysts, lower temperatures are often preferred. A deposition period of 15 – 60 min typically gives well-defined bimetallic compositions.

1.4 Pt-Ru Bimetallic Catalysts

The platinum-ruthenium (Pt-Ru) bimetallic system has been extensively studied since the early 1900s. Synergistic effects have been observed for a variety of reactions, primarily skeletal isomerization reactions (hydrogenolysis of C−C bonds) for catalytic reforming of alkanes to increase octane values by conversion into aromatics, cycloalkanes, and branched acyclic alkanes [46-48]. Pt-Ru catalysts have also been used for the selective hydrogenation of multi-functional olefins for the production of higher value chemicals [49]; exemplary reactions include selective hydrogenation of cinnamaldehyde [50,51], citral [52], ortho-chloronitrobenzene [53,54], glycerol [55] and α, β-unsaturated aldehydes [56,57]. With the combination of high activity for hydrogenation of C=O bonds from Ru and facile hydrogenation ability of C=C bonds

from Pt, specific Pt-Ru catalysts have shown high activity for hydrogenation of a variety of chemicals and selective hydrogenation of specific functional groups of multi-functional olefins.

More recently, Pt-Ru catalysts have been used for fuel cell applications where alcohols are used as H_2 sources at the anode of PEM fuel cells. Specifically, it has been shown that anodic Pt-Ru catalysts provide optimal performance for direct methanol fuel cells (DMFC) relative to Pt monometallic catalysts. Platinum catalysts typically lose activity due to poisoning from strongly-adsorbed CO generated during methanol reforming. The presence of surface Ru minimizes effects of CO poisoning by the direct interaction between Ru and Pt surface sites. Electrochemical studies have suggested that the existence of the Ru-OH species (from the H_2O vapor co-feed) helps remove CO adsorbed on adjacent Pt surface sites [58]. The reaction scheme is shown in equations 1.1 and 1.2 below.

$$Ru + H_2O \rightarrow Ru - OH + H^+ + e^- \qquad \text{Eq. 1.1}$$

$$Ru - OH + Pt - CO \rightarrow Ru + Pt + CO_2 + H^+ + e^- \qquad \text{Eq. 1.2}$$

This interaction can occur only when the two metallic components form bimetallic surface compositions instead of separate particles or ensembles of separate metal atoms on the catalyst surface. Several research groups have reported that bimetallic Pt-Ru catalysts with a 1:1 bulk molar ratio give the best performance [59-62]. It is intuitive that the bifunctional mechanism described above requires the Pt and Ru sites to be in contiguous positions to facilitate CO removal. However, in most cases, the Pt-Ru catalysts have been prepared by bulk methods [63-65] (co-impregnation, successive

impregnation, galvanostatic pulse electrodeposition) that do not necessarily form surface compositions which are consistent with overall composition, since conventional preparation methods usually have poor control of surface composition; co-impregnation and successive impregnation typically result in both monometallic and bimetallic particles (of variable composition) which make it difficult to determine the position of the two metallic components. New preparation methods for true bimetallic Pt-Ru catalysts are crucial to improve catalysts performance.

1.5 Ethylene Oxide and Ethylene Epoxidation Catalysts

The world-wide production of ethylene oxide (EO) currently exceeds 25 Mt/yr, placing the synthesis of this oxygenated organic chemical high on the list of the world's most commonly produced chemicals [66,67]. In 1931, Theodore Lefort developed a Ag-based catalyst capable of directly epoxidizing ethylene to EO, which replaced the previously used chlorohydrin process [68]. Since 1937, when Union Carbide started their first EO plant, the selective, partial oxidation of ethylene has been performed using Lefort's Ag-based catalyst [66,68-71]. The reaction pathway, as typically displayed in many catalysis textbooks, is shown in Figure 1.6 and is deceptively simple. It involves only 2 reactants and 3 potential products, where r_1 represents the desired, mildly exothermic and selective pathway leading to the formation of EO ($\Delta H = -105$ kJ/mol). Alternatively, ethylene and/or EO can undergo combustion to CO_2 and H_2O by one or both of two highly exothermic pathways including the parallel (r_2: $\Delta H = -1326$ kJ/mol) and sequential routes (r_3: $\Delta H = -1222$ kJ/mol). Industrially, the relative rates of the three pathways $[r_1/(r_2 + r_3)]$ and careful control of process conditions (to avoid thermal

runaway) are of the utmost importance. Over the past 70 years, this reaction has been studied extensively and considerable progress has been made in understanding the fundamental kinetic and mechanistic details of this reaction [68-82]. One theme that has emerged is the importance of having an atomic oxygen adsorbed on the Ag surface during reaction conditions that is considered to be electron deficient or "electrophilic-type" which is responsible for the selective reaction (r_1) leading to the formation of EO. Alternatively an electron rich or "nucleophilic-type" Ag-O species can abstract a hydrogen atom from adsorbed ethylene by the non-selective reaction pathway (r_2) to form CO_2 and H_2O. Reaction pathway (r_3) typically represents acid-catalyzed isomerization of gas phase EO to form acetaldehyde, which undergoes facile combustion to CO_2 and H_2O because of the high reactivity of both the aldehydic C-H bond as well as the three equivalent C-H species at the α-position [83].

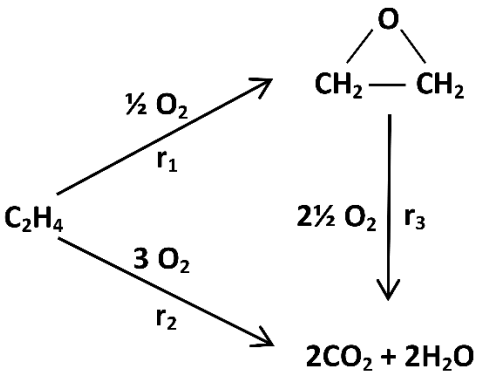

Figure 1.6 Reaction network for the production of EO from ethylene.

In addition to Ag and a "promoting amount" of Cs, Re and Re co-promoters must be added to current catalyst formulations to improve the selectivity to EO [84-86]. A chlorine-containing moderator such as ethyl chloride (CH_3CH_2Cl) is also continuously fed to the reactor at ppm levels because it similarly increases the selectivity to EO. The

use of Cs as a promoter has been discussed at length, but its specific role in the selective oxidation of ethylene is still the subject of considerable debate [87-96]. For example, Waugh and coworkers [71,87-89] recently argued that the role of Cs is mainly geometric in nature and claimed that Cs is preferentially bound to Ag on unselective, stepped silver sites. In this mechanism, Cs is thought to be responsible for blocking adsorption of oxygen onto these inherently less selective sites. This contradicts earlier work by Lambert and coworkers [90-92] who argued that Cs promotion was mainly electronic in nature. In their interpretation, Cs affected the secondary chemistry by decreasing the rate of EO isomerization to acetaldehyde [reaction (r_3)], which at typical reaction conditions combusts immediately in the presence of Ag. Monnier and coworkers [93-96,97] proposed a different type of electronic argument regarding the role of Cs as a promoter in the epoxidation of butadiene to form 3,4-epoxy-1-butene (EpB). In their case, the highly polarizable nature and large ionic radius of Cs^+ was hypothesized to lower the desorption energy of the EpB precursor adsorbed on Ag by shifting electron density from Cs^+ to those Ag sites. Experiments were conducted using Cs^+, Tl^+, Rb^+ and K^+ salts sharing identical counter-anions and revealed that the promoter enhancement of catalytic selectivity decreased as follows: $Cs^+ \approx Tl^+ > Rb^+ >> K^+$. The Pauling polarizabilities (and, hence, the ability to respond to changes in the positive character of the active $Ag^{\delta+}$ sites) of Tl^+, Cs^+, and Rb^+ are the largest of all ions in the periodic table [93,95]. This trend permitted the authors to argue that promotion by Cs cannot be explained by a site blocking mechanism since all of these cations, including K^+, have rather similar ionic radii and should be present in similar positions on the surface of the Ag (and possibly the support) to give similar performance trends. Recent work by Barteau and coworkers

[77,98] have also suggested that Cs may interact with the oxametallacyle intermediate through long-range, dipole-dipole electrostatic effects to shift the reaction path towards EO instead of acetaldehyde.

Similar arguments have also been proposed regarding the role of Cl as a moderator and include both ensemble/geometric [99] and electronic effects [70,88,92,100-102]. In the case of Cl, however, an electronic effect is more clearly favored. For example, Lambert et al. [100] investigated the effect of using different halogen-containing moderators (F, Cl, Br, I) on the selectivity to EO and found that selectivity decreases as follows: Cl > F $\approx$ Br > I, which tracks with the reported electron affinities (3.61, 3.40, 3.36 and 3.06 eV for Cl, F, Br, I, respectively). From this trend, Lambert concluded that the electronic nature of Cl promotion was unequivocal, with valence charge withdrawal from an oxygen adsorbed to an adjacent Ag site by Cl being responsible for the observed selectivity increases. The charge withdrawal resulted in a more electrophilic oxygen atom under reaction conditions that preferentially added to the electron-rich C=C double bond to form EO, rather than undergo nucleophilic attack at a C-H bond, thus increasing the selectivity to EO. Interestingly, a recent DFT investigation has also postulated that subsurface Cl may lower the desorption energy, as in the case of Cs, of the adsorbed EO intermediate in addition to drawing electron density from adjacent oxygen atoms [102].

The use of Re as a promoter is much less understood, as recently stated by Barteau [103]. This is especially relevant because the patent literature as early as 1988 [84-86] described that significant enhancements in EO selectivity were achieved by Re promotion of Ag-Cs/α-Al_2O_3 catalysts. In 1987 Shell Oil introduced their high selectivity

(HS) series of catalysts containing high-valent Re oxyanions to the marketplace with significant improvements in EO selectivity relative to their previous high activity (HA) supported Cs-Ag series of catalysts. Selectivity improvements of 5-7 percentage points were obtained by incorporation of promoter amounts of Re salts [104]. More recent patent examples [69,105-108] describe EO catalysts containing not only Cs and Re promoted silver but also Re co-promoters consisting of high-valent oxyanions of the transition metals Mo, W, Cr, Ti, Hf, Zr, V, Ta, Hf, and Nb, as well as high-valent oxyanions of non-metals such as S, P, and B. In all cases, these catalysts achieved selectivities to EO in excess of the previously-hypothesized, upper limit of 85.7% [69].

In some cases, the reported selectivity was even as high as 92% [105]. Given the overwhelming industrial significance of EO and the use of Re-containing high selectivity EO catalysts for more than 25 years, it is surprising to find so few open literature reports [103,109,110] addressing the role of Re in the current generation of high-selectivity Ag-Cs-Re/α-Al_2O_3 catalysts or the role and significance of adding Re co-promoters to the Ag-Cs-Re system. It is important to study the mechanism of how Cs, Re and Re co-promoters increase the selectivity during this epoxidation reactions.

CHAPTER 2:

EXPERIMENTAL PROCEDURES

2.1 Catalyst Preparation of Pt-Ru Bimetallic System

Two series of Pt@Ru/C and Ru@Pt/C bimetallic catalysts have been prepared by electroless deposition (ED) method. For Pt@Ru/C compositions, a new ED bath was developed using $Ru(NH_3)_6Cl_3$ as the Ru precursor salt and formic acid (HCOOH) as the reducing agent. For Ru@Pt/C preparations, a standard bath using H_2PtCl_6 and dimethylamine borane (DMAB) as Pt precursor salt and reducing agent, respectively, was employed. Sample sizes of 0.5 g base catalysts (Pt/C or Ru/C) in a 100 mL ED bath were used for all ED experiments. Conditions for the ED baths were chosen based on the PZC of the base catalyst, the rate of deposition of the secondary metal, and the stability of the bath.

For Pt@Ru/C catalysts (Ru deposition on Pt/C), $Ru(NH_3)_6Cl_3$ and HCOOH were dissolved using DI water to form stock solutions. Based on the desired weight loadings of Ru on Pt/C, the proper volumes of $Ru(NH_3)_6Cl_3$ solution and DI water were added to a Pyrex^{TM} beaker to give 100 mL of ED bath and the desired initial concentrations of $Ru(NH_3)_6^{3+}$. The bath pH was adjusted to a specific value between pH 2-4 with hydrochloride acid (HCl) and the bath temperature was maintained at values between 70 – 120 ℃ by immersion into a temperature-regulated oil bath. At temperatures > 100 ℃, a reflux condenser was used to maintain H_2O in the ED bath. HCOOH was next added to the bath solution to determine thermal stability. For ED experiments, 0.5 g of 20 wt% Pt/XC-72 base catalyst was added to the bath after a 30 min time interval (final bath stability check). Additional aliquots of HCOOH were added at different time intervals during the ED experiment to ensure adequate concentrations of reducing agent. One mL liquid aliquots were taken from the bath periodically during the deposition for Ru

analysis using atomic absorption spectroscopy (AAS) performed by a Perkin Elmer AAnalyst 400 spectrometer.

For Pt deposition on Ru/C, H_2PtCl_6 and DMAB, were used as the Pt salt and reducing agent, respectively. H_2PtCl_6 and DMAB were dissolved in DI water to form separate stock solutions, and proper volumes of H_2PtCl_6 solution and DI water were used to form a 100 mL ED bath with desired Pt salt content. Bath pH was adjusted between pH 9-11 using a NaOH solution. The ED bath temperature was maintained at specific temperatures between 50 – 90 ℃. 0.5 g of 20 wt% Ru/C base catalyst was added into ED bath. Additional DMAB was also added during ED to ensure complete deposition of $PtCl_6^{2-}$. One mL samples were periodically taken from the bath and concentrations of unreacted $PtCl_6^{2-}$ were analyzed by atomic absorption spectroscopy (AAS).

Once deposition of Ru or Pt was completed, samples were filtered using a Büchner flask and funnel. After filtration, catalysts were then rinsed with an amount of deionized water at least five times the total volume of the ED bath, and left to dry in the Büchner flask and funnel overnight. The catalysts were then stored at ambient conditions in sealed bottles.

2.2 Catalyst Characterization of Pt-Ru Bimetallic System

Monometallic Pt/C, Ru/C and bimetallic Pt@Ru/C, Ru@Pt/C catalysts were characterized using H_2 titration of oxygen pre-covered metal sites. A Micromeritics Autochem II 2920 automated chemisorption analyzer with a high sensitivity thermal conductivity detector (TCD) was used for all chemisorption measurements. All samples were pretreated *in situ* in flowing H_2 for 3 h at 300 ℃ and then purged with flowing Ar

for 0.5 h before cooling to 40 ℃ in Ar. A gas flow of 10% O_2/balance He was passed over the samples for 30 min to form O-covered Pt or Ru surface species. After purging with pure Ar flow for 30 min to remove residual gas phase and weakly adsorbed O_2, pulses of 10% H_2/balance Ar were dosed at 5 min intervals until all surface oxygen reacted with H_2 to form H_2O and Pt-H or Ru-H surface species.

Temperature programmed reduction (TPR) using a CHEMBET-3000 (Quantachrome Instruments) was used to determine optimal H_2 titration temperatures of O-precovered surfaces and the subsequent extent of Pt-Ru interactions for the bimetallic compositions. All catalysts were reduced in flowing H_2 for 3 h at 300 ℃ and then purged with flowing N_2 for 30 min at 300 ℃ before cooling to 40 ℃ in N_2. A gas stream of O_2 was then flowed for 30 min to form O-precovered Ru and Pt surface species. After purging with N_2 for 30 min to remove residual gas and weakly adsorbed O_2, 10% H_2/balance N_2 was passed over the sample while heating from 40 ℃ to 400 ℃ at 10 ℃/min ramp rate. Hydrogen consumption was measured using a thermal conductivity detector (TCD). Figure 2.1 is the schematic of the TPR-MS system.

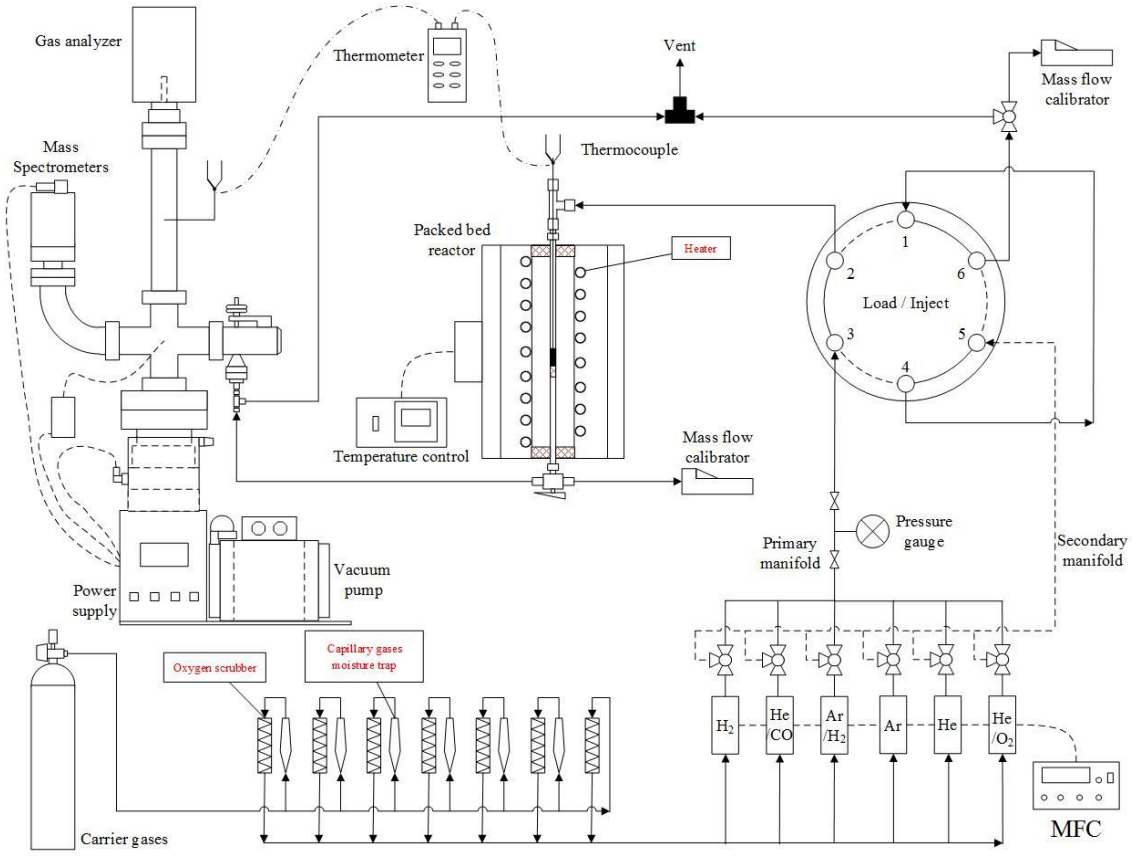

Figure 2.1 The schematic of the TPR-MS system.

X-ray photoelectron spectroscopy (XPS) measurements were collected using a hemispherical analyzer on a Kratos Axis Ultra DLD XPS with a monochromated Al Kα x-ray source. The monochromatic Al Kα source was operated at 15 keV and 150 W, incident at 45 °with respect to the surface normal. The pass energy was fixed at 40 eV for the detailed scans. All samples were pretreated at 280 °C in H_2 for 2 h followed by Ar flow for 2 h and cooled to room temperature in Ar flow in a catalysis chamber attached to the UHV chamber by means of a gate valve and a linear translation arm. After pretreatment, the samples were transferred without exposing to air into the UHV chamber for XPS measurements.

Scanning transmission electron microscopy (STEM) was used to obtain High Angle Annular Dark Field (HAADF) images of the base catalysts and the ED prepared bimetallic catalysts using a cold field emission, probe aberration corrected, 200 kV electron microscope, the JEOL JEM-ARM200CF. The JEM-ARM200CF has an imaging resolution of down to below 0.078 nm and energy resolution of 0.35 eV. HAADF micrographs were acquired with either of the two detectors (JEOL and Gatan) for HAADF fitted in the JEM-ARM200CF. Microanalyses of the catalysts were done using X-Ray Energy Dispersive Spectroscopy (XEDS) to generate elemental maps of Ru and Pt. The XEDS maps were acquired through an Oxford Instruments X-Max100TLE SDD detector also fitted to the JEM-ARM200CF. The ED prepared catalysts with the highest loading of secondary metal were selected for STEM imaging and XEDS in order to obtain the best possible imaging contrast and spectroscopic signal, respectively.

2.3 Catalyst Preparation of Ag-based EO Catalysts

Different series of Ag, Ag-Cs, Ag-Re, Ag-Cs-Re and Ag-Cs-Re-Mo compositions supported on α-alumina were prepared using the incipient wetness (plus 5% excess liquid) method. $Ag_2C_2O_4$ and α-Al_2O_3 rings (SA5562, 8mm rings, BET surface area = 0.60 m^2g^{-1} using Kr adsorption, and pore volume = 0.53 cm^3g^{-1} from Norpro-St. Gobain) were used as the Ag precursor salt and support, respectively. The silver ($Ag_2C_2O_4$) and promoter salts ($CsNO_3$, NH_4ReO_4 and $(NH_4)_2MoO_4$) were added to an aqueous solution containing sufficient ethylenediamine (EN) to give a 3:1 molar ratio of EN to Ag, or [EN]/[$Ag_2(C_2O_4)$ = 1.5:1. For each impregnation batch, the appropriate amount of impregnation solution and 20 g of α-Al_2O_3 rings were added a 100 mL fluted flask and

tumbled under vacuum at 60 ℃ until the rings tumbled freely. The rings were then calcined using forced air flow (100 L/min) at 260 ℃ for a total of 5 – 7 min. The rings were crushed and sieved to 20-40 mesh (850-425 μm) before evaluation. Figure 2.2 shows the rings before impregnation, rings after impregnation and calcination, and after crushing to 20-40 mesh sieved particles.

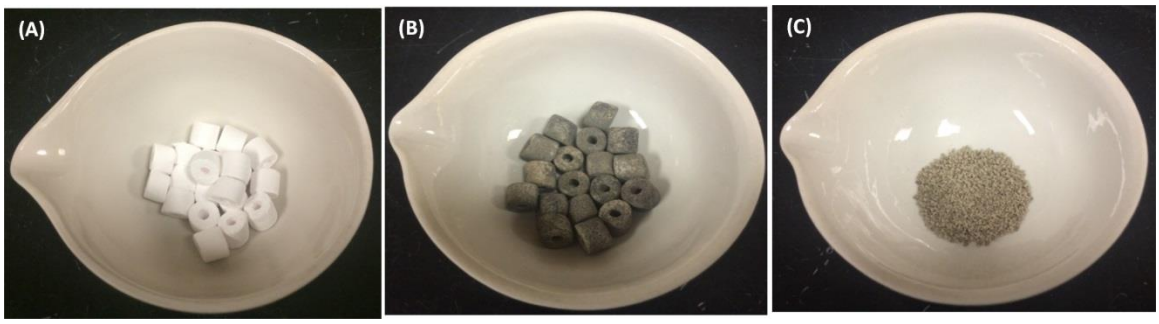

Figure 2.2 Pictures of (A) SA5562 α-Al_2O_3 rings (B) Ag-Cs-Re-Mo/α-Al_2O_3 catalyst (C) sieved Ag-Cs-Re-Mo/α-Al_2O_3 catalyst for reaction.

2.4 Catalyst Characterization of Ag-based EO Catalysts

The weight loadings of Ag, Cs and Re for selected samples were measured by inductively coupled plasma (ICP) using a Perkin-Elmer Optima 2100 DV for Re and by atomic absorption spectroscopy (AAS) using a Perkin Elmer AAnalyst 400 spectrometer for Ag and Cs. Solid samples were dissolved, digested, and diluted to appropriate concentrations before elemental analysis.

Scanning electron microscopy (SEM) micrographs were collected using a Zeiss Ultraplus Thermal Field Emission Scanning Electron Microscope. Electrons were collected using a high efficiency scintillator detector with an optically-coupled photomultiplier. The incident electron beam energy was set to 6.0 keV. Micrographs were recorded at 30,000x and 50,000x magnification. Prior to analysis, the extruded rings

were cut in half and only the interior portions of the samples were scanned to ensure that only non-attrited surfaces were analyzed.

XPS measurements were performed using a Kratos AXIS Ultra DLD XPS system equipped with a hemispherical energy analyzer and a monochromatic Al Kα source. The monochromatic Al Kα source was operated at 15 keV and 150 W; pass energy was fixed at 40 eV for the detailed scans. All samples were prepared as pressed powders supported on a gold-plated stainless steel stub for the XPS measurements. A catalyst pretreatment cell attached to the UHV system permitted samples to be pretreated in H_2-containing and O_2-containing gas streams at elevated temperatures.

2.5 Epoxidation Reactions

The crushed and sieved 20-40 mesh (850-425 μm) catalysts were evaluated in a tubular, 316 stainless steel reactor. The reactor with 0.19 in. ID, 0.25 in. OD was tightly encased (press-fitted) in a 1 in. OD aluminum jacket to better ensure isothermal operation. A gas hourly space velocity (GHSV) of 4500 hr^{-1} feed with 8% O_2, 25% C_2H_4, 1-3 ppm ethyl chloride (EtCl), and balance CH_4 at 250 psig were regulated using Brooks 5850E mass flow controllers. Two g of 20/40 mesh catalyst particles were loaded into the reactor for the epoxidation reaction. After exiting the reactor, the pressure was reduced to 1 atm by a Veriflo back pressure regulator, and the gas flow was directed into Valco switching valves containing a sample loop that diverted gas contents to either a thermal conductivity or flame ionization detector. Analysis was performed using an on-line, Agilent 7890A gas chromatograph with two Poraplot Q columns for quantitative analysis of CO_2, H_2O, EO, and acetaldehyde and ethylene glycol, if present.

CHAPTER 3:

PREPARATION AND CHARACTERIZATION OF PT-RU BIMETALLIC CATALYSTS SYNTHESIZED BY ELECTROLESS DEPOSITION METHODS

Reprinted with permission from [W. Diao, J. M. M. Tengco, J. R. Regalbuto, J. R. Monnier, ACS Catal. 5 (2015) 5123-5134].

DOI: 10.1021/acscatal.5b01011

3.1 Abstract

Two series of Pt@Ru/C and Ru@Pt/C bimetallic catalysts have been prepared by electroless deposition (ED) method. For Pt@Ru/C compositions, a new ED bath was developed using $Ru(NH_3)_6Cl_3$ as Ru precursor and HCOOH as reducing agent. For Ru@Pt/C preparations, a standard bath using H_2PtCl_6 and DMAB as Pt precursor and reducing agent, respectively, was employed. The Pt@Ru/C and Ru@Pt/C bimetallic catalysts have been characterized by temperature programmed reduction (TPR), selective chemisorption, X-ray photoelectron spectroscopy (XPS), and scanning transmission electron microscopy (STEM) with X-ray energy dispersive spectroscopy (XEDS). TPR and selective chemisorption (H_2 titration of oxygen pre-covered surfaces) experiments have confirmed the existence of strong surface interactions between Pt and Ru as evidenced by hydrogen spillover of Pt to Ru (Pt-assisted reduction of oxygen pre-covered Ru). XPS analyses also showed e^- transfer from Pt to Ru on the bimetallic surface, again indicating strong surface interactions between Pt and Ru. Finally, the STEM images and XEDS elemental maps provided strong visual evidence of targeted deposition of the secondary metal on the primary metal. The elemental maps confirmed that individual nanoparticles of both Pt@Ru/C and Ru@Pt/C catalysts prepared by ED were bimetallic, with excellent association between the primary and the secondary metals.

3.2 Introduction

As we discussed in section 1.3, Pt-Ru bimetallic catalysts are widely used for direct methanol fuel cells, biomass upgrading and hydrocarbon refining. Ensemble effect, electronic effect and bifunctional effect provide unique properties for Pt-Ru bimetallic

catalysts compare to the corresponding Pt or Ru monometallic catalysts. To achieve better performance, strong metal-metal interactions and true bimetallic surface are needed.

This interaction can occur only when the two metallic components form bimetallic surface compositions instead of separate particles or ensembles of separate metal atoms on the catalyst surface. Several research groups have reported that bimetallic Pt-Ru catalysts with a 1:1 bulk molar ratio give the best performance [59-62]. It is intuitive that the bifunctional mechanism described above requires the Pt and Ru sites to be in contiguous positions to facilitate CO removal. However, in most cases, the Pt-Ru catalysts have been prepared by bulk methods [63-65,111] (co-impregnation, successive impregnation, galvanostatic pulse electrodeposition) that do not necessarily form surface compositions which are consistent with overall composition, since conventional preparation methods have poor control of surface composition; co-impregnation and successive impregnation typically result in both monometallic and bimetallic particles (of variable composition) which make it difficult to determine the position of the two metallic components.

Thus, preparative methods that form bimetallic catalysts with bimetallic surfaces of known composition should be critical to improve catalyst performance. We use the method of electroless deposition (ED) to deposit a secondary metal salt onto a pre-existing metal site that has been activated by a suitable reducing agent [8,33,36,37,40,112,113]. The process may include both catalytic deposition of the metal salt in solution onto the pre-existing supported metal and autocatalytic deposition of the metal salt onto the just reduced, deposited metal. In principle, however, the ED process

forms only bimetallic particles without formation of isolated secondary metal particles on the catalyst support. With the kinetic control of electroless deposition, the final composition of a particular bimetallic catalyst can be controlled to give rather precise combinations of the two metallic components.

Unlike conventional bimetallic catalyst preparation methods (co-impregnation and successive impregnation) which result in both monometallic and bimetallic particles with varying composition, the electroless deposition (ED) method offers the ability to synthesize true bimetallic catalysts with bimetallic surfaces. By controlling the base catalyst, secondary metal ion source, reducing agent, bath temperature, and pH, our group has successfully synthesized multiple bimetallic catalyst systems, such as Cu-Pd, Ag-Pt, Pd-Co, Au-Pd, Ag-Pd [8,33,36,37,40].

In this study, two series of Ru@Pt/C (Pt deposited on Ru surfaces) and Pt@Ru/C (Ru deposited on Pt surfaces) catalysts have been synthesized. The focus of this manuscript is limited to the preparation and characterization of these compositions. Characterization data from temperature programmed reduction (TPR), selective chemisorption, X-ray photoelectron spectroscopy (XPS), and scanning transmission electron microscopy (STEM) are presented to confirm formation of Pt-Ru bimetallic surfaces with strong metal-metal interactions. Results for evaluation of these catalysts for direct methanol fuel cells (DMFC) are the subject of a forthcoming paper. Future work will also include evaluation of these catalysts for paraffin reforming reactions and Fischer-Tropsch applications.

3.3 Experimental

3.3.1 Catalysts Preparation

For Ru deposition on Pt, ruthenium(III) hexaammine chloride ($Ru(NH_3)_6Cl_3$) supplied by Sigma-Aldrich and formic acid (HCOOH, 99% purity) supplied by Fluka analysis were used as the Ru metal salt and reducing agent, respectively. $Ru(NH_3)_6Cl_3$ and HCOOH (FA) were dissolved using DI water to form separate stock solutions. The proper volumes of $Ru(NH_3)_6Cl_3$ solution and DI water were added to a Pyrex^{TM} beaker to give 100 mL of ED bath and the desired initial concentrations of $Ru(NH_3)_6^{3+}$. The bath pH was adjusted to a specific value between pH 2-4 with hydrochloride acid (HCl, 36.5-38%) supplied by BDH and the bath temperature was maintained at values between 70 – 120 ℃ by immersion into a temperature-regulated oil bath. At temperatures > 100 ℃, a reflux condenser was used to maintain H_2O in the ED bath. HCOOH was next added to the bath solution to determine thermal stability (no reduction of the Ru^{3+} salt by HCOOH). Stabilities were ensured over a 120 min time interval. For ED experiments, a 20 wt% Pt/XC-72 base catalyst was added to the bath after a 30 min time interval (final bath stability check). Additional aliquots of FA were added at different time intervals during the ED experiment to ensure adequate concentrations of reducing agent. One ml liquid aliquots were taken from the bath periodically during the deposition for Ru analysis using atomic absorption spectroscopy (AAS) performed using a Perkin Elmer AAnalyst 400 spectrometer. For every ED experiment, the pH value of bath was maintained constant at the initial pH value using an HCl solution of pH 1 and NaOH solution at pH 11.

For Pt deposition, hexachloroplatinic acid (H_2PtCl_6) and dimethylamine borane (DMAB, 97% purity), both supplied by Sigma-Aldrich, were used as the Pt salt and reducing agent, respectively. The kinetics and energetics of Pt deposition using DMAB have been described in detail in earlier work by Beard [33,34,114]. As above, H_2PtCl_6 and DMAB were dissolved in DI water to form separate stock solutions, and proper volumes of H_2PtCl_6 solution and DI water were used to form a 100 ml ED bath with desired Pt salt content. Bath pH was adjusted between pH 9-11 using a NaOH solution (NaOH pellets from J.T. Baker). The ED bath temperature was maintained at specific temperatures between 50 – 90 ℃. Before ED experiments, a solution containing DMAB was added to the $PtCl_6^{2-}$ solution to check bath stability; stability was ensured for a minimum of 60 min. For ED experiments, the 20 wt% Ru/C base catalyst was added after 30 min. Additional DMAB was also added during ED to ensure complete deposition of $PtCl_6^{2-}$. One ml samples were periodically taken from the bath and concentrations of unreacted $PtCl_6^{2-}$ were analyzed by atomic absorption spectroscopy (AAS). All the bimetallic catalysts prepared by electroless deposition method were washed with sufficient amounts of water (~2 L/g catalyst) to remove inorganic residues and by-products. The catalysts were then dried *in vacuo* at room temperature and stored at ambient conditions in sealed bottles.

3.3.2 Catalyst Characterization

The concentrations of Pt and Ru surface sites for the base Pt/XC-72 and Ru/XC-72 catalysts were determined by pulse chemisorption using H_2 titration of oxygen pre-covered Pt and Ru sites. A Micromeritics Autochem II 2920 automated chemisorption analyzer with a high sensitivity thermal conductivity detector (TCD) was used for all

chemisorption measurements. Before analysis, all samples were pretreated *in situ* in flowing H_2 for 3 h at 300 ℃ and then purged with flowing Ar for 0.5 h before cooling to 40 ℃ in Ar. A gas flow of 10% O_2/balance He was passed over the samples for 30 min to form O-covered Pt or Ru surface species. After purging with pure Ar flow for 30 min to remove residual gas phase and weakly adsorbed O_2, pulses of 10% H_2/balance Ar were dosed at 5 min intervals until all surface oxygen reacted with H_2 to form H_2O and Pt-H or Ru-H surface species.

Previous work has shown that surface Pt-O species was easily titrated by dosing pulses of 10% H_2/Ar at 40 ℃; however, titration of O-Ru sites required higher temperatures [115]. The higher temperature required for Ru-O titration will be discussed in more depth in the Results section. In this study, H_2 was dosed at 40 ℃ for Pt/XC-72 and at 250 ℃ for Ru/XC-72. The hydrogen titration stoichiometry was assumed to be H_2/Pt = 3/2 and H_2/Ru = 5/2 according to the following equations. The assignment of O/Ru = 2/1 stoichiometry is taken from the work of Corro [116].

H_2 titration:

$$\begin{matrix} O \\ | \\ Pt \end{matrix} + \frac{3}{2}H_2 \xrightarrow{40℃} \begin{matrix} H \\ | \\ Pt \end{matrix} + H_2O \qquad \text{Eq. 3.1}$$

H_2 titration:

$$\begin{matrix} O & O \\ \diagdown & \diagup \\ Ru \end{matrix} + \frac{5}{2}H_2 \xrightarrow{250℃} \begin{matrix} H \\ | \\ Ru \end{matrix} + 2H_2O \qquad \text{Eq. 3.2}$$

Hydrogen titration experiments gave Pt and Ru dispersions of 21.5%, and 5.8%, respectively, corresponding to average Pt and Ru diameters of 5.3 nm and 21.1 nm, respectively. The total surface sites for Pt@Ru/XC-72 and Ru@Pt/XC-72 bimetallic

catalysts were also measured at both 40 ℃ and 250 ℃ using the same pretreatment procedure as for the monometallic catalysts.

Temperature programmed reduction (TPR) using a CHEMBET-3000 (Quantachrome Instruments) was used to determine optimal H_2 titration temperatures of O-precovered surfaces and the subsequent extent of Pt-Ru interactions for the bimetallic compositions. All catalysts were reduced in flowing H_2 for 3 h at 300 ℃ and then purged with flowing N_2 for 30 min at 300 ℃ before cooling to 40 ℃ in N_2. A gas stream of O_2 was then flowed for 30 min to form O-precovered Ru and Pt surface species. After purging with N_2 for 30 min to remove residual gas and weakly adsorbed O_2, 10% H_2/balance N_2 was passed over the sample while heating from 40 ℃ to 400 ℃ at 10 ℃/min ramp rate. Hydrogen consumption was measured using a thermal conductivity detector (TCD).

X-ray photoelectron spectroscopy (XPS) measurements were collected using a hemispherical analyzer on a Kratos Axis Ultra DLD XPS with a monochromated Al Kα x-ray source. The monochromatic Al Kα source was operated at 15 keV and 150 W, incident at 45 °with respect to the surface normal. The pass energy was fixed at 40 eV for the detailed scans. All samples were pretreated at 280 ℃ in H_2 for 2 h followed by Ar flow for 2 h and cooled to room temperature in Ar flow in a catalysis chamber attached to the UHV chamber by means of a gate valve and a linear translation arm. After pretreatment, the samples were transferred without exposing to air into the UHV chamber for XPS measurements. In this study, all catalysts were supported on highly conductive XC-72 carbon, so no charge neutralization was needed to offset surface charging. All samples were analyzed as received and after 280 ℃ reduction in H_2 for 2 h. The before

reduction (BR) and after reduction (AR) data for C 1s, Ru $3d_{5/2}$ and Pt $4f_{7/2}$ were analyzed for all samples. All Ru $3d_{5/2}$ and Pt $4f_{7/2}$ binding energy (BE) peak positions were corrected using the C 1s binding energy value of 284.2 eV and all peak intensities were normalized to that for the C 1s peak for quantitative comparison.

Powder X-ray diffraction (XRD) analyses of the bimetallic catalysts with highest loadings of secondary metal as well as the monometallic core nanoparticles were performed on a Rigaku Miniflex II benchtop diffractometer with a CuKα radiation source (λ = 1.5406 Å) operated at 30 kV and 15 mA. Powder samples were loaded on an amorphous glass-backed, low background holder. Scanning was done over the 2θ range of 30 °-75 ° with sampling width of 0.02 ° and dwell time of 2 °/min. The diffractometer was fitted with a Rigaku D/tex Ultra silicon strip detector which is capable of detecting nanoparticles in samples with metal loadings as low as 1 wt% and particles as small as 1 nm [117].

Scanning transmission electron microscopy (STEM) was used to obtain High Angle Annular Dark Field (HAADF) images of the base catalysts and the ED prepared bimetallic catalysts using a cold field emission, probe aberration corrected, 200 kV electron microscope, the JEOL JEM-ARM200CF. The JEM-ARM200CF has an imaging resolution of down to below 0.078 nm and energy resolution of 0.35 eV. HAADF micrographs were acquired with either of the two detectors (JEOL and Gatan) for HAADF fitted in the JEM-ARM200CF. Microanalyses of the catalysts were done using X-Ray Energy Dispersive Spectroscopy (XEDS) to generate elemental maps of Ru and Pt. The XEDS maps were acquired through an Oxford Instruments X-Max100TLE SDD detector also fitted to the JEM-ARM200CF. The ED prepared catalysts with the highest

loading of secondary metal were selected for STEM imaging and XEDS in order to obtain the best possible imaging contrast and spectroscopic signal, respectively.

3.4 Results and Discussion

3.4.1 Catalyst Synthesis

3.4.1.1 Pt@Ru/XC-72 Preparation

Several different Ru precursor salts were tested for development of an ED bath for Ru deposition on Pt/XC-72 base catalyst. Most could not be used because of (1), insolubility in water [e.g., $Ru(NH_3)_6Cl_2$], (2), precipitation at basic conditions typically used for ED [e.g., (K_2RuCl_5)], or (3), too stable for reduction with conventional reducing agents [e.g., $K_4Ru(CN)_6$)]. Consequently, $Ru(NH_3)_6Cl_3$ was selected as the preferred choice for Ru deposition. To ensure there was no strong electrostatic adsorption (SEA) of $Ru(NH_3)_6^{3+}$ on the Pt/XC-72 catalyst, the pH of the reaction was maintained below the point of zero charge (PZC) of the catalyst [14,15]. In this case, the reaction was conducted at acidic conditions of less than pH 4.8, the PZC of 20 wt% Pt/XC-72. A recent study by Mustain has shown that formic acid (HCOOH, FA) is an effective reducing agent in acidic solutions [118]. Therefore, development of an ED bath using $Ru(NH_3)_6Cl_3$ as the Ru precursor and formic acid as reducing agent at acidic conditions was required for deposition of Ru on the base Pt/XC-72 catalyst. A sample weight of 0.5 g of the base 20 wt% Pt/XC-72 catalyst in a 100 ml ED bath was used for each experiment. All deposition experiments were conducted for 2 h, and the first 30 min served to test bath stability with only the $Ru(NH_3)_6Cl_3$ precursor and formic acid present in the bath . After 30 min, the Pt/XC-72 was added to the ED bath and additional aliquots

of formic acid solution were added at 30 min time intervals to compensate for any non-selective decomposition of formic acid.

The initial set of experiments examined the effects of bath temperature on the rate and extent of Ru deposition on the Pt surface of 20 wt% Pt/XC-72. In Figure 3.1, the concentration of 110 ppm Ru^{3+} corresponded to one monodisperse layer coverage of Ru on the Pt surface (based on Pt chemisorption measurements which will be discussed in section 3.2.1). All deposition temperature values are of the oil bath and not of the aqueous solution inside the beaker/flask itself. At T > 90 ℃, a reflux condenser was used to prevent evaporation of H_2O from the ED bath. From Figure 3.1, the first 30 min confirmed the thermal stability of the Ru^{3+} salt in the presence of FA before the addition of Pt/XC-72. In addition to the bath stability test, an earlier control experiment with only $Ru(NH_3)_6Cl_3$ and 20 wt% Pt/XC-72 in solution was also conducted at ED conditions. There was no Ru uptake at pH 3, confirming that no strong electrostatic adsorption between Ru^{3+} and the carbon support occurred. Thus, all Ru uptakes in Figure 3.1 must be due to electroless deposition of Ru on Pt and not adsorption on the carbon support. The deposition curves in Figure 3.1 also show that uptake at 70 ℃ and 90 ℃ ceased after approximately 30 min of exposure (60 min overall time). No further Ru deposition occurred, even when additional aliquots of formic acid were added to the bath. However, when the deposition temperature was increased to 110 ℃ all the Ru^{3+} was deposited. The deposition rate was also fastest at 120 ℃; all of the Ru deposition was completed in less than 5 min. From these experiments, we can conclude that deposition of $Ru(NH_3)_6^{3+}$ on Pt/XC-72 is highly temperature-dependent and that both the extent and rate of deposition increase with temperature. The reason for only partial deposition at low temperature

(70 ℃ and 90 ℃) is most likely due to the strong adsorption of CO, the oxidation product of reducing agent formic acid, on surface Pt sites; CO poisoning on Pt surface suppresses and limits further deposition of Ru on Pt surface. A recent study by Baldauf for electrochemical methanol oxidation has shown that poisoning by CO on Pt surfaces occurs at pH 2 and ambient temperatures [119].

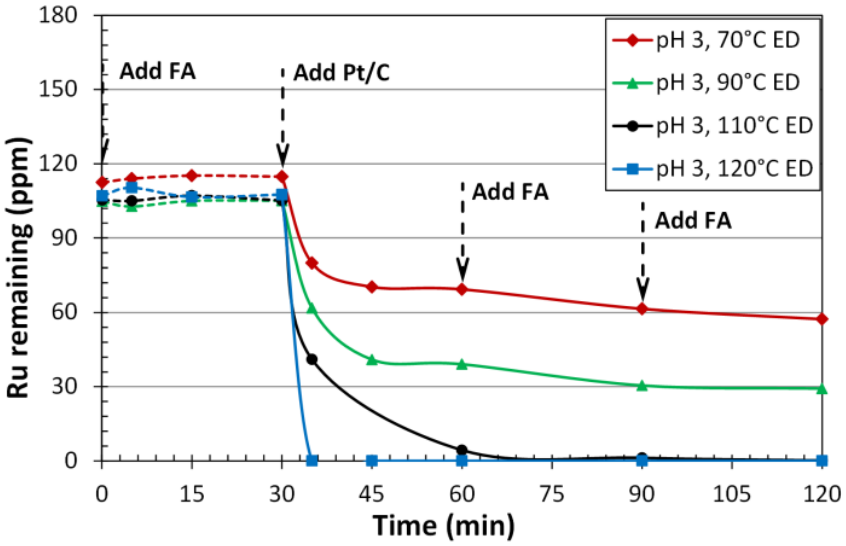

Figure 3.1 Temperature effect of Ru deposition on Pt/XC-72. Deposition conditions maintained at bath pH 3, deposition time of 2 h, total mole ratio of HCOOH to $Ru(NH_3)_6Cl_3$ = 18 : 1, and initial Ru^{3+} concentration of 110 ppm. Initial concentration of HCOOH corresponded to $[HCOOH]/[Ru^{3+}]$ = 6/1. The two other aliquots of HCOOH added at 60 and 90 min gave final mole ratio = 18/1.

The effects of bath pH on deposition of Ru on Pt are shown in Figure 3.2. The reaction temperature was kept at 90 ℃ and all conditions other than pH were the same as in Figure 3.1.

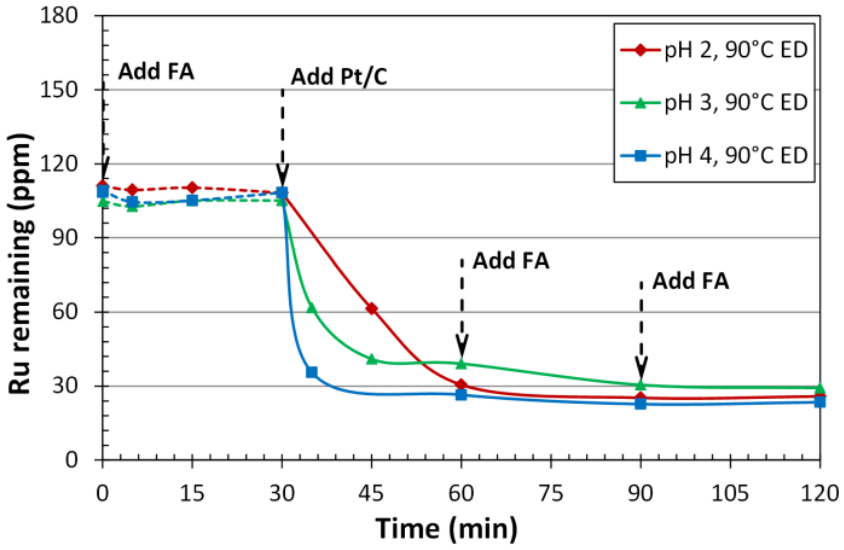

Figure 3.2 Bath pH effect of Ru deposition on Pt/XC-72. With exception of variable pH, ED conditions were same as stated in Figure 3.1.

The curves in Figure 3.2 show that the extents of Ru^{3+} deposition were similar for all three pH values, indicating that pH had little effect on the amount of deposition of $Ru(NH_3)_6^{3+}$ on Pt/XC-72. However, the rates of deposition increased at higher pH values, most likely because the concentration of $HCOO^-$, the active form of the reducing agent was higher based on the K_a of formic acid at 25 ℃ (1.8×10^{-4}).

After bath temperature and pH effects were determined, temperatures of 110 ℃ and pH 3 were chosen to prepare the different weight loadings of Ru on the base 20 wt% Pt/XC-72 catalyst; results are summarized in Table 3.1. The amount of Ru deposited was controlled by the initial concentrations of $Ru(NH_3)_6Cl_3$ in the ED bath since ~100% deposition occurred in all cases. This simple relationship of $Ru(NH_3)_6Cl_3$ in the ED bath being proportional to Ru deposition made it straightforward to prepare an extensive series of Ru-Pt bimetallic catalysts, one of the positive features of the ED process. The theoretical coverages of Ru on Pt/XC-72 are shown in the last column of Table 3.1 and are based on the assumption that Ru is deposited in a monodisperse manner on the Pt

surface with a deposition ratio of Ru : Pt = 1 : 1. Surface compositions are discussed in more detail in section 3.2.

Table 3.1 Summary of Pt@Ru/XC-72 catalysts prepared by ED. The compositions are expressed as the weight loadings of Ru deposited on the 20 wt% Pt/XC-72 base catalyst.

Catalysts	Pt wt loading (%)	Ru wt loading (%)	Theoretical monodisperse coverage θ_{Ru} on Pt	Bulk Pt/Ru atomic ratios
Pt@Ru 1	20	0.35	0.16	29.6 : 1
Pt@Ru 2	20	0.67	0.30	15.5 : 1
Pt@Ru 3	20	1.03	0.46	10.1 : 1
Pt@Ru 4	20	1.14	0.51	9.1 : 1
Pt@Ru 5	20	1.49	0.68	7.0 : 1
Pt@Ru 6	20	1.83	0.83	5.7 : 1
Pt@Ru 7	20	2.11	0.96	4.9 : 1

3.4.1.2 Ru@Pt/XC-72 Preparation

In order to compare with Pt@Ru catalysts, an inverse series of Ru@Pt/XC-72 catalysts were also prepared using electroless deposition. In this case, the base catalyst was 20 wt% Ru/XC-72, also supplied by Premetek. The Ru dispersion was 5.8% corresponding to an average Ru particle size of 21.1 nm, assuming the H_2 and O_2 adsorption stoichiometries cited earlier. Chloroplatinic acid was used as the Pt source and DMAB was the reducing agent. Bath pH was maintained at > 9**,** which was above the point of zero charge (PZC) of the base 20 wt% Ru/XC-72 catalyst, to avoid strong electrostatic adsorption of $PtCl_6^{2-}$ on the carbon support. Each experiment used 0.5 g of the base catalyst in a 100 mL ED bath and the results are summarized in Figure 3.3. All experiments were conducted for 2 h at 70 ℃ and the first 30 min were used to test the

thermal stabilities of the ED baths. The Ru/XC-72 catalyst was added to the ED bath at 30 min and additional DMAB was added after 30 min time intervals. The deposition curves in Figure 3.3 show the $PtCl_6^{2-}$ salt was thermally stable with respect to reduction in the presence of DMAB at pH 10 before the addition of 20 wt% Ru/XC-72. Besides the bath stability test, an earlier control experiment with only H_2PtCl_6 and Ru/XC-72 in a pH 10 solution (without reducing agent) was also conducted under ED conditions. The results showed no $PtCl_6^{2-}$ uptake, which demonstrated that no strong electrostatic adsorption occurred. Thus, based on the control experiment and the bath stability test, we confirm that Pt should be deposited only on the Ru surface and not adsorbed on the carbon support or reduced in solution. However, when Ru/XC-72 was added at t = 30 min, only negligible amounts levels of Pt were deposited between 30-60 min, almost certainly because all DMAB added to the bath has been thermally decomposed to produce gas phase H_2 between 0-30 min at basic pH values [30]. At 60 min, a second aliquot of DMAB was added to the solution in the presence of Ru/XC-72, this time resulting in facile deposition of Pt on the Ru surface in ≤ 30 min. In Figure 3.3, the concentration of 110 ppm Pt, or 564 umoles $PtCl_6^{2-}$/L, corresponds to one monodisperse layer coverage of Pt on the Ru surface, assuming a 1/1 ratio of Pt to surface Ru. Different weight loadings of Pt on the Ru surface of Ru/XC-72 catalysts were also synthesized by changing the initial concentrations of $PtCl_6^{2-}$ in the bath, since all $PtCl_6^{2-}$ in solution was deposited by ED. Table 3.2 shows the summary of Ru@Pt/XC-72 catalysts prepared by this ED method. As before, the theoretical coverages of Ru on Pt/XC-72 shown in the last column of Table 3.2 are based on the assumption that Pt is deposited in a monodisperse manner on the Ru surface with a deposition ratio of Pt : Ru = 1 : 1. All loadings of

secondary metal in Table 3.1 and Table 3.2 were determined from the change of concentration in the ED bath, and not from total digestion of metals from the finished catalyst. Based on the phase diagram study by Hutchinson [120], the bimetallic Pt-Ru compositions in this study (bulk Ru atomic percentages between 0 – 16% and 94.5 – 100%) should remain as core-shell structures, and not alloys, at all conditions discussed in this study.

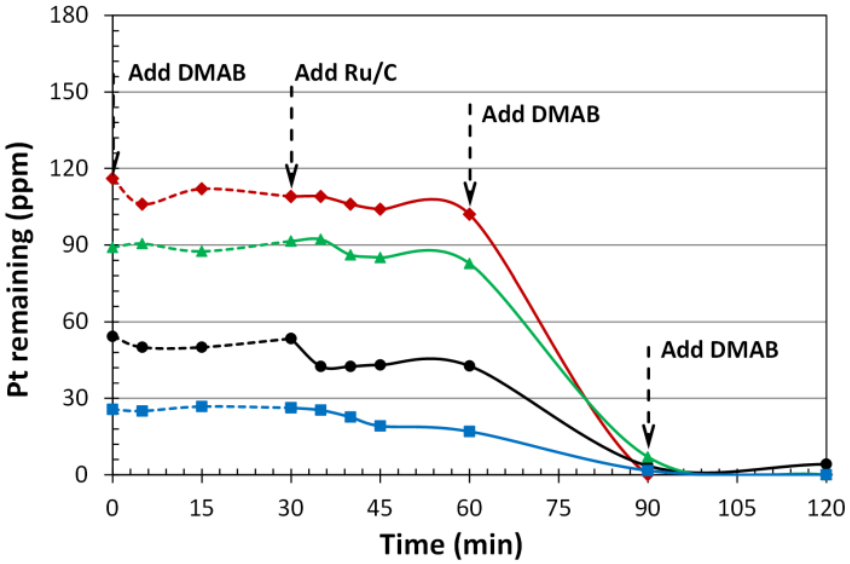

Figure 3.3 Pt deposition on Ru/XC-72 with different initial concentrations of $PtCl_6^{2-}$. Initial ratio of [DMAB]/[$PtCl_6^{2-}$] = 6/1. Similar amounts of DMAB added at 60 and 90 min to give total ratio of [DMAB]/[$PtCl_6^{2-}$] = 18/1 during the ED experiment.

Table 3.2 Summary of Ru@Pt/XC-72 catalysts prepared by ED. The compositions are expressed as the weight loadings of Pt deposited on the 20 wt% Ru/XC-72 base catalyst.

Catalysts	Ru wt loading (%)	Pt wt loading (%)	Theoretical monodisperse coverage θ_{Pt} on Ru	Bulk Ru/Pt atomic ratios
Ru@Pt 1	20	0.52	0.23	74.2 : 1
Ru@Pt 2	20	0.99	0.45	39.0 : 1
Ru@Pt 3	20	1.73	0.79	22.3 : 1
Ru@Pt 4	20	2.27	1.05	17.0 : 1

3.4.2 Catalyst Characterization

3.4.2.1 Chemisorption

The concentrations of Pt and Ru surface sites for the base Pt/XC-72 and Ru/XC-72 catalysts were determined by pulse chemisorption using hydrogen titration of oxygen pre-covered Pt/Ru sites. In general, if adsorbate interactions differ for two metals present on a bimetallic surface, the number of surface sites of each metal can be simply determined. For example, since group IB metals (Cu, Ag, and Au) do not dissociatively chemisorb H_2 at 40 ℃ while Pd or Pt does, H_2 chemisorption or H_2 titration of oxygen pre-covered Pt or Pd can be used to determine the surface coverage of group IB metals on Pt and Pd surfaces [8,27,37].

Previous work has shown that oxygen pre-covered Pt surfaces are readily titrated by pulses of 10% H_2/Ar at 40 ℃. However, titration of O-Ru sites requires higher temperatures [115,121,122]. The pulse chemisorption results in Figure 3.4 confirmed this; no measurable titration of O-covered Ru occurred at 40 ℃. The situation is much different for O pre-covered Pt; for the first five pulses, H_2 was completely consumed, and unreacted H_2 was observed beginning with 6^{th} pulse and continued until all Pt-O sites were titrated and Pt surface sites were saturated with adsorbed H.

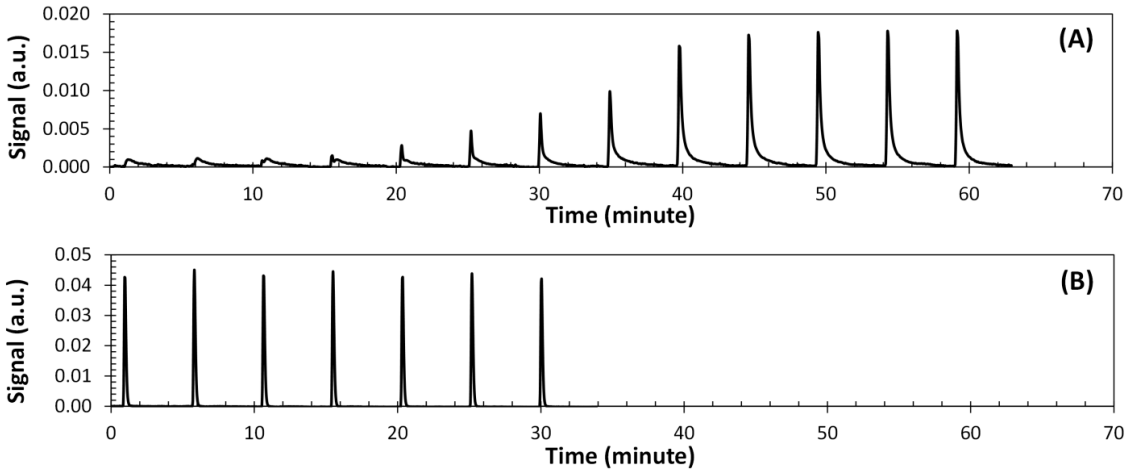

Figure 3.4 H_2 pulse titrations for O pre-covered (A) 20 wt% Pt/XC-72 and (B) 20 wt% Ru/XC-72 at 40 ℃.

To determine the temperature dependency for reduction of O pre-covered Ru, temperature programmed reduction at 10℃/min (in 10% H_2/balance N_2) over the temperature range 40 – 400 ℃ was conducted. The results are shown in Figure 3.5 and indicate that H_2 titration does not begin until temperatures greater than 150 ℃ is reached. For comparison the similar experiment for 20 wt% Pt/XC-72 is also shown and indicates that H_2 titration occurs rapidly at 40 ℃. To ensure complete and facile titration of O pre-covered Ru, H_2 titration at 250 ℃ was selected and the pulse chemisorption data are shown in Figure 3.6. Interestingly, even for the first ten pulses of H_2 only a constant-valued and partial consumption of H_2 occurred, indicating that the kinetics of Ru-O titration was a slow process even at 250 ℃. The contact time of the H_2 pulse over the Ru-O surface permitted only a limited amount of reaction of H_2 with Ru-O titration to occur. A blank chemisorption experiment for the XC-72 support at the same pretreatment conditions gave no H_2 uptake, indicating that all H_2 uptake values were due to the metallic components.

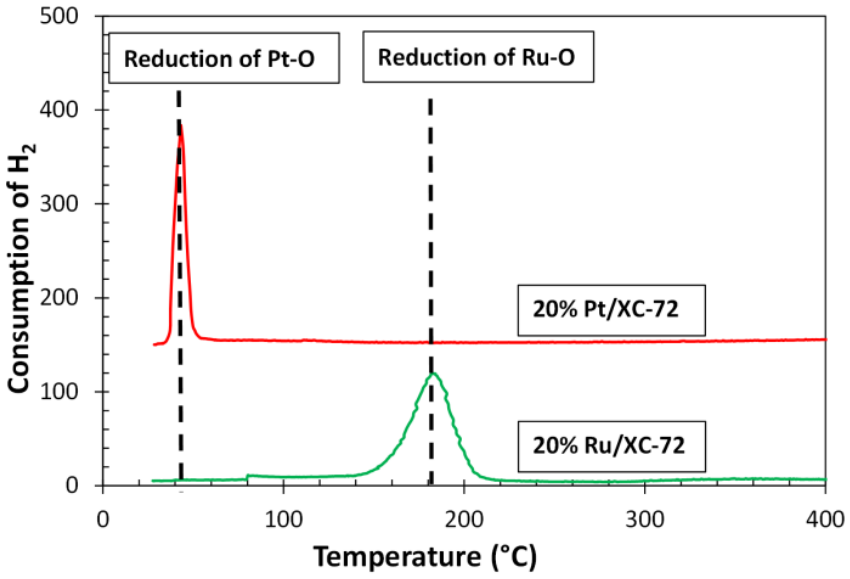

Figure 3.5 TPR of O pre-covered Ru/XC-72 and Pt/XC-72 samples. Temperature ramp rate was 10°C/min and sweep gas was N_2.

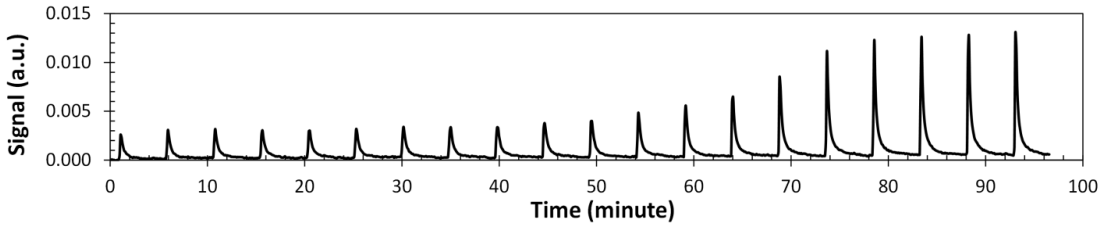

Figure 3.6 H_2 pulse spectrum for titration of O pre-covered Ru/XC-72 at 250 ℃.

From H_2 uptake values, the concentrations of Pt and Ru surface sites were calculated to be 1.33×10^{20}/g catalyst and 6.86×10^{19}/g catalyst, respectively, corresponding to 21.5% Pt dispersion and 5.8% Ru dispersion. For the bimetallic catalysts, if there are no chemisorptive interactions between adjacent Pt and Ru sites, H_2 titrations at 40 ℃ and 250 ℃ should separately determine the surface concentrations of Pt and Ru surface sites, respectively. However, H_2 titration experiments for bimetallic Pt@Ru/XC-72 and Ru@Pt/XC-72 catalysts at both 40 ℃ and 250 ℃ always gave H_2 uptake at 40 ℃ (Pt sites) higher than expected, in fact even higher than the total number

of Pt atoms deposited on the Ru surface for Ru@Pt/XC-72 catalysts. Conversely, H_2 uptakes at 250 ℃ (Ru sites) were always lower than expected.

3.4.2.2 Temperature Programmed Reduction

To better understand the H_2 titration results, temperature programmed reduction (TPR) of O pre-covered, bimetallic Ru-Pt catalysts were conducted from 40 – 400 ℃, and the results summarized in Figure 3.7(A) for ED of Ru on Pt surfaces and (B) for ED of Pt on Ru surfaces. The TPR curves for monometallic Ru/XC-72 and Pt/XC-72 catalysts are also shown as well as that for a physical mixture of each of the monometallic catalysts. The results show clearly that reduction of oxygen pre-covered Pt/XC-72 occurred sharply at the initial temperature of 40 ℃, and reduction of oxygen pre-covered Ru/XC-72 was highest at 180 ℃. The difference in reduction temperatures confirms that either the surface Ru-O bond is much stronger than the Pt-O bond or that dissociative adsorption of H_2 on Ru-O is a thermally-activated process. The TPR profile of a physical mixture of Ru/XC-72 and Pt/XC-72 shows both the Pt reduction and Ru reduction peaks, indicating no physical interaction between the Pt and Ru particles. TPR experiments for Pt@Ru/XC-72 bimetallic catalysts are also shown in Figure 3.7(A). For both 1.1% Ru-20% Pt/XC-72 (theoretical θ_{Ru} = 0.51) and 2.1% Ru-20% Pt/XC-72 (theoretical θ_{Ru} = 0.96), only the low temperature reduction peak indicative of Pt-O was observed; the Ru-O species was also titrated at 40 ℃, explaining why during chemisorption studies the quantity of H_2 consumed was larger than expected. It also indicates there is intimate interaction between the surface Ru and Pt sites, since the titration occurred rapidly at 40 ℃. For both Pt@Ru compositions, Ru is the minority component and there are accessible Pt atoms adjacent to surface Ru atoms. Thus, after

titration of the Pt-O site, H_2 can be readily dissociated on the Pt sites to facilitate reduction of adjacent Ru-O at the same temperature. Since there was no TPR peak at 180 ℃ the Ru atoms must have been rather evenly distributed on the Pt surface and not in aggregates of isolated Ru-O ensembles on the carbon support. These results also indicate that Ru-O species can be reduced at 40 ℃ if adsorbed H (from Pt) is present and that the temperature-demanding step for reduction of Ru-O is dissociative adsorption of H_2 on Ru.

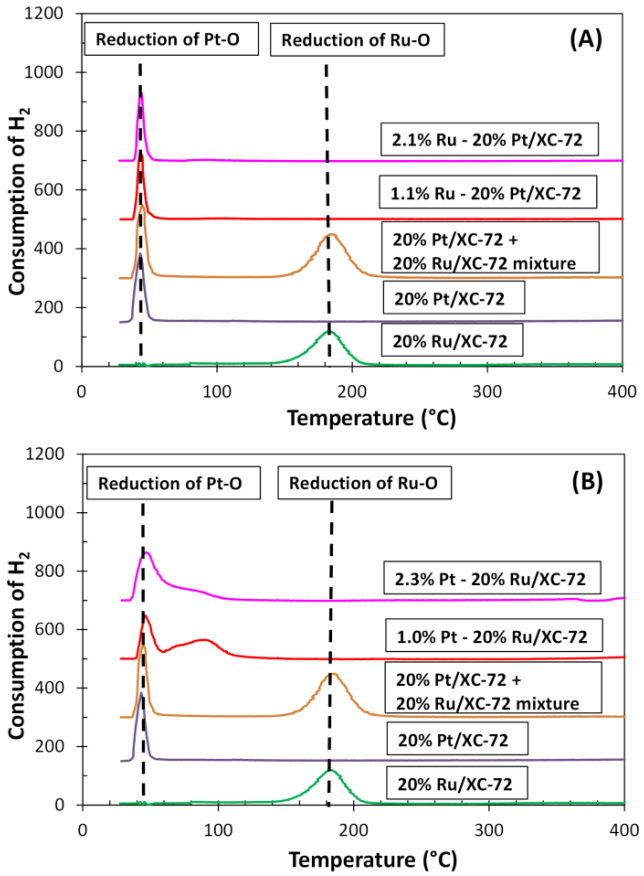

Figure 3.7 TPR of O pre-covered (A) Pt@Ru/XC-72 and (B) Ru@Pt/XC-72 samples. Temperature ramp rate was 10 ℃/min and sweep gas was N_2. TPR curves for 20% Ru/XC-72 and 20% Pt/XC-72 are shown again for reference.

TPR profile of Ru@Pt/XC-72 catalysts are shown in Figure 3.7(B). The first three TPR curves from the bottom are the same as for Figure 3.7(A). The TPR curve for 1.0% Pt-20% Ru/XC-72 (theoretical θ_{Pt} = 0.45) shows the reduction of Ru-O has been shifted

from 180 ℃ to a broad peak between 60 – 100 ℃. Similarly, for 2.3% Pt-20% Ru/XC-72 (theoretical θ_{Pt} = 1.05) the Ru-O reduction peak was shifted to even lower temperatures, existing both as a shoulder of the broader Pt-O reduction peak and as a component of the Pt-O peak at 40 ℃. The presence of Pt lowers the reduction temperature to less than 100 ℃ due again to Pt-assisted reduction of Ru-O. However, because Pt is now the minority component, there are insufficient Pt sites to assist in reduction of all Ru-O species at 40 ℃. In addition to insufficient Pt sites adjacent to Ru-O sites, the relatively slow kinetics of H spillover from Pt to Ru may be an additional reason for the reduction peak shoulder between 40 – 100 ℃. The broadness of the reduction peak between 40 – 100 ℃ also indicates that, once formed, Ru^o sites also participate in the reduction of adjacent Ru-O sites. Combining these two series of TPR experiments with chemisorption measurements, it confirms that the secondary metal (Ru or Pt) was deposited only on the primary metal (Pt or Ru) during ED process and that there are proximal, bimetallic interactions between the two metals.

3.4.2.3 X-ray photoelectron spectroscopy (XPS)

X-ray photoelectron spectroscopy (XPS) was used to determine possible electronic interactions between Ru and Pt to investigate the nature of the bimetallic interaction. The before reduction (BR) and after reduction (AR) data for Ru $3d_{5/2}$ and Pt $4f_{7/2}$ binding energies of 20 wt% Ru/XC-72 and 20 wt% Pt/XC-72 are shown in Figure 3.8. The BE positions and heights of all peaks have been referenced to the C 1s peak of the carbon support for all comparisons. The C 1s peak positions for all samples were constant at 284.2 eV which is very close to the standard binding energy (BE) of 284.5 eV for conductive carbon surfaces [123]. For the before reduction sample, the BE for Ru

$3d_{5/2}$ corresponds to Ru^{2+} and/or Ru^{4+} (280.70 eV), revealing the presence of RuO_x on the surface. After reduction at 280 ℃ the BE = 279.96 eV indicates complete reduction to Ru^0 (280.0 eV). The Pt $4f_{7/2}$ peak is at 70.96 eV for both before and after reduction at 280 ℃, indicating metallic Pt in both cases. Thus, the 20 wt% Pt/XC-72 base catalyst is completely reduced and stable as received from the vendor, while the surface of 20 wt% Ru/XC-72 catalyst was passivated as RuO_x when received from the vendor.

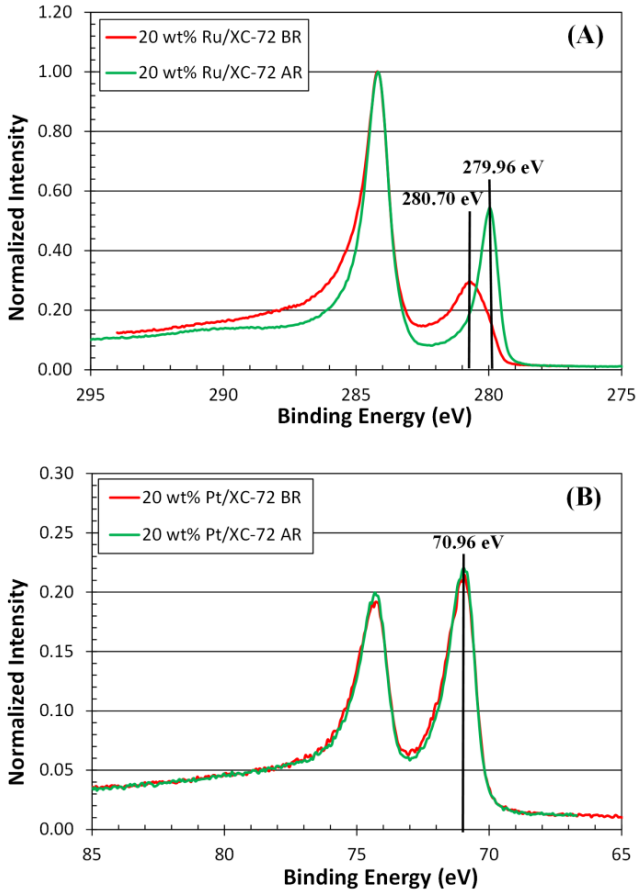

Figure 3.8 XPS of base catalysts before reduction (BR) and after reduction (AR) at 280 ℃ for (A) Ru $3d_{5/2}$ and (B) Pt $4f_{7/2}$. Carbon 1s BE at 284.2 eV also shown in (A).

The Ru $3d_{5/2}$ peaks of 0.51 ML Pt@Ru/C and 0.45 ML Ru@Pt/C for before and after reduction analyses are shown in Figure 3.9, along with analogous data for the monometallic catalysts. For the catalysts before reduction, the Ru $3d_{5/2}$ peaks are shifted

to lower BEs (280.70 eV → 280.32 eV) for both bimetallic catalysts, indicating e^- transfer from surface Pt to surface Ru atoms. After reduction the Ru $3d_{5/2}$ BE values are similar for both Ru only and Ru-Pt bimetallic catalysts, indicating the existence of only Ru^o. For quantitative comparison, the heights of the normalized Ru^o $3d_{5/2}$ peaks decrease in the order Ru/C > 0.45 ML Ru@Pt/C > 0.51 ML Pt@Ru/C, in agreement with the expected decrease of Ru surface/near surface concentrations. The substantial decrease in surface Ru for the 0.45 ML Ru@Pt/C (compared to Ru/C) also confirms that Pt atoms have been deposited only on the Ru surface, otherwise the decrease in Ru peak intensity would not have been as great.

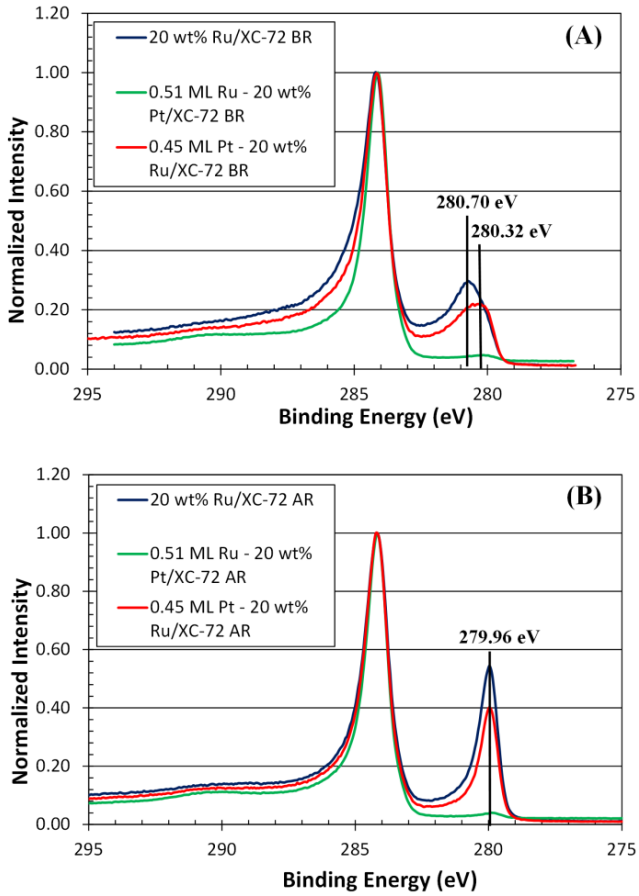

Figure 3.9 Ru $3d_{5/2}$ peaks of Ru/C, Pt@Ru/C and Ru@Pt/C (A) before and (B) after 280 ℃ reduction.

The Pt $4d_{7/2}$ peaks of Pt/C, 0.51 ML Pt@Ru/C and 0.45 ML Ru@Pt/C for before and after reduction analyses are shown in Figure 3.10 (A) and (B), respectively. For the before reduction sample of 0.45 ML Ru@Pt/C, the Pt $4d_{7/2}$ peak has shifted to higher binding energy (70.96 eV → 72.28 eV), indicating e- transfer from Pt to Ru atoms, corroborating the results of Figure 3.9, which showed e- transfer from Pt to Ru for the 0.51 ML Pt@Ru/C sample. In fact, the Pt $4d_{7/2}$ BE value of 72.28 eV is very near the published value of 72.40 eV for Pt^{2+} [$Pt(OH)_2$], indicating a high level of e^- transfer to the oxidized Ru sites [123]. Even after reduction at 280 ℃ a BE shift for Pt $4f_{7/2}$ to 71.33 eV is still present but not as dramatic. The heights of the normalized peaks are in same order as the decrease of surface Pt concentration. The XPS results are summarized in the Table 3.3 below.

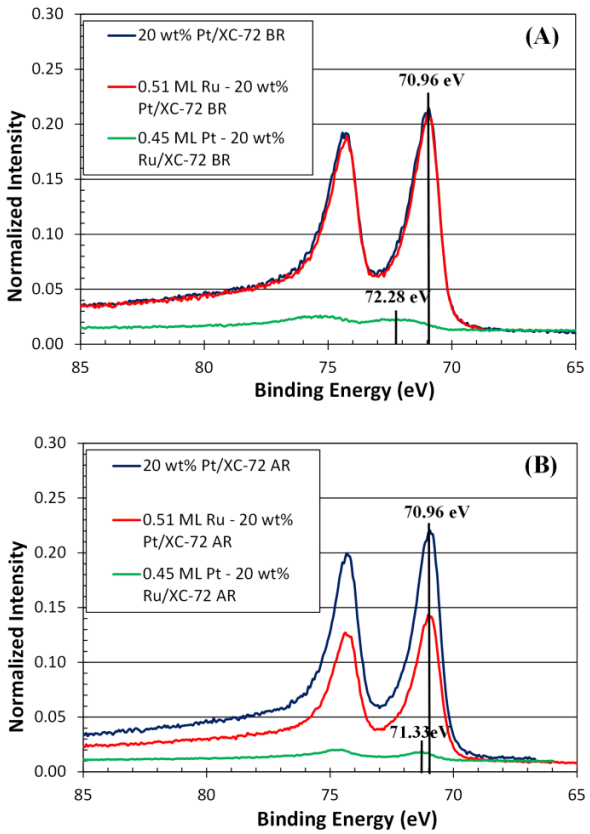

Figure 3.10 Pt $4f_{7/2}$ peaks for Pt/C, Pt@Ru/C and Ru@Pt/C (A) before and (B) after 280 ℃ reduction.

Table 3.3 Summary of binding energies for Ru $3d_{5/2}$ and Pt $4f_{7/2}$.

Sample	Ru $3d_{5/2}$ before reduction (eV)	Ru $3d_{5/2}$ after reduction (eV)	Pt $4f_{7/2}$ before reduction (eV)	Pt $4f_{7/2}$ after reduction (eV)
20 wt% Pt	N/A	N/A	70.96	70.96
20 wt% Ru	280.70	279.96	N/A	N/A
0.51 ML Ru-20 wt% Pt	280.04	279.87	70.92	70.96
0.45 ML Pt-20 wt% Ru	280.32	279.95	72.28	71.33

In conclusion, XPS analyses confirm that bimetallic interactions exist on the surface of the catalysts, which agree well with the results from chemisorption and TPR. Further, the directions of the binding energy shifts of both Ru $3d_{5/2}$ and Pt $4d_{7/2}$ peaks demonstrate e^- transfer from Pt to Ru on the bimetallic surface. The shift is more significant for the minority component in the bimetallic system due to the dilution effect of subsurface layers of the majority component.

3.4.2.4 Powder X-ray Diffraction (XRD)

Comparison of XRD patterns of the ED-prepared catalysts with the corresponding monometallic base catalysts are shown in Figure 3.11; the reference patterns of Ru^o and Pt^o are also shown. Other than intensity changes, which can be attributed to amount of sample used during analysis, there are no obvious differences of the patterns for the ED catalysts and their corresponding monometallic base catalysts. There is a slight sharpening of the peaks for both Pt and Ru peaks, which has been attributed to sintering under ED conditions. Schaal observed that sintering of the base metal occurred in some cases due to strong interactions between particular reducing agents and metals such as Pd or Pt [124]. It is also possible that the apparent increase in size may be due to epitaxial deposition of the secondary metal on the primary metal, since the atomic sizes of Ru and

Pt are identical and would not be distinguishable by XRD if lattice parameters of the shell component are the same as the core component.

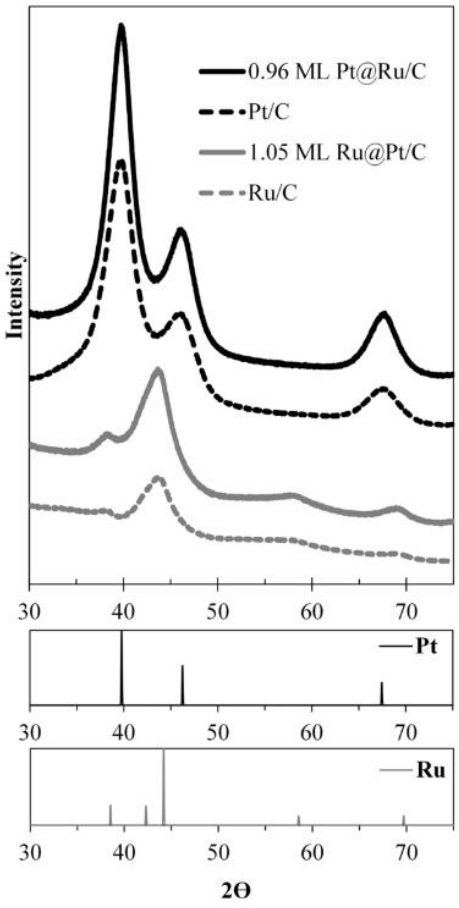

Figure 3.11 XRD patterns of Pt/C, Ru/C, Pt@Ru/C and Ru@Pt/C with standard patterns of Pt and Ru phases.

Using the Scherrer equation, the measured peak narrowing corresponds to ~ 3 Å increase in particle sizes for both primary metals. Even though there was deposition of the secondary metal from ED bath analysis, failure to observe their XRD peaks can be attributed to the formation of very thin overlayers of the secondary metal in spite of the ultra-low detection limit of the XRD system. In addition, the peaks observed in the patterns are not shifted relative to the standard positions of the primary metals, indicating that lattice parameters remain the same and there is no alloy formation. These results

provide evidence that (1), ED does not favor formation of separate particles of the secondary metal, but that the secondary metal deposits as an overlayer and (2), the deposited secondary metal overlayer is too thin to be detected by XRD, indicating that the secondary metal is highly dispersed on the primary metal.

3.4.2.5 Scanning Transmission Electron Microscopy (STEM)

Selected HAADF-STEM images of the base catalysts are shown in Figure 3.12. From these micrographs, the base catalyst particles have significant heterogeneity in size and morphology of the particles. There is considerable clustering of the particles particularly for the 20 wt% Pt/C catalyst. Irregularities in the size distribution and shape of these particles, however, are not considered influential in the electroless deposition process. Deposition of the secondary metal occurs only on the surface of the accessible primary metal particles which are measured by chemisorption.

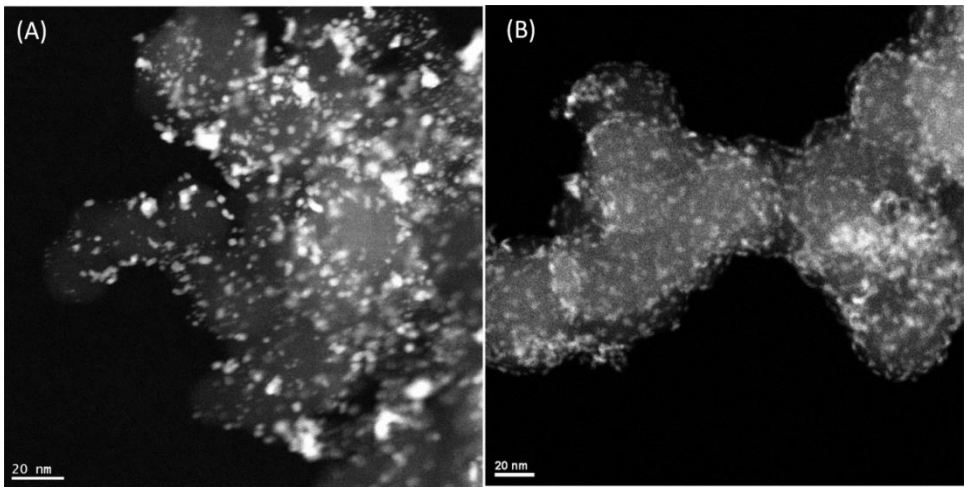

Figure 3.12 STEM-HAADF micrographs for (A) 20 wt% Pt/C and (B) 20 wt% Ru/C.

Representative micrographs of the 0.96 ML Pt@Ru/C and 1.05 ML Ru@Pt/C samples are shown in Figure 3.13 (A) and (E). In standard HAADF electron microscopy, also known as Z-contrast imaging, atoms of more massive elements that have higher Z

number produce greater electron scattering. The scattering of electrons are recorded as bright regions in the Z-contrast images. Thus, atoms of heavier elements such as platinum (Z=78) should be brighter than ruthenium (Z=44) in HAADF micrographs, while the carbon support and vacuum are the darkest regions. In the Z-contrast image of the 1.05 ML Ru@Pt/C catalyst (E) the Pt atoms can be made out as faintly brighter regions over a background of less bright Ru nanoparticles. For the 0.96 ML Pt@Ru/C (A) however, since Ru atoms are deposited over Pt, entire particles show up bright and thus regions where Ru is deposited cannot be made out without XEDS mapping of Ru deposition sites.

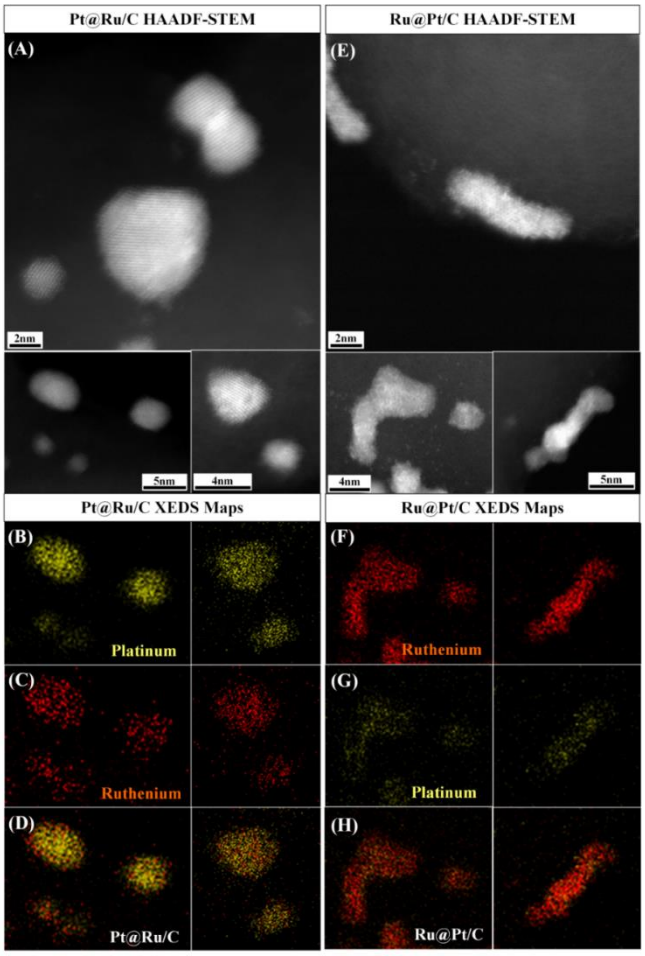

Figure 3.13 STEM-HAADF micrographs and XEDS maps of (A) – (D) for Pt@Ru/C and (E) - (H) for Ru@Pt/C.

The XEDS maps of representative spots of the ED catalysts, (B) - (D) for 0.96 ML Pt@Ru/C and (F) - (H) for and 1.05 ML Ru@Pt/C, show a more distinct evidence of targeted deposition of the secondary metal on the primary metal. There is correspondence in the location of primary metal, mapped in (B) and (F), to that of the secondary metal, shown in (C) and (G), respectively. This is observed in overlaid maps presented in (D) and (H) and was present in virtually all nanoparticles mapped by XEDS. For the 0.96 ML Pt@Ru/C, the Ru map overlaid on the Pt map (D) confirms that Ru is indeed present and deposited on the surface of the nanoparticles, which was not clearly observed in HAADF images. Furthermore, the Pt map for the 1.05 ML Ru@Pt/C catalyst (G) corresponds well with the brighter regions of the HAADF image of the same spot (E) which, as discussed earlier, are presumed to be deposited Pt based on Z-contrast. In the XEDS maps, points of Ru and Pt signal in locations not corresponding to nanoparticles can be attributed to background scattering of spurious x-rays and artifact signal contributions. From these STEM and XEDS images, it is visually established that individual nanoparticles of the catalysts prepared by ED are bimetallic, with excellent association between the primary and secondary metal.

In summary, TPR, XPS and STEM characterization data have shown that the Pt-Ru catalysts prepared by ED form true bimetallic surfaces with strong interactions between Pt and Ru. Figure 3.14 shows a model for the surface composition of Pt-Ru bimetals and the resulting mechanism of step-wise reduction that occurs during H_2 titration of the oxygen pre-covered Pt-Ru bimetallic system. After pretreatment in flowing O_2, both Pt-O and Ru-O are formed on the bimetallic surface. During dosing with H_2 at 40 ℃, the Pt-O surface undergoes reduction to form Pt-H (and H_2O) which can

then react with oxygen adsorbed on contiguous Ru-O sites. This Pt-assisted reduction of Ru-O is facile and also occurs at 40 ℃ to form Ru-H sites which then assist in reduction of additional and adjacent Ru-O species. For the case of Ru@Pt/C catalysts, where Ru is the majority component, O chemisorbed on Ru sites not close to Pt will undergo reduction more slowly and will appear as higher temperature reduction events in the temperature programmed mode of operation [Figure 3.7(B)] and during chemisorption. The continuous outward formation of Ru^{o} results in the sequential reduction of the bimetallic surface. For Pt@Ru/C catalysts, where Ru is the minority component, all O-precovered Ru surface sites are adjacent to surface Pt atoms. The Pt-assisted reduction of Ru-O then occurs completely at 40 ℃, as illustrated in Figure 3.14(B). This is also consistent with the TPR data that showed no isolated Ru reduction peak for Pt@Ru/C catalysts.

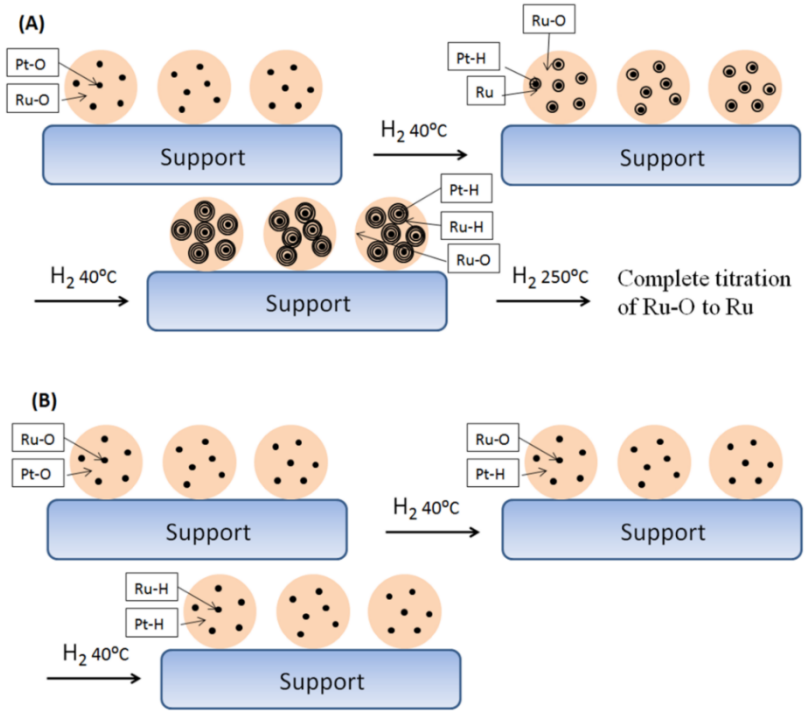

Figure 3.14 Proposed mechanism for H_2 titration of O pre-covered bimetallic surface of (A) Ru@Pt/C catalysts and (B) Pt@Ru/C catalysts.

3.5 Conclusion

Two series of Pt@Ru/C and Ru@Pt/C bimetallic catalysts have been prepared by electroless deposition (ED) method. For Pt@Ru/C preparation, a new ED bath was developed using $Ru(NH_3)_6Cl_3$ as Ru precursor and HCOOH as reducing agent. Temperature and pH effects were studied by varying temperatures from 70 ℃ to 130 ℃ and pH from 2 to 4. A deposition temperature of 110 ℃ (to minimize effects of CO poisoning on Pt surface during deposition) and pH 3 (to avoid strong electrostatic adsorption) were chosen to synthesize Pt@Ru/C catalysts with variable and controlled Ru weight loadings. For Ru@Pt/C preparation, a standard bath using H_2PtCl_6 and DMAB as Pt precursor and reducing agent, respectively, was employed. Several Ru@Pt/C catalysts with different Pt weight loadings were synthesized by controlling initial Pt concentrations in the ED bath at the preferred conditions of 70 ℃ and pH 10.

The Pt@Ru/C and Ru@Pt/C bimetallic catalysts have been characterized by temperature programmed reduction (TPR), selective chemisorption, X-ray photoelectron spectroscopy (XPS), X-ray powder diffraction (XRD) and scanning transmission electron microscopy (STEM). TPR data showed that for Ru@Pt/C catalysts, where Ru was the major component, the peak for the reduction of oxygen pre-covered Ru shifted from 180 ℃ (for monometallic 20 wt% Ru/C) to temperatures between 60 ℃ and 100 ℃. However, for Pt@Ru/C catalysts, where Ru was the minor component, TPR profile resembled that for monometallic 20 wt% Pt/C; both oxygen-covered Pt and Ru surface sites underwent reduction at 40 ℃. Selective chemisorption (H_2 titration of oxygen pre-covered surfaces) experiments also confirmed the existence of strong surface interactions between Pt and Ru, which are explained as hydrogen spillover (Pt-assisted reduction of

oxygen pre-covered Ru). XPS analyses showed that binding energies (BE) shifted to lower values for the Ru $3d_{5/2}$ peak, and to higher values for the Pt $4d_{7/2}$ peak. The directions of the binding energy shifts indicate e^- transfer from Pt to Ru on the bimetallic surface, again indicating strong surface interactions between Pt and Ru. There were no obvious differences between the XRD patterns for the ED catalysts and their corresponding base catalysts, revealing that deposition of the second metal by ED bath formed only thin overlayers of the secondary metal, and not three-dimensional aggregates. In addition, the peaks observed in the XRD patterns were not shifted relative to the standard positions of the primary metals; the similar lattice parameters remain the same, suggesting no alloy formation. Finally, The STEM and XEDS images provided strong, visual evidence of targeted deposition of the secondary metal on the primary metal. The XEDS images confirmed that individual nanoparticles of the catalysts prepared by ED were bimetallic, with excellent association between the primary and the secondary metals. No monometallic Pt or Ru particles were detected for either of the families of bimetallic particles.

CHAPTER 4:

AN INVESTIGATION ON THE ROLE OF RE AS A PROMOTER IN AG-CS-RE-AL_2O_3 HIGH-SELECTIVITY ETHYLENE EPOXIDATION CATALYSTS

Reprinted with permission from [W. Diao, C. D. DiGiulio, M. T. Schaal, S. Ma, J. R. Monnier, J. Catal. 322 (2014) 14-23].

DOI: 10.1016/j.jcat.2014.11.007

4.1 Abstract

A series of Cs-Ag, Re-Ag, Cs-Re-Ag and Cs-Re-Mo-Ag (supported on α-Al_2O_3) catalysts has been prepared and evaluated for ethylene epoxidation to determine the mechanism of selectivity enhancement for high selectivity ethylene oxide (EO) catalysts which contain high-valent Re oxyanions and other co-promoters, such as MoO_4^{2-}. Optimal amounts of Re (as NH_4ReO_4) and Mo [as $(NH_4)_2MoO_4$] on Cs-promoted, Ag/α-Al_2O_3 increase EO selectivity from approximately 79% to 83%. Analyses by XPS and SEM suggest the origin of both Re and Cs promotion are electronic. SEM shows that neither Re nor Mo changes the morphology or particle sizes of the Ag particles. XPS analyses show that Re shifts Ag 3d BE to higher values which enhances electrophilic attack by oxygen adsorbed on Ag (Ag-O) at the electron-rich C=C bond of C_2H_4. In the subsequent step, Cs lowers the Ag 3d BE to facilitate desorption of the EO precursor to form gas phase EO. That is, Re and Cs promote different steps of the mechanism of EO formation. A reaction scheme detailing the mechanism of EO formation over Re-modified, Cs-promoted Ag catalysts is presented.

4.2 Introduction

As we discussed in section 1.5, Ag, Cs, Re and Re co-promoters are the major components for current generation of EO catalysts. The first patent describing Re-containing EO catalysts was disclosed in 1984. However, there are only a very limited number of published journal articles that discuss the role of Re in EO catalysts, remarkable considering the economic importance of this industrial reaction. It is very important to study the mechanism of promoters that increase EO selectivity, which may

help with the design of next generation EO catalysts hiving even higher selectivities. Further, knowledge gained with ethylene epoxidation may lead to the formation of catalysts for the direct epoxidation (using O_2) of propylene to propylene oxide, which has been likened by some as one of the holy grails of catalysis [125].

In this study, the role of Re as a promoter and the role of Mo as a co-promoter will be addressed through analysis of rate data collected in experiments conducted under industrially relevant conditions and after steady-state operation was achieved (> 50 h on-line). The reaction conditions investigated are similar to those used commercially and the activity and selectivity values agree quite well with examples available in the patent literature [85]. Among the analysis and characterization tools utilized in this work, X-ray photoelectron spectroscopy (XPS) was particularly instructive in characterizing the oxidation states of Ag, Cs, Re and Mo. A site model is proposed to postulate how the Cs-Re-Ag system functions under reaction conditions and how the presence of Mo affects this working model as it relates to the importance of electrophilic oxygen adsorbed on the Ag surface during reaction.

4.3 Experimental

4.3.1 Catalyst Preparation

The different series of Ag-based catalysts used in this investigation were prepared using silver oxalate ($Ag_2C_2O_4$), as described in the patent literature [84-86]. The $Ag_2C_2O_4$ was slowly dissolved into an aqueous solution containing a 3:1 molar ratio of ethylenediamine (EN) to $Ag_2C_2O_4$. The target Ag loadings were maintained at 12 wt % on the α-Al_2O_3 catalyst carrier. The impregnation volume was calculated using the pore

volume of the carrier plus 5% excess. The α-Al_2O_3 catalyst carrier (SA5562, 8 mm rings, BET surface area = 0.60 m^2g^{-1} using Kr adsorption, and pore volume = 0.53 cm^3g^{-1}) was obtained from Norpro-St. Gobain. The silver and promoter salts were added to the support in a single step by addition of small aliquots of stock solutions of $CsNO_3$, NH_4ReO_4 and, optionally, $(NH_4)_2MoO_4$ to the $Ag_2C_2O_4$-containing impregnation solution. Twenty grams of α-Al_2O_3 rings and the appropriate amount of the $Ag_2C_2O_4$-impregnation solution were added to a 100 mL fluted flask and tumbled under vacuum at 60 ℃ until the rings tumbled freely. After impregnation, the rings were calcined using forced air flow (100 L/min) at 260 ℃ for a total of 5 – 7 min. The nominal weight loadings of Ag, Cs, and Re for selected samples were confirmed using Atomic Absorption Spectroscopy (AAS) performed using a Perkin Elmer AAnalyst 400 spectrometer or by ICP analysis for Re (Perkin-Elmer Optima 2100 DV). In all cases, the analyzed weight loadings were quite close (± 6%) to the nominal weight loadings, indicating that catalyst performance can be described in terms of nominal promoter loadings. Table 4.1 provides an example of nominal vs. analyzed Ag and Cs loadings for two of the reference Ag-Cs/α-Al_2O_3 catalysts used in this investigation.

Table 4.1. Nominal vs. analyzed Ag and Cs loadings for two representative catalysts.

Catalyst	Ag loading (nom.) (%)	Ag loading (anal.) (%)	Cs loading (nom.) (ppm)	Cs loading (anal.) (ppm)
Ag-Cs/α-Al_2O_3	12.0	11.8	350	330
Ag-Cs/α-Al_2O_3	12.0	12.1	350	329

4.3.2 Catalyst Characterization

Scanning electron microscopy (SEM) micrographs were collected using a Zeiss Ultraplus Thermal Field Emission Scanning Electron Microscope. Electrons were

collected using a high efficiency scintillator detector with an optically-coupled photomultiplier. The incident electron beam energy was set to 6.0 keV. Micrographs were recorded at 30,000x and 50,000x magnification. Prior to analysis, the extruded rings were cut in half and only the interior portions of the samples were scanned.

The Ag dispersion and average particle size of the unpromoted Ag catalyst were measured using a Micromeritics Autochem II 2920 automated chemisorption analyzer. Prior to O_2 chemisorption, 0.5 g of catalyst was reduced in flowing 10% H_2/balance Ar at 200 ℃ for 1 h, then exposed to 100% Ar at 200 ℃ for 1 h to remove any residual H_2. The catalyst was then cooled to 170 ℃, and using the method described by Vannice et al. [126], the sample was exposed to pulses of 10% O_2/balance He. The O_2/He mixture was pulsed in 4 min intervals until no further uptake of O_2 was observed, as indicated by equal peak areas measured by the downstream thermal conductivity detector. The oxygen uptake was then quantitatively determined by integrating the early adsorption curves and comparing the area to the latter curves, after O_2 uptake was complete. The O_2 adsorption stoichiometry was assumed to be ½ O_2/Ag = 1 (as used by Vannice) to give a Ag dispersion of 0.95%, corresponding to an average Ag diameter of 0.12 μm. Titration with O_2 for samples containing Cs, Re and Mo was not performed because Cs [90], Re [127] and Mo [128] might interact with O_2, which would skew the results and make accurate calculations of the average Ag particle sizes unreliable.

XPS measurements were performed using a Kratos AXIS Ultra DLD XPS system equipped with a hemispherical energy analyzer and a monochromatic Al Kα source. The monochromatic Al Kα source was operated at 15 keV and 150 W; pass energy was fixed at 40 eV for the detailed scans. All samples were prepared as pressed powders supported

on a gold-plated stainless steel stub for the XPS measurements. A catalyst pretreatment cell attached to the UHV system permitted samples to be pretreated in H_2-containing and O_2-containing gas streams (12 h at each condition) at elevated temperatures, typically at 250 ℃ for H_2 pretreatment and 260 – 280 ℃ for oxidation by O_2, before being analyzed by XPS. Peak fitting was conducted using XPSPEAK 4.0 for the sum of Gaussian and Lorentzian functions as the model. A charge neutralizer was used to compensate for the surface charge. Ca $2p_{3/2}$ was taken as the binding energy reference defined at 346.6 eV for peak corrections. Ca 3s is also located in the Re 4f region, which complicated the peak fitting for Re 4f. The pre-rhenium modified sample was analyzed with XPS for extracting the association constants between Ca 2p and Ca 3s in terms of the peak separation and intensity ratio. These constants were used later to define the Ca 3s peak based on Ca 2p in the peak fitting of Re 4f.

4.3.3 Catalyst Evaluation

Catalysts were evaluated in a tubular, 316 stainless steel reactor of 0.19 in. ID, 0.25 in. OD. The reactor was tightly encased (press-fitted) in a 1 in. OD aluminum jacket to ensure isothermal operation. Gas flows were regulated using Brooks 5850E mass flow controllers and gas feed composition was 8% O_2, 25% C_2H_4, 1-3 ppm ethyl chloride (EtCl) moderator, balance CH_4 at 250 psig and a gas hourly space velocity (GHSV) of 4500 hr^{-1}. Methane, rather than N_2 was used as the inert diluent, since the specific heat capacity of CH_4 is more than twice as high as that of N_2, helping to ensure a more isothermal catalyst bed during ethylene epoxidation. Feed compositions and flow rates were kept constant unless otherwise stated and were chosen to be similar to those reported in the patent literature [84-86]. Prior to evaluation, the catalyst rings were

broken and sieved to 20/40 mesh (850 – 425 μm) and 2.0 g were loaded into the reactor. Two thermocouples were initially used to monitor temperature, one in the 1 in. OD aluminum shell and the other immersed in the catalyst bed. After confirmation of good agreement between the two thermocouples, the shell temperature was assumed to be the reaction temperature. After exiting the catalyst bed, the pressure was let down to 1 atm by a Veriflo back pressure regulator and the gas flow was directed into Valco switching valves containing a sample loop that diverted gas sample loop contents to either a thermal conductivity or flame ionization detector. Analysis was performed using an on-line, Agilent 7890A gas chromatograph with two Poraplot Q columns for quantitative analysis of CO_2, H_2O, EO, and acetaldehyde and ethylene glycol, if present. Typically, only CO_2, H_2O, and EO were observed as products, so only the high sensitivity thermal conductivity detector was used. After GC analysis, the following equations were used to calculate the EO concentration in the product stream and the selectivity to EO as a function of catalyst time on line. Since the capacity of the sample loop was expressed in nanomoles, all product amounts were expressed in the same units.

$$\%\ EO\ in\ product\ stream = \frac{nmol\ EO}{nmol\ sample\ loop} \times 100 \qquad \text{Eq. 4.1}$$

$$EO\ Sel.(\%) = \frac{nmol\ EO}{nmol\ EO + \frac{1}{2} nmol\ CO_2} \times 100 \qquad \text{Eq. 4.2}$$

EO selectivity is typically reported at constant EO concentrations; unless otherwise stated, the value of 2.0 mole % EO was used in this study. EO concentrations were manipulated by adjusting reactor shell temperatures after pseudo steady state

behavior was reached. When Re was present, the catalysts were pretreated *in situ* for 12-18 h in a 20% O_2/balance CH_4 flow stream at 260 ℃ before being brought online, as described in a recent patent by Lockmeyer [107]. A similar pretreatment for non-Re containing catalysts evaluated in this study had no effect on catalyst activity or selectivity. Thus, in all other cases catalysts were brought online without a pretreatment in the reaction gas mixture. The catalysts were usually run for 24-48 h before initial shell temperature adjustments were made.

4.4 Results and Discussion

4.4.1 Catalyst Evaluation Protocol

The results shown in Figure 4.1 demonstrate the standard protocol for evaluation of an EO catalyst; in this case, a representative example of a run performed using Ag-Cs-Re/α-Al_2O_3 catalysts is provided. The catalyst composition is designated as 12% Ag, 350 ppm Cs, 100 ppm Re/α-Al_2O_3, where the promoter amounts correspond to the amounts of Cs and Re metal ions in ppm/g catalyst. This designation is used throughout this paper. The bottom pane in Figure 4.1 indicates that the start-up temperature for this catalyst was 210 ℃. The temperature was held constant for the first 35 h, while both activity and selectivity were transient. After 35 h, the shell temperature was adjusted to 216 ℃ to achieve 2 mole % EO in the product stream. The temperature was then held at 216 ℃ for 16 h to allow performance to stabilize again before two smaller temperature adjustments were made to maintain EO concentration at 2.0 mole %. The catalyst was then evaluated for approximately 70 h to obtain pseudo steady-state performance and to ensure that the catalyst formulation was stable at these conditions before the run was terminated. Values

for C_2H_4 and O_2 conversions, EO and CO_2 concentrations, and EO selectivity were typically recorded for each catalyst. Since CO_2 was not co-fed during reaction, calibration of the CO_2, ethylene, and EO response factors were determined and used to record carbon mass balances for the different catalysts at all reaction conditions. Acetaldehyde and ethylene glycol were not observed at normal reaction conditions. In all cases, the carbon mass balance closure was at least ±3% and routinely better than ± 2%. In summary, the reactor performance data included in subsequent sections was collected using the same protocol and the selectivity to EO (and any other relevant performance data) was reported after pseudo steady-state operation had been achieved.

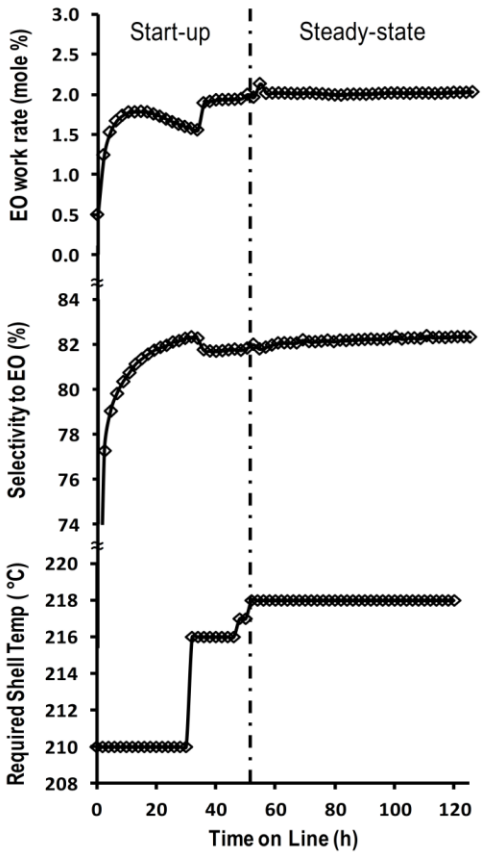

Figure 4.1 An example of a typical run for evaluation of EO catalysts (Conditions: 25% ethylene, 8% O_2, 2 ppm EtCl, bal. CH_4; Catalyst: 12% Ag, 350 ppm Cs, 100 ppm Re/α-Al_2O_3).

4.4.2 Optimization of Cs, Re and Mo

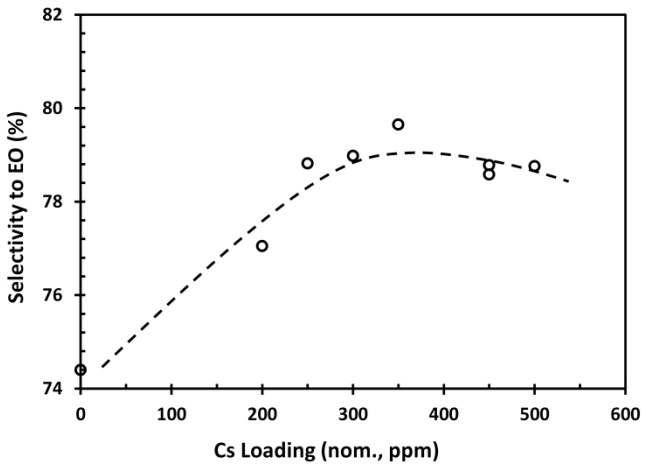

Figure 4.2 The effect of Cs addition on EO selectivity for 12 wt % Ag/α-Al_2O_3 EO catalyst (Conditions: 25% ethylene, 8% O_2, 2 ppm EtCl, bal. CH_4, where unless otherwise denoted the conditions for the remaining Figures. were collected under identical conditions).

The results shown in Figure 4.2 show the selectivities to EO as a function of Cs loading are in very good agreement with those reported by Lauritzen [85]. The optimal Cs loading ranged from approximately 300 to 450 ppm of Cs. Since higher Cs loadings (e.g. >450 ppm) generally decreased activity, 350 ppm of Cs was selected as the optimum level of Cs promotion for 12 wt % Ag/α-Al_2O_3 catalyst. For other catalysts containing variable amounts of Re and/or Mo, the Cs loading was held constant at 350 ppm, since the Cs loading exhibited a broad maximum in this region. Thus, the assumption was made that changes in optimal Cs loadings when other promoters were added should not significantly affect catalyst performance. The results in Figure 4.3 show the effects of Re promotion on activity and EO selectivity for a series of Re-promoted Ag-Cs catalysts. In Figure 4.3(a) and (c), the Ag, Cs and Re salts were impregnated in a single step onto the α-Al_2O_3 support, while in Figure 4.3(b) and (d), the NH_4ReO_4 promoter was added to the support and then calcined at 450 ℃ for four hours prior to the subsequent addition of both

Ag and Cs salts. The purpose was to determine whether Re promoted EO formation by interaction with the Al_2O_3 support (i.e., lower the rate of sequential combustion of EO on acid sites of the support or by acting as a transition layer between the Al_2O_3 and Ag particles) or whether Re needed to be in intimate contact with the Ag surface to form more selective surface sites. Comparison of the data in Figure 4.3 for the samples with different Re salt impregnation methods indicates little difference in catalytic activity or selectivity to EO. This is perhaps not surprising, however, if after calcination at 450 ℃, NH_4ReO_4 on Al_2O_3 is converted to Re_2O_7 as expected [129], which is highly soluble in H_2O and should dissolve from the Al_2O_3 support during the subsequent, aqueous impregnation of Ag and Cs salts. The similar performance of the two series of catalysts, despite changes in the impregnation methodology, supports the case for Re re-dissolution and redistribution during the subsequent Ag and Cs salts impregnation step. If ReO_2, Re_2O_5, or ReO_3, which are all insoluble in H_2O, were formed during calcination at 450 ℃, we should expect differences in catalyst performance for the different impregnation methods. To specifically address re-dissolution of Re from the support, a Re-modified support was washed in DI H_2O and ICP analysis of the filtrate confirmed that the majority of Re deposited during the support modification step was easily washed from the support at 25 ℃. Subsequent XPS analysis (discussed later in Figure 4.9) confirmed that Re existed as Re^{7+} (i.e., Re_2O_7) after extended pretreatment in O_2 at 260-280 ℃, which is consistent with the re-dissolution observations. Thus, similar trends should be expected for the two series of catalysts in Figure 4.3, which suggest that Re is distributed on both the Ag and Al_2O_3 components of the catalyst surface. The results in Figure 4.3 that show similar selectivities to EO for Re added before or during Ag and Cs

impregnation are in very good agreement with those reported by Lauritzen [85]. Previous reports in the patent literature have stated that NH_4ReO_4 could be added before, during or after Ag was added with the same results in EO selectivity, suggesting random distribution of Re on both Al_2O_3 and Ag surfaces [85,106,130].

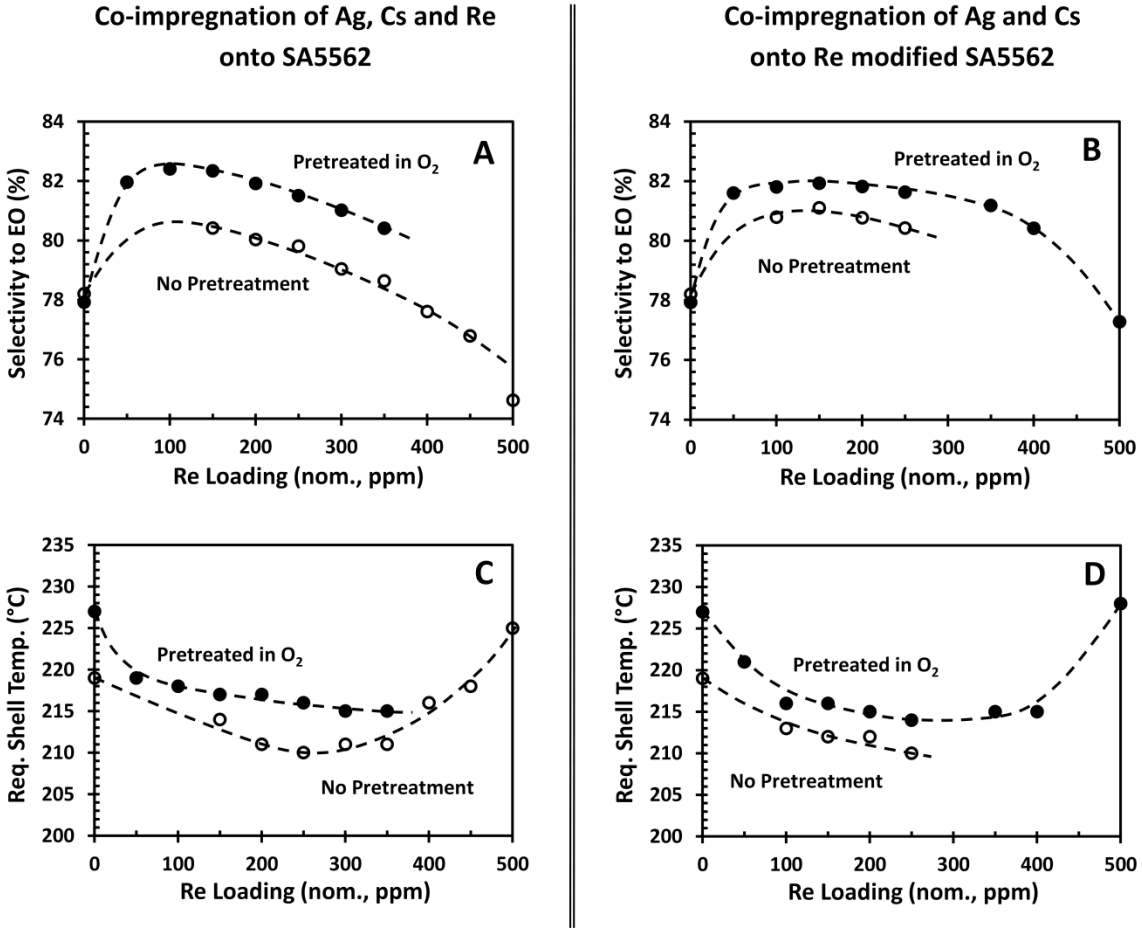

Figure 4.3 The effects of Re promotion, support modification and catalyst pretreatment on EO selectivity and activity for a series of Re-promoted 12 wt % Ag, 350 ppm Cs/α-Al_2O_3 catalysts, where (A and C) were prepared using co-impregnation of Ag, Cs and Re and (B and D) were prepared using co-impregnation of Ag and Cs on to a Re modified support. As denoted, some catalysts were subjected to a pretreatment step containing 20% O_2/CH_4 at 260 ℃ for 12 h prior to start-up.

In addition to changes in the sequence of Re salt addition, the effect of a 12-18 h *in situ* pretreatment step in 20% O_2/balance inert (CH_4 in this study) at 260 – 280 ℃ was

also investigated and the data are also shown in Figure 4.3. Selectivities for Re-modified catalysts were approximately 2 - 3 percentage points higher following the *in situ* calcination treatments, due to either better redistribution of Re on the Ag surface or oxidation of Re species to the +7 state. The surface free energies of both Re_2O_7 and MoO_3, 32 – 40 ergs/cm^2 and 50 – 70 ergs/cm^2, respectively, are much lower than the values for Al_2O_3 (650 – 830 ergs/cm^2) and Ag^o (1200 – 1300 ergs/cm^2), all at 200 – 300 ℃. This means that diffusion of oxidized Re and Mo from Al_2O_3 to Ag is thermodynamically favored to lower the overall surface free energy of the Re-Ag-Al_2O_3 system [131,132]. The higher EO selectivities were accompanied by slightly lower activities, which required higher temperatures to achieve 2% EO product levels. Recent work of Okal [133] has shown that high temperature calcination of 1.0 wt % Re/γ-Al_2O_3 increased the extent of oxidation of the supported Re species resulting in enhanced surface migration of Re^{7+} species to redistribute Re on the γ-Al_2O_3 surface. Previous work of Lockemeyer et al. [107] demonstrated significant increases in selectivity to EO for a similar calcination in air pretreatment conducted using a series of optimally-promoted Ag catalysts containing approximately 370 ppm Re (as well as other promoters); after the pretreatment step, the selectivity to EO improved from 82.0% at a work rate of 1.5 mole % EO at 224 ℃ to 88.6% for the same work rate at 242 ℃. The increase in EO selectivity, even at the higher temperatures required to achieve 1.5 mole% EO, suggests the *in situ* calcination re-distributed the Re on the Ag surface, lowering the total number of active Ag sites, but forming more selective sites. This is consistent with our results in Figure 4.3.

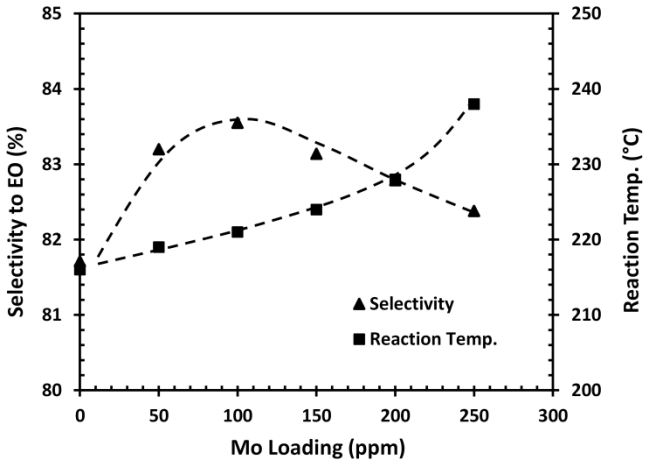

Figure 4.4 Determination of the optimum Mo co-promoter loading required for a 12 wt % Ag, 350 ppm Cs, 200 ppm Re/α-Al_2O_3 catalyst.

Lauritzen [85] also indicated that EO selectivities increased further if other high-valent oxyanion promoters were used along with NH_4ReO_4. These included the ammonium salts of MoO_4^{2-}, WO_4^{2-}, and SO_4^{2-}; addition of 32 ppm S (as SO_4^{2-}) to a catalyst already containing 186 ppm Re and optimal Cs increased EO selectivity from 81.9 to 83.1% selectivity. Likewise, addition of 96 ppm Mo (as MoO_4^{2-}) to a similar Re, Cs promoted catalyst raised selectivity to 83.5%. Lauritzen referred to the additional high valent oxyanions as Re co-promoters. If Re was removed and only the co-promoters were added, there was no significant increase in selectivity. Thus, Re was required for the selectivity enhancements. The results in Figure 4.4 show the effects of addition of varying amounts of $(NH_4)_2MoO_4$ to catalysts also containing 200 ppm Re and 350 ppm Cs. The results show a broad maximum in EO selectivity between 50 – 150 ppm Mo; at 100 ppm Mo the selectivity is 1.9 percentage points higher than the Re-promoted sample containing no Mo co-promoter. The temperatures needed to achieve 2% EO also increase with higher Mo loadings, suggesting the effective Mo is deposited on the Ag surface and that the number of active sites decreases with Mo loading. This is expected, but different

from the Re results (50 – 350 ppm Re) in Figure 4.3(c) and (d), where the temperatures needed to attain 2% EO actually decrease as EO selectivity increases. In the case of Re, promotion actually increases the activity of the Ag sites, even though Re is apparently deposited on the Ag surface. Finally, the cumulative effects of Cs, Re, and Mo are shown in Figure 4.5 and Table 4.2 and indicate that the addition of Re promoter and Mo co-promoter increases the selectivity to EO by more than three percentage points relative to only Cs as a promoter. Catalyst activity is expressed in work rate, the term commonly used to describe activity for EO formation, which is simply the molar concentration of EO in the reactor effluent.

Table 4.2 Comparison of catalyst activity and selectivity for Cs, Re and/or Mo promoted EO catalysts. (Conditions: 25% C_2H_4, 8% O_2, 2 ppm ethyl chloride, GHSV: 4500 hr^{-1}).

Catalyst Composition	**C_2H_4 Conversion** (%)	**EO work Rate** (mole %)	**EO Selectivity** (%)	**Temp.** (℃)
12% Ag	10.5	1.94	74.5	224
12% Ag, 350 ppm Cs	10.3	2.00	79.7	224
12% Ag, 350 ppm Cs, 200 ppm Re	10.1	2.04	81.7	214
12% Ag, 350 ppm Cs, 200 ppm Re, 150 ppm Mo	9.8	2.02	83.1	224

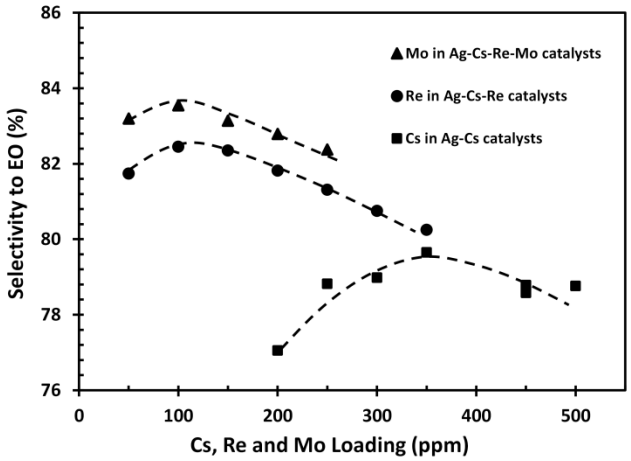

Figure 4.5 Summary detailing the effects of Cs, Cs-Re and Cs-Re-Mo promotion on a 12 wt % Ag/ α-Al_2O_3 catalyst.

The results in Figure 4.5 even suggest that Cs may not be necessary as a promoter since Re and Mo appear to be responsible for the large enhancement in EO selectivity. The results shown in Table 4.3 compare the relevant performance characteristics for a series of Ag catalysts containing: (1), no promoters, (2), an optimum amount of Cs, but no Re, (3), an optimum amount of Re, but no Cs and (4), an optimum amount of Cs and Re promoters, where the optimum Cs and Re loadings were determined using the results shown in Figures 4.4 and 4.5. The results for the Cs-promoted and Cs-Re promoted catalysts exhibit strong promoter effects relative to the unpromoted Ag catalyst. However, the Re-only promoted catalyst is markedly different. In order to obtain ~ 2.0% EO the required reactor temperature was 262 ℃, while the selectivity to EO under these conditions was only 49.9% at more than 60% O_2 conversion. Because EO selectivities normally decrease with higher temperatures, performance of the Re-Ag/Al_2O_3 catalyst is also shown at ~ 40% O_2 conversion (entry 3' in Table 4.3) as done by others [84-86] and at 225 °C (entry 3'' in Table 4.3), which is much closer to the evaluation temperatures for the other catalysts in Table 4.3. The results for 41.5% O_2 conversion at 250 ℃ still gave only 60.7% EO selectivity, which is also in good agreement with results of Lauritzen [85] who observed that EO selectivity was 54.3% for a catalyst promoted only with Re, while a similar catalyst promoted with both Cs and Re was 79.8% selective to EO; both comparisons were made at 40% O_2 conversion. At 225 ℃, the catalyst was essentially inactive with only 0.35% EO being formed, making any comparisons irrelevant. Thus, it appears that one of the roles of Cs is to offset the Re effects; that is, Re is necessary but not sufficient for high selectivity and high activity to EO. This is a possible scenario if Re

and Cs promote distinctly different steps of the epoxidation reaction. This will be discussed at a later point.

Table 4.3 Effects of Cs and/or Re on catalyst activity and selectivity.

Catalyst Composition	**EO conc** (mole %)	**EO Select** (%)	**Temp** (℃)	**C_2H_4 conv** (%)	**O_2 conv** (%)
(1) 12% Ag	1.94	74.5	224	10.4	28.7
(2) 12% Ag, 350 ppm Cs	2.00	79.7	224	10.3	26.7
(3) 12% Ag, 100 ppm Re	1.93	49.9	262	15.9	60.5
(4) 12% Ag, 350 ppm Cs, 100 ppm Re	2.03	82.4	218	9.8	23.5
(3') 12% Ag, 100 ppm Re	1.6	60.7	250	11.4	41.5
(3'') 12% Ag, 100 ppm Re	0.35	79.5	225	1.8	4.4

4.4.3 Discussion

In order to determine whether Re and Re co-promoters modify catalyst performance by changing Ag particle sizes and/or morphology, scanning electron microscopy (SEM) was used to image the different compositions. Previously, Minahan et al. [134-136] claimed the main role of Cs was to act as a binder or transition layer between the Ag particles and the α-Al_2O_3 surface which increased the strength of interaction between Ag and the support. SEM micrographs for unpromoted catalysts depicted small silver particles in addition to regions containing a thin film of Ag present on the surface of the Al_2O_3. Alternatively, Minahan observed that the Cs-promoted catalysts exhibited only a thin film of Ag and small particles were not observed in the "as-prepared" state. Thus, in this study, the Re and co-promoters might function in the same manner, especially since both the α-Al_2O_3 and high-valent oxy anions are oxide

compositions.

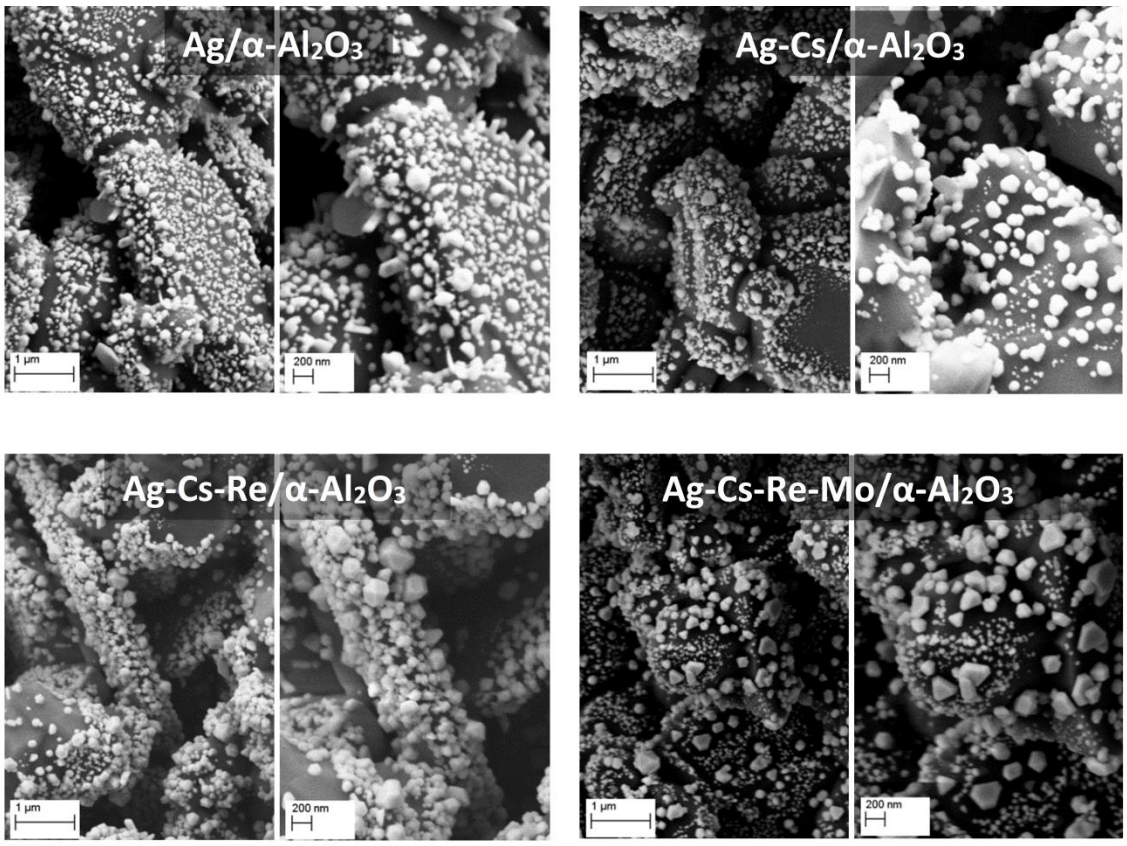

Figure 4.6 SEM micrographs demonstrating the size and morphology of Ag for the following EO catalysts: 12 wt% Ag/α-Al_2O_3 (top left), 12 wt% Ag, 350 ppm Cs/α-Al_2O_3 (top right), 12 wt% Ag, 350 ppm Cs, 200 ppm Re/α-Al_2O_3 (bottom left), 12 wt% Ag, 350 ppm Cs, 200 ppm Re, 150 ppm Mo/α-Al_2O_3 (bottom right).

The SEM micrographs for the catalytic formulations reported in Table 4.2 are shown in Figure 4.6. The compositions of each catalyst are shown for each image; the smooth, light gray regions depict the α-Al_2O_3 carrier and the smaller, white particles are the supported Ag particles. All micrographs in Figure 4.6 show distinct Ag particles of varying size and shape. A wide variety of geometric shapes were observed, including hexagons, octagons, hexagonal sheets, octagonal sheets, prisms, pyramids, triangular sheets, spherical particles, and even some needle-like protrusions extending from the

surface of the support. Visual comparison of the micrographs for the unpromoted Ag catalyst and the catalysts promoted with Cs, Cs-Re, and Cs-Re-Mo, respectively, show no obvious trends in particle sizes or shapes. XRD analysis (data not reported for brevity) similarly did not reveal changes in the relative contributions of different crystalline planes in the XRD diffraction patterns and were indistinguishable from one another. Thus, the average particle size of 0.12 μm determined by O_2 chemisorption at 170 ℃ for the unpromoted Ag catalyst was assumed to be representative for all catalysts evaluated in this investigation. We conclude that because no apparent morphological changes in the Ag particles caused by addition of promoters were observed, the mechanism for higher EO selectivity must occur either through a site-blocking process, as stated by Waugh et al. [71,87-89], or through an electronic interaction, as proposed by Monnier and others [77,90-96,98]. However, the results in Table 4.3 show that when 350 ppm of Cs is added to the Ag-Re catalyst, the required shell temperature to achieve 2.0 mole % EO drops from 262 ℃ to 218 ℃, while the selectivity to EO increases from 49.85 to 82.35%. In this case, it is hard to envision how the blocking of additional sites by Cs could result in much higher activity and selectivity to EO. Rather, it seems that Cs is required to offset some of the negative aspects of Re promotion.

In order to better explore possible electronic interactions between Cs, Ag, and Re, XPS studies were conducted on the following four catalysts: (1), 12% Ag/α-Al_2O_3, (2), 350 ppm Cs, 12% Ag/α-Al_2O_3, (3), 200 ppm Re, 350 ppm Cs, 12% Ag/α-Al_2O_3, and (4), 200 ppm Re, 12% Ag/α-Al_2O_3. The XPS results in Figure 4.7 show the Ag 3d binding energies for the catalysts following 12 h pretreatments at 280 ℃ in flowing O_2 in the catalysis cell attached to the XPS chamber; the results in Figure 4.3 indicated that EO

selectivities following *in situ* calcination at 260 ℃ for 12-15 h were 1 – 2 percentage points higher than the same catalysts that did not receive the *in situ* calcination. All "as prepared" catalysts had been subjected to a rapid calcination sequence using forced air flow (100 L/min) at 260 ℃ for a total of 5 – 7 min; the heat-up time from 25 ℃ to 260 ℃ required < 2 min. This was done to approximate calcination procedures used by others [84-86,107] for preparation of similar compositions. Thus, the calcination conditions of the freshly prepared catalysts were less demanding than calcination in the attached catalysis cell of the XPS.

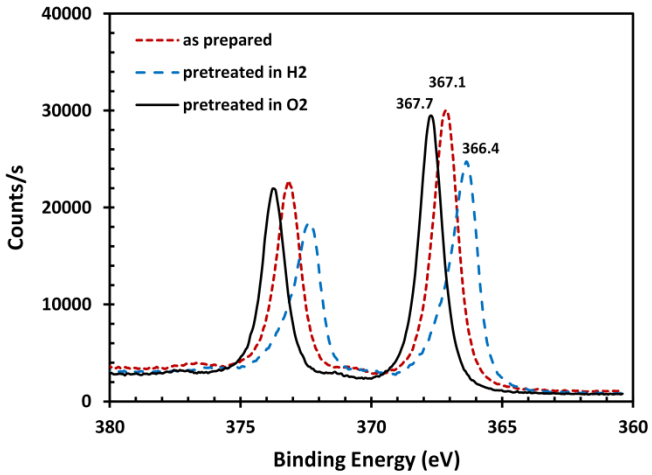

Figure 4.7 Ag $3d_{5/2}$ spectra of 12 wt% Ag/α-Al_2O_3 for (1), as prepared sample, (2), after pretreatment in 100% H_2 at 280 ℃ for 12 h, and (3), after pretreatment in 10% O_2/balance He at 280 ℃ for 12 h. Both H_2 and O_2 pretreatments performed *in situ* in catalysis cell attached to XPS chamber.

Because of the uncertainty of Ag 3d binding energies of supported Ag catalysts, presumably due to charging effects of the insulating alumina support and possible Ag particle size effects, it is difficult to compare BE values among different studies. For example, Hoflund [134] claimed Ag $3d_{5/2}$ BE values of 368.0, 367.7, and 367.3 eV for Ag^o, Ag_2O, and AgO species, respectively, present on Cs-promoted, Ag/α-Al_2O_3 catalysts following different pretreatments, while Goodman [137] measured values ranging from

367.8 – 368.8 eV for variable, fractional coverages of Ag metal particles on Al_2O_3/Re(0001) planar surfaces. Finally, Lambert [138] observed the Ag $3d_{5/2}$ BE of 367.0 eV for Ag^o particles supported on {0001} α-Al_2O_3 surfaces. From just these three studies, $3d_{5/2}$ BE values ranging from 367.0 to 368.8 eV for Ag^o have been reported. A further complication is that in some cases the oxides of silver show an anomalous negative BE shift compared to the metal. In one study [139] the Ag_2O and AgO BE shifts were approximately 0.3 eV and 0.8 eV to lower binding energies, respectively, compared to the value of 368.2 eV for Ag^o. The predominant cause of this peculiar shift has been attributed to initial-state factors of ionic charge and lattice potential. Thus, comparisons of Ag binding energies are valid only within a given study for similar Ag morphologies and particle sizes. As the images in Figure 4.6 indicate, all supported Ag particles exhibited similar morphologies and sizes on the same α-Al_2O_3 support. To confirm the Ag $3d_{5/2}$ BEs for Ag^o and Ag^+ (or $Ag^{\delta+}$) species in this study, the XPS spectra in Figure 4.7 are shown for 12% Ag/α-Al_2O_3 following different pretreatments. The $3d_{5/2}$ values following reduction at 280 ℃ and after calcination at 280 ℃ (both for 12 h) are 366.4 and 367.7 eV, corresponding to Ag^o and Ag^+ or $Ag^{\delta+}$, both respectively. We do not make a hard distinction between Ag^+ and $Ag^{\delta+}$ in this study, since we have no reference compound to confirm the BE of Ag^+, but the shifts to higher Ag $3d_{5/2}$ BE values indicate e^- transfer away from Ag. The intermediate value of 367.1 eV for the "as prepared" sample suggests the Ag was not as oxidized following the shorter calcination period at 260 ℃. More importantly, it indicates we do not have the anomalous, negative BE shift referenced above for the series of catalysts in this study.

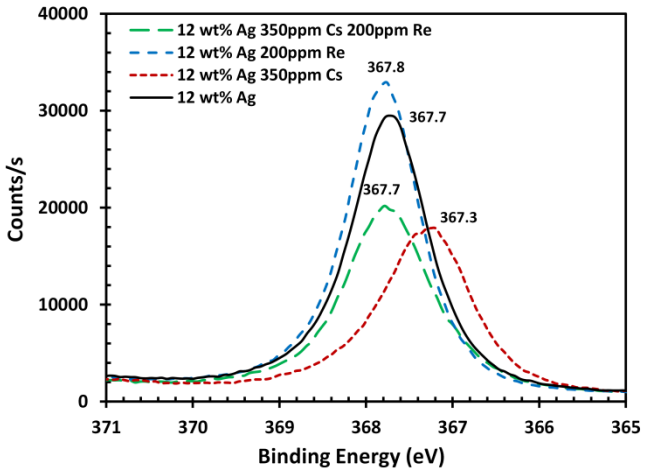

Figure 4.8 Ag $3d_{5/2}$ spectra for (1), 12 wt% Ag/α-Al_2O_3, (2), 12 wt% Ag, 350 ppm Cs/α-Al_2O_3, (3), 12 wt% Ag, 200 ppm Re/α-Al_2O_3, and (4), 12 wt% Ag, 350 ppm Cs, 200 ppm Re/α-Al_2O_3 after *in situ* pretreatment in 10% O_2/balance He at 280 ℃ for 12 h. Only Ag $3d_{5/2}$ binding energy shown for purposes of clarity.

The Ag $3d_{5/2}$ BE values for the four "as prepared" catalysts were all similar with values of 367.2 ± 0.1 eV; the $3d_{5/2}$ values following H_2 reduction were also all very similar with values of 366.6 ± 0.1 eV. However, the Ag $3d_{5/2}$ binding energies shown in Figure 4.8 for the same samples after calcination at 280 ℃ for 12 h differ according to catalyst composition. The addition of 350 ppm Cs to 12 wt% Ag lowers the Ag $3d_{5/2}$ BE from 367.7 eV to 367.3 eV, suggesting transfer of e^- density from the highly polarizable Cs^+ to the e--deficient $Ag^{\delta+}$ species, which is consistent with earlier results of Monnier [93,140] and the polarizability trends from Douglas [141]. Polarizability is the tendency of an electron cloud of an atom, ion, or molecule to be distorted from its normal shape by a nearby ion. In this case the electron cloud is that of Cs^+ and the nearby ion is $Ag^{\delta+}$; Cs^+ has the largest ionic radius of any naturally-occurring element and has completely-filled atomic orbitals through the fourth period of the periodic table, making it highly polarizable.

The Ag $3d_{5/2}$ BE value is shifted back to 367.8 eV when 200 ppm Re is added to the 12 wt% Ag, 350 ppm Cs composition, indicating that the interaction of the high-valent Re cation with $Ag^{\delta+}$ offsets the opposite effect of Cs^{+}; the Ag $3d_{5/2}$ BE of the 12 wt% Ag, 200 ppm Re catalyst is essentially the same, also showing the same ability of Re to affect the electronic structure of Ag.

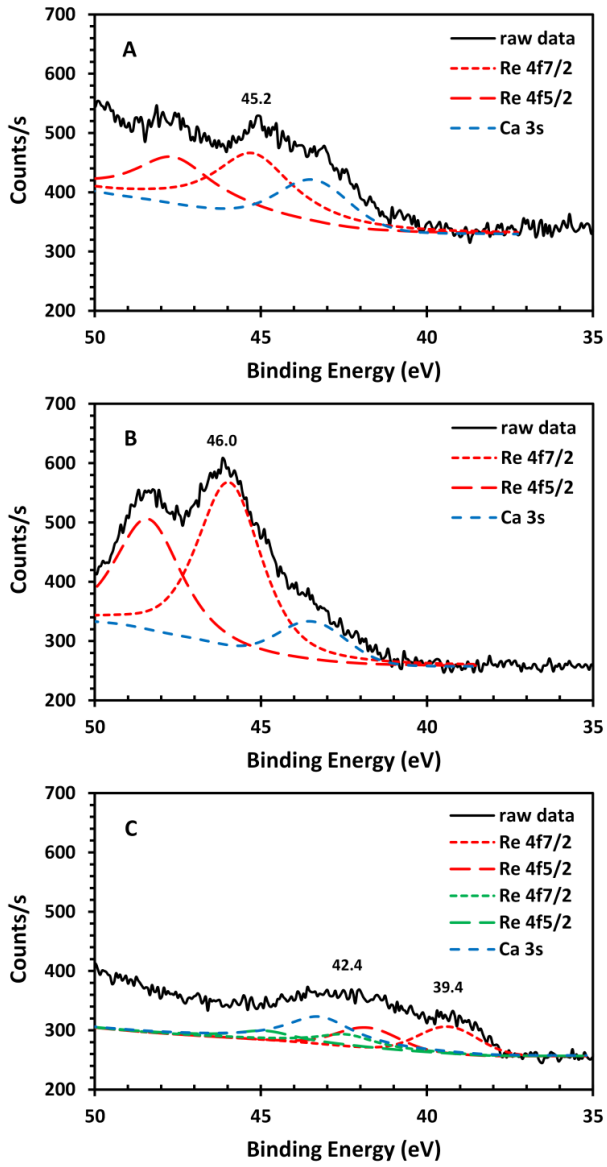

Figure 4.9 Re $4f_{7/2}$ spectra of 12 wt% Ag, 350ppm Cs, 200ppm Re/α-Al_2O_3 for (a), as prepared sample (b), after pretreatment in 10% O_2/balance He at 280 ℃ for 12 h, and (c), after pretreatment in 100% H_2 at 280 ℃ for 12 h. Both H_2 and O_2 pretreatments performed *in situ* in catalysis cell attached to XPS chamber.

The Re 4f XPS spectra for the 12 wt% Ag, 350 ppm Cs, 200 ppm Re/α-Al_2O_3 catalyst after different pretreatment conditions are shown in Figure 4.9. The BE values of the Re $4f_{7/2}$ peaks are shown in each of the three spectra. The as prepared sample shows a BE at 45.2 eV indicative of a mixture of both Re^{6+} and Re^{7+} species [129,133]. Following calcination at 280 ℃, all Re is oxidized to Re^{7+}, with a $4f_{7/2}$ BE of 46.0 eV (Figure 4.9B), which indicates that the *in situ* pretreatment at 260 ℃ for 12 h oxidizes all Re to the Re^{7+} state before catalyst evaluation. This suggests the existence of Re^{7+} is linked to the higher selectivity values for EO following the *in situ* calcination in Figure 4.3. The effects of catalyst composition on BE values for Ag and Re are summarized in Table 4.4. Finally, reduction of the catalyst at 280 ℃ for 12 h reduces the majority of the Re to the metallic state (BE = 39.4 eV) with a smaller contribution from Re^{4+} (BE = 42.4 eV) (Figure 4.9C).

Table 4.4 Binding Energy of Ag $3d_{5/2}$ and Re $4f_{7/2}$ after *in situ* pretreatment in 10% O_2 /balance He at 280 ℃ for 12 h.

Catalyst composition	**Ag $3d_{5/2}$ B.E (eV)**	**Re $4f_{7/2}$ B.E (eV)**
(1) 12 wt% Ag/α-Al_2O_3	367.7	N/A
(2) 12 wt% Ag, 350 ppm Cs/α-Al_2O_3	367.3	N/A
(3) 12 wt% Ag, 200 ppm Re/α-Al_2O_3	367.8	45.6
(4) 12 wt% Ag, 350 ppm Cs, 200 ppm Re/α-Al_2O_3	367.7	46.0

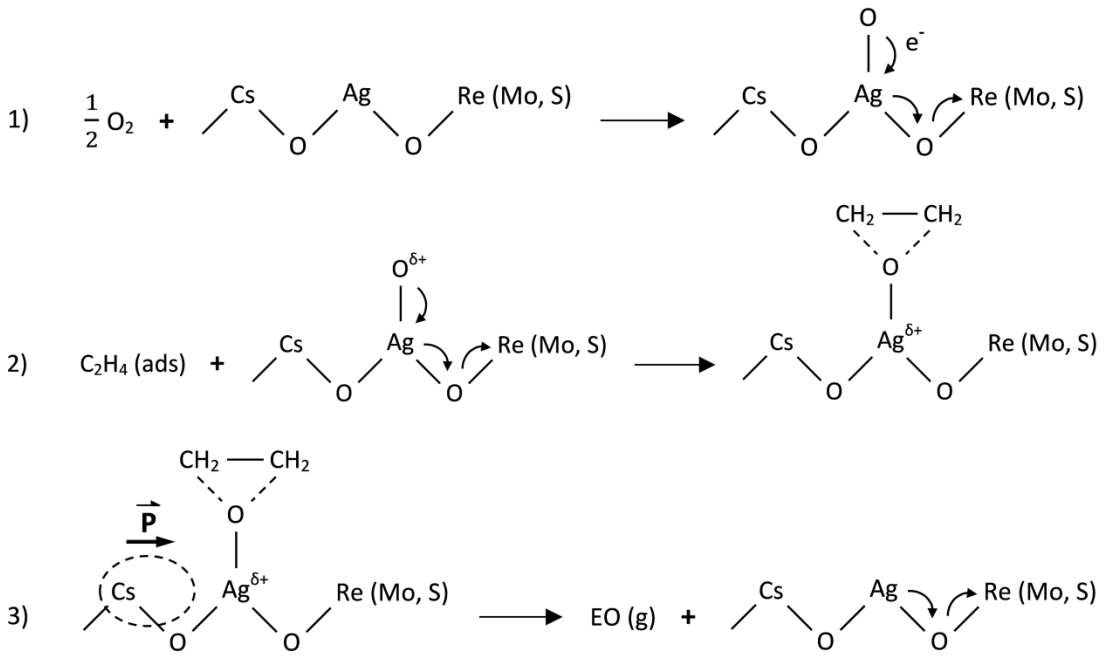

Figure 4.10 Mechanistic scheme for ethylene epoxidation using Cs-Re(Mo) promoted Ag catalysts.

The XPS data and catalyst evaluation suggests the following site model postulating how the Cs-Re-Ag system functions under reaction conditions. In Figure 4.10, Step 1 shows that the presence of the high-valent Re oxide species, along with the other high-valent, Re co-promoters (Mo and S), draws e- density from the Ag site to increase the electrophilicity of the adsorbed O atom so that, in Step 2 electrophilic attack of adsorbed O at the e^- - rich C=C bond is favored, rather than nucleophilic attack at a C-H bond of C_2H_4. However, formation of the adsorbed EO species also increases the positive charge on Ag, since the O is shared by both Ag and C_2H_4. This is the situation that exists for Re-promoted, Ag catalysts; the strongly-adsorbed EO intermediate undergoes combustion to CO_2 and H_2O and because desorption of EO becomes more rate limiting, overall activity also declines, as shown in Table 4.3. This is the same situation Monnier [93,94] described for butadiene epoxidation over unpromoted Ag catalysts,

where both selectivity to 3,4-epoxy-1-butene and conversion of butadiene were adversely affected due to strong adsorption of the adsorbed epoxide intermediate. However, as Monnier also observed for butadiene epoxidation, the presence of Cs in Step 3 results in Cs-assisted desorption of EO by the participation of the highly polarizable electron cloud surrounding the Cs^+ cation. This results in the higher EO selectivity and C_2H_4 conversion values shown in Table 4.3 and Figure 4.3. That this is feasible is shown in Table 4.4; the Ag $3d_{5/2}$ BE is shifted 0.4 eV from 367.7 to 367.3 eV when 350 ppm Cs is added to the Ag catalyst. This site model indicates two different types of promoters are required for high selectivity EO catalysts, a high valent Re (and optional Mo and S) promoter to increase the electrophilicity of O adsorbed on Ag as well as Cs to offset the effect of Re and lower the desorption energy of adsorbed EO. Thus, two different types of promoter are required for Re-containing, high selectivity EO catalysts.

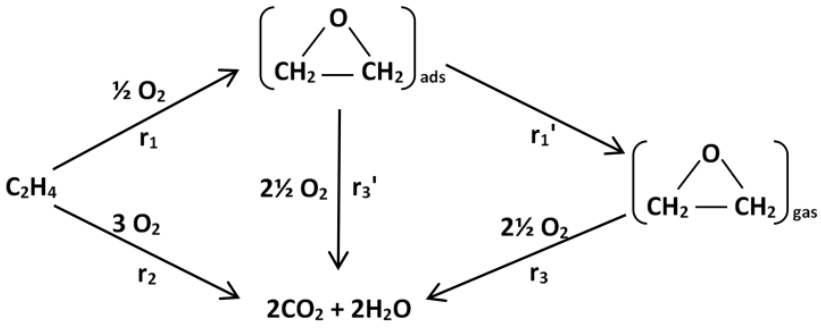

Figure 4.11 Reaction network for the production of EO for Re-containing catalysts.

Finally, the reaction pathway shown in Figure 1.6 should be rewritten as shown in Figure 4.11 to include the effect of Re and other high-valent promoters. Reaction pathway (r_1) has been changed to include (r_1') for desorption of adsorbed EO. In the presence of Cs, (r_1') is high enough that it becomes negligible, but in the absence of Cs, (r_1') must be included to determine the rate of gas phase EO formation. If unable to

desorb efficiently, (r_3') also provides a pathway for combustion to CO_2 and H_2O. As stated earlier, the primary role of Re and co-promoters is to increase the electrophilicity of O adsorbed on Ag. This is reflected by increasing the ratio of (r_1)/(r_2) and even (r_1)/(r_3').

4.5 Conclusion

A series of Cs-Ag, Re-Ag, Cs-Re-Ag and Cs-Re-Mo-Ag catalysts supported on α-Al_2O_3 have been prepared and evaluated for ethylene epoxidation. While all current generation, high selectivity EO catalysts contain high-valent Re oxyanions and other high-valent oxyanions, such as MoO_4^{2-} as co-promoters for Re, virtually nothing in the open literature has been published regarding the mechanism of selectivity enhancement for these catalysts. We have found, in agreement with patent literature, that addition of optimal amounts of Re (as NH_4ReO_4) and Mo [as $(NH_4)_2MoO_4$] to Cs-promoted, Ag/α-Al_2O_3 increase EO selectivity from approximately 79% to 83%. Cesium is required for the high selectivity to EO, since removal of Cs from an optimal Cs-Re-Ag/α-Al_2O_3 results in dramatic loss of EO selectivity from 83% to less than 50%. Thus, Re is necessary, but not sufficient for high selectivity to EO. XPS and SEM analyses of the above catalysts indicate that the role of Re and Cs are both electronic in nature. From SEM analyses, the presence of Re (and Mo) does not change either the morphology or particle sizes of the Ag particles relative to Ag/α-Al_2O_3 and Cs-Ag/α-Al_2O_3 catalysts. However, the presence of Re^{7+} species on the Ag surface shifts the Ag 3d BE to higher values, making the Ag site more electron-deficient and the resulting O adsorbed on Ag more electrophilic. This increases the interaction with the electron-rich C=C double bond

of C_2H_4 and conversely lowers nucleophilic attack at one of the four C-H bonds; the former pathway leads to EO formation while the latter leads to combustion to CO_2 and H_2O. XPS analysis also shows the presence of Cs on Ag lowers the Ag 3d BE, suggesting that Cs lowers the desorption energy of the EO precursor strongly bound to the Re-modified, Ag surface site. In the absence of Cs, strongly-bound EO undergoes combustion to CO_2 and H_2O, explaining why the Re-Ag/α-Al_2O_3 catalyst is much less selective to EO than the analogous Cs-Re-Ag/α-Al_2O_3 catalyst. Rhenium and Cs promote two different steps of the overall mechanism; Re increases the rate of electrophilic attack by Ag-O at the C=C bond of C_2H_4, while Cs lowers the desorption energy of the adsorbed EO precursor to form EO. The role of Cs is even more pronounced for the Re-modified, Ag catalysts than for unpromoted Ag catalysts since Re increases the electron deficiency of the adjacent Ag site. A reaction scheme detailing the mechanism of EO formation over Re-modified Ag catalysts has also been presented.

CHAPTER 5:

CONCLUSIONS

In this study, for Pt-Ru system, two series of Pt@Ru/C and Ru@Pt/C bimetallic catalysts were synthesized by electroless deposition method. For Ru@Pt/C catalysts (Pt deposition on Ru/C) preparation, a standard ED bath condition for Pt deposition was used. H_2PtCl_6 and DMAB as Pt precursor and reducing agent were used in the ED bath with pH 10 and temperature 70 ℃. By changing the initial concentration of Pt in solution, different weight loadings and coverage of Ru@Pt/C catalysts were synthesized. For Pt@Ru/C catalysts (Ru deposition on Pt/C) preparation, a new ED bath was developed using HCOOH as reducing agent and $Ru(NH_3)_6Cl_3$ as Ru precursor. After bath temperature and pH effect study, pH 3 and temperature 110 ℃ were used to prepare different weight loadings and coverage of Pt@Ru/C catalysts. The Pt@Ru/C and Ru@Pt/C bimetallic catalysts were then characterized by temperature programmed reduction (TPR), selective chemisorption, X-ray photoelectron spectroscopy (XPS), X-ray powder diffraction (XRD) and scanning transmission electron microscopy (STEM). Selective chemisorption (H_2 titration of oxygen pre-covered surfaces) and TPR and experiments confirmed the existence of strong surface interactions between Pt and Ru as evidenced by hydrogen spillover of Pt to Ru (Pt-assisted reduction of oxygen pre-covered Ru). XPS analyses also indicated strong surface interactions between Pt and Ru. The binding energy (BE) shifts of Pt to higher BE value and Ru to lower BE value suggested e^- transfer from Pt to Ru on the bimetallic surface. No peak shown of secondary metal (Pt or Ru) in XRD analysis indicated the secondary metal is highly dispersed on the primary metal. Finally, The STEM and XEDS images provided strong, visual evidence of targeted deposition of Ru on Pt/C and Pt on Ru/C. The XEDS images confirmed that individual nanoparticles of the catalysts prepared by ED were bimetallic, with excellent association

between the primary and the secondary metals. No monometallic Pt or Ru particles were detected for either of the families of bimetallic particles.

For ethylene epoxidation study of Ag-based catalysts, a series of α-Al_2O_3 supported Ag, Ag-Cs, Ag-Re, Ag-Cs-Re and Ag-Cs-Re-Mo catalysts were prepared using impregnation method. The Ag-based catalysts were then characterized using SEM and XPS. A flow reactor with a feed of 8% O_2, 25% C_2H_4, 1-3 ppm ethyl chloride (EtCl), and balance CH_4 at 250 psig was used for catalyst evaluation. Addition of optimal amounts of Re (as NH_4ReO_4) and Mo [as $(NH_4)_2MoO_4$] to Cs-promoted, Ag/α-Al_2O_3 increased EO selectivity from approximately 79% to 83%. Cesium is required for the high selectivity to EO, since removal of Cs from an optimal Cs-Re-Ag/α-Al_2O_3 resulted in dramatic loss of EO selectivity from 83% to less than 50%. Thus, Re is necessary, but not sufficient for high selectivity to EO. From SEM analyses, the presence of Cs, Re, and Mo did not change either the morphology or particle sizes of the Ag particles relative to Ag/α-Al_2O_3 catalysts. XPS analyses showed that Re shifts Ag 3d BE to higher values which enhances electrophilic attack by oxygen adsorbed on Ag (Ag-O) at the electron-rich C=C bond of C_2H_4. In the subsequent step, Cs lowered the Ag 3d BE to facilitate desorption of the EO precursor to form gas phase EO. That was, Re and Cs promoted different steps of the mechanism of EO formation. The detail mechanism of Cs, Re and its co-promoter increasing selectivity of Ag-based catalysts for ethylene epoxidation was proposed in this study. Also, a reaction scheme detailing the mechanism of EO formation over Re-modified, Cs-promoted Ag catalysts was presented.

REFERENCES

[1] G. Ertl, H. Knozinger, J. Weitkamp (Eds.), Handbook of Heterogeneous Catalysis, VCH Verlagsgesellschaft, Weinheim, 1997, p. 13, 35-38, 191-286, 365-367.

[2] R. A. van Santen, J. W. Niemantsverdriet, Chemical Kinetics and Catalysis, Plenum Press, New York, 1995, p. 1-6.

[3] J. Hagen, Industrial Catalysis: A Practical Approach, 2nd ed., Wiley-VCH & Co., Weinheim, Germany, 2006.

[4] G. Rothenberg, Catalysis: Concepts and Green Applications, Wiley-VCH, Weinheim, 2008.

[5] J. A. Rodriguez, Surf. Sci. Rep. 24 (1996) 223-287.

[6] M. Kuhn, J. A. Rodriguez, J. Catal. 154 (1995) 355-363.

[7] W. M. H. Sachtler, Appl. Surf. Sci. 19 (1984) 167-180.

[8] Y. Zhang, W. Diao, C. T. Williams, J. R. Monnier, Appl. Catal., A 469 (2014) 419-426.

[9] A. A. Rodriguez, C. T. Williams, J. R. Monnier, Appl. Catal., A 475 (2014) 161-168.

[10] Y. -J. Song, J. R. Monnier, P. T. Fanson, C. T. Williams, J. Catal. 315 (2014) 59-66.

[11] J. T. Wrobleski, M. Boudart, Catal. Today 15 (1992) 349-360.

[12] A. J. van Dillen, R. J. A. M. Terörde, D. J. Lensveld, J. W. Geus, K. P. de Jong, J. Catal. 216 (2003) 257-264.

[13] J. W. Geus, Stud. Surf. Sci. Catal. 16 (1983) 1-33.

[14] J. R. Regalbuto, Strong Electrostatic Adsorption of Metals onto Catalyst Supports. In Catalyst Preparation Science and Engineering; Regalbuto, J. R., Ed.; CRC Press: Boca Raton, 2006, p. 297-318.

[15] J. R. Regalbuto, Electrostatic Adsorption. In Synthesis of Solid Catalysts; de Jong, K. P., Ed.; Wiley-VCH Verlag GmbH & Co.: Weinheim, 2009, p. 33-58.

[16] K. P. de Jong, Curr. Opin. Solid State Mater. Sci. 4 (1999) 55-62.

[17] J. W. Geus, Production of Supported Catalysts by Impregnation and Viscous Drying. In Catalyst Preparation: Science and Engineering; J. R. Regalbuto (Ed.), CRC Press, Boca Raton, 2006, p. 341-372.

[18] C. Louis, Deposition-precipitation Synthesis of Supported Metal Catalysts. In Catalyst Preparation: Science and Engineering; J. R. Regalbuto (Ed.), CRC Press, Boca Raton, 2006, p. 319-339.

[19] J. P. Brunelle, Pure Appl. Chem. 50 (1978) 1211-1229.

[20] M. S. Heise, J. A. Schwarz, J. Colloid. Interface. Sci. 107 (1985) 237-243.

[21] M. S. Heise, J. A. Schwarz, J. Colloid. Interface. Sci. 113 (1986) 55-61.

[22] M. S. Heise, J. A. Schwarz, J. Colloid. Interface. Sci. 123 (1988) 51-58.

[23] J. A. Schwarz, M. S. Heise, J. Colloid. Interface. Sci. 135 (1990) 461-467.

[24] H. Cho, "The Rational Synthesis of Supported Noble Single or Bimetallic Catalysts by Electrostatic Adsorption" University of South Carolina, 2013.

[25] J. Park,, J. R. Regalbuto, J. Colloid. Interface. Sci. 175 (1995) 239-252.

[26] G. Ertl, H. Knözinger, J. Weitkamp (Eds.), Preparation of Solid Catalysts, Wiley-VCH, Weinheim, 1999.

[27] Y. Zhang, W. Diao, J. R. Monnier, C. T. Williams, Catal. Sci. Technol. 5 (2015) 4123-4132.

[28] E. Lamy-Pitara, J. Barbier, Appl. Catal. A 149 (1997) 49-87.

[29] V. Sudha, M. V. Sangaranarayanan, J. Chem. Sci. 117 (2005) 207-218.

[30] S. Djokic, Mod. Aspect. Electroc. 35 (2002) 51-133.

[31] M. Schlesinger, Electroless Deposition of Nickel. In Modern Electroplating, 5th ed.; M. Schlesinger, M. Paunovic (Eds.), Wiley, New York, 2010, p. 447-458.

[32] Y. Okinaka, Electroless Plating of Gold and Gold Alloys. In Electroless Plating: Fundamentals and Applications; G. O. Mallory, J. B. Hajdu (Eds.), William Andrew Publishing, Norwich, 1990, p. 401-420.

[33] K. D. Beard, D. Borrelli, A. M. Cramer, D. Blom, J. W. Van Zee, J. R. Monnier, ACS Nano 3 (2009) 2841-2853.

[34] K. D. Beard, J. W. Van Zee, J. R. Monnier, Appl. Catal., B 88 (2009) 185-193.

[35] W. Riedel, Electroless Nickel Plating, Finishing Publications Ltd., Great Britain, 1991, p. 1-10, 26-32, 54-56.

[36] M. T. Schaal, A. Y. Metcalf, J. H. Montoya, J. P. Wilkinson, C. C. Stork, C. T. Williams, J. R. Monnier, Catal. Today 123 (2007) 142-150.

[37] M. T. Schaal, A. C. Pickrell, C. T. Williams, J. R. Monnier, J. Catal. 254 (2008) 131-143.

[38] W. Diao, J. M. M. Tengco, J. R. Regalbuto, J. R. Monnier, ACS Catal. 5 (2015) 5123-5134.

[39] K. D. Beard, M. T. Schaal, J. W. Van Zee, J. R. Monnier, Appl. Catal., B 72 (2007) 262-271.

[40] J. Rebelli, M. Detwiler, S. Ma, C. T. Williams, J. R. Monner, J. Catal. 270 (2010) 224-233.

[41] J. Rebelli, "Preparation, characterization, and evaluation of bimetallic catalysts prepared by electroless deposition methods" University of South Carolina, 2011.

[42] I. Ohno, O. Wakabayashi, S. Haruyama, J. Electrochem. Soc. 132 (1985) 2323-2330.

[43] G. Mallory, J. Hajdu (Eds.), Electroless Plating: Fundamentals and Applications, American Electroplaters and Surface Finishers Society, Orlando, 1990, p. 1-73, 289-295, 305-320, 401-420, 423-433, 441-461.

[44] C. F. Baes, P. E. Mesmer (Eds.), The Hydrolysis of Cations, Wiley, New York, 1976.

[45] B. D. Barker, Surf. Technol. 12 (1981) 77-88.

[46] G. Diaz, F. Garin, G. Maire, J. Catal. 82 (1983) 13-25.

[47] Y. Zhang, A. Maroto-Valiente, I. Rodriguez-Ramos, Q. Xin, A. Guerrero-Ruiz, Catal. Today 93-95 (2004) 619-626.

[48] G. Diaz, F. Garin, G. Maire, S. Alerasool, R. D. Gonzalez, Appl. Catal., A 124 (1995) 33-46.

[49] A. Amano, G. Parravano, Adv. Catal. 9 (1957) 716-726.

[50] H. Vu, F. Goncalves, R. Philippe, E. Lamouroux, M. Corrias, Y. Kihn, D. Plee, P. Kalck, P. Serp, J. Catal. 240 (2006) 18-22.

[51] J. Teddy, A. Falqui, A. Corrias, D. Carta, P. Lecante, I. Gerber, P. Serp, J. Catal. 278 (2011) 59-70.

[52] M. Chatterjee, F. Zhao, Y. Ikushima, Adv. Synth. Catal. 346 (2004) 459-466.

[53] M. Liu, J. Zhang, J. Liu, W. Yu, J. Catal. 278 (2011) 1-7.

[54] M. Liu, W. Yu, H. Liu, J. Zheng, J. Colloid Interface Sci. 214 (1999) 231-237.

[55] E. P. Maris, R. J. Davis, J. Catal. 249 (2007) 328-337.

[56] P. Claus, Top. Catal. 5 (1998) 51-62.

[57] P. Gallezot, D. Richard, Catal. Rev. Sci. Eng. 40 (1998) 81-126.

[58] J. W. Long, R. M. Stroud, K. E. Swider-Lyons, D. R. Rolison, J. Phys. Chem. B 104 (2000) 9772-9776.

[59] M. P. Hogarth, G. A. Hards, Platin. Met. Rev. 4 (1996) 150-159.

[60] A. Hamnett, Catal. Today 38 (1997) 445-457.

[61] S. Wasmus, A. Kuver, J. Electroanal. Chem. 461 (1999) 14-31.

[62] T. R. Garrick, W. Diao, J. M. Tengco, J. R. Monnier, J. W. Weidner, ECS Trans. 53 (2013) 79-84.

[63] E. V. Steigerwalt, G. A. Deluga, C. M. Lukehart, J. Phys. Chem. B 106 (2002) 760-766.

[64] J. Choi, K. Park, B. Kwon, Y. Sung, J. Electrochem. Soc. 150 (2003) 973-978.

[65] Z. He, J. Chen, D. Liu, H. Zhou, Y. Kuang, Diamond Relat. Mater. 13 (2004) 1764-1770.

[66] C. H. Bartholomew, R. J. Farrauto, Fundamentals of Industrial Catalytic Processes, John Wiley and Sons, New York, 2006, p. 597.

[67] J. L. Pellegrino, L. Sousa, H. Kenchington, Energy and Environmental Profile of the U.S. Chemical Industry, Report prepared by Energetics Inc. for the U.S. Department of Energy, 2000.

[68] J. P. Dever, K. F. George, W. C. Hoffman, H. Soo, in: J.I. Kroschwitz, M. Howe-Grant (Eds.), Kirk-Othmer Encyclopedia of Chemical Technology, John Wiley and Sons, New York, 2004, p. 632.

[69] W. M. H. Sachtler, C. Backx, R. A. Van Santen, Catal. Rev. Sci. Eng. 23 (1981) 127-149.

[70] R. A. Van Santen, H. P. C. E. Kuipers, Adv. Catal. 35 (1987) 265-321.

[71] K.C. Waugh, M. Hague, Mechanisms in Homogeneous and Heterogeneous Epoxidation Catalysis; S. T. Oyama (Ed.) Elsevier, Oxford, 2008, p. 233.

[72] R. B. Grant, R. M. Lambert, J. Catal. 92 (1985) 364-375.

[73] R. Haul, G. Neubauer, J. Catal. 105 (1987) 39-54.

[74] J. T. Gleaves, A. G. Sault, R. J. Madix, J. R. Ebner, J. Catal. 121 (1990) 202-218.

[75] V. I. Bukhtiyarov, A. I. Boronin, V. I. Savchenko, J. Catal. 150 (1994) 262-267.

[76] V. I. Bukhtiyarov, A. I. Boronin, I. P. Prosvirin, V. I. Savchenko, J. Catal. 150 (1994) 268-273.

[77] C. Stegelmann, N. C. Schiodt, C. T. Campbell, P. Stoltze, J. Catal. 221 (2004) 630-649.

[78] S. Linic, M. A. Barteau, J. Am. Chem. Soc. 124 (2002) 310-317.

[79] S. Linic, M. A. Barteau, J. Am. Chem. Soc. 125 (2003) 4034-4035.

[80] S. Linic, M. A. Barteau, J. Catal. 214 (2003) 200-212.

[81] W. -X. Li, C. Stampfl, M. Scheffler, Phys. Rev. B 68 (2003) 165412-1-165412-15.

[82] M. -L. Bocquet, D. Loffreda, J. Am. Chem. Soc. 127 (2005) 17207-17215.

[83] J. March, Advanced Organic Chemistry: Reactions, Mechanisms, and Structure, McGraw-Hill, New York, 1968, p. 153.

[84] A. M. Lauritzen, US Patent 4 761 394 (1976), to Shell Oil Company.

[85] A. M. Lauritzen, US Patent 4 766 105 (1988), to Shell Oil Company.

[86] A. M. Lauritzen, US Patent 4 833 261 (1989), to Shell Oil Company.

[87] J. Couves, M. Atkins, M. Hague, B. H. Sakakini, K. C. Waugh, Catal. Lett. 99 (2005) 45-53.

[88] M. Atkins, J. Couves, M. Hague, B. H. Sakakini, K. C. Waugh, J. Catal. 235 (2005) 103-113.

[89] K. C. Waugh, M. Hague, Catal. Today 157 (2010) 44-48.

[90] R. B. Grant, R. M. Lambert, Langmuir 1 (1985) 29-33.

[91] R. B. Grant, R. M. Lambert, J. Catal. 93 (1985) 92-99.

[92] S. A. Tan, R. B. Grant, R. M. Lambert, J. Catal. 106 (1987) 54-64.

[93] J. R. Monnier, J. L. Stavinoha Jr., R. L. Minga, J. Catal. 226 (2004) 401-409.

[94] J. R. Monnier, Stud. Surf. Sci. Catal. 110 (1997) 135-149.

[95] J. R. Monnier, J. W. Medlin, M. A. Barteau, J. Catal. 203 (2001) 362-368.

[96] J. W. Medlin, J. R. Monnier, M. A. Barteau, J. Catal. 204 (2001) 71-76.

[97] J. R. Monnier, G. W. Hartley, J. Catal. 203 (2001) 253-256.

[98] J. T. Jankowiak, M. A. Barteau, J. Catal. 236 (2005) 379-396.

[99] C. T. Campbell, B. E. Koel, J. Catal. 92 (1985) 272-283.

[100] R. M. Lambert, R. L. Cropley, A. Husain, M. S. Tikhov, Chem. Commun. 10 (2003) 1184-1185.

[101] J. R. Monnier, J. L. Stavinoha Jr., G. W. Hartley, J. Catal. 226 (2004) 321-333.

[102] D. Torres, F. Illas, R. M. Lambert, J. Catal. 260 (2008) 380-383.

[103] J. C. Dellamorte, J. Lauterbach, M. A. Barteau, Catal. Today 120 (2007) 182-185.

[104] Shell Chemicals Magazine (Autumn/Winter 2010) 12.

[105] W. E. Evans, M. Matusz, P. M. McCallister, WO Patent 0 786 03 (2012), to Shell Oil Company.

[106] N. Rizkalla, A. Rokicki, US Patent 0 281 724 (2011), to Scientific Design Company.

[107] J. R. Lockemeyer, R. C. Yeates, D. Reinalda, US Patent 0 160 655 (2010).

[108] A. Bortinger, A. D. Schmitz, US Patent 7 553 795 (2009).

[109] J. Deng, J. Yang, S. Zhang, X. Yuan, J. Catal. 138 (1992) 395-399.

[110] J. Yang, J. Deng, X. Yuan, S. Zhang, Appl. Catal. A 92 (1992) 73-80.

[111] C. Coutanceau, A. F. Rakotondrainibe, A. Lima, E. Garnier, S. Pronier, J. Leger, C. J. Lamy, Appl. Electrochem. 34 (2004) 61-66.

[112] I. Ohno, Mater. Sci. Eng., A 146 (1991) 33-49.

[113] R. P. Galhenage, K. Xie, W. Diao, J. M. M. Tengco, G. S. Seuser, J. R. Monnier, D. A. Chen, Phys. Chem. Chem. Phys. 2015, DOI: 10.1039/C5CP00075K

[114] M. Ohashi, K. D. Beard, S. Ma, D. Blom, J. W. Van Zee, J. R. Monnier, Electrochim. Acta 55 (2010) 7376-7384.

[115] D. Liu, Y. M. Lopez-De Jesus, J. R. Monnier, C. T. Williams, J. Catal. 269 (2010) 376-387.

[116] G. Corro, R. Gomez, React. Kinet. Catal. Lett. 12 (1979) 145-150.

[117] K. O'Connell, J. R. Regalbuto, Catal. Lett. 145 (2015) 777-783.

[118] W. E. Mustain, H. Kim, V. Narayanan, T. Osborn, P. A. Kohl, J. Fuel Cell Sci. Tech. 4 (2010) 041013-1-041013-7.

[119] M. Baldauf, D. M. Kolb, J. Phys. Chem. 100 (1996) 11375-11381.

[120] J. M. Hutchinson, Platinum Met. Rev. 16 (1972) 88-90.

[121] G. Blanchard, H. Charcosset, Stud. Surf. Sci. Catal. 4 (1980) 515-524.

[122] H. Kubicka, React. Kinet. Catal. Lett. 5 (1976) 223-228.

[123] J. F. Moulder, W. F. Stickle, P. E. Sobol, K. D Bomben, In Handbook of X-ray Photoelectron Spectroscopy; Physical Electronics Inc., Eden Prairie, MN, 1995.

[124] M. T. Schaal, J. Rebelli, H. M. McKerrow, C. T. Williams, J. R. Monnier, Appl. Catal., A 382 (2010) 49-57.

[125] S. J. Khatib, S. T. Oyama, Cat. Rev. Sci. Eng. 57 (2015) 306-344.

[126] S. R. Seyedmonir, D. E. Strohmayer, G. J. Guskey, G. L. Geoffroy, M. A. Vannice, J. Catal. 93 (1985) 288-302.

[127] C. Bolivar, H. Charcosset, R. Frety, M. Primet, L. Tournayan, C. Betizeau, G. Leclercq, R. Maurel, J. Catal. 45 (1976) 163-178.

[128] L. Rodrigo, K. Marcinkowska, A. Adnot, P. C. Roberge, S. Kaliaguine, J. M. Stencel, L. E. Makovsky, J. R. Diehl, J. Phys. Chem. 90 (1986) 2690-2696.

[129] J. Okal, Appl. Catal. A 287 (2005) 214-220.

[130] D. Stacchiola, G. Wu, M. Kaltchev, W. T. Tysoe, Surf. Sci. 486 (2001) 9-23.

[131] S. H. Overbury, P. A. Bertrand, G. A. Somorjai, Chem. Rev. 75 (1975) 547-560.

[132] L. Z. Mezey, J. Giber, Jpn. J. Appl. Phys. 21 (1982) 1569-1572.

[133] J. Okal, L. Kepinski, L. Krajczyk, W. Tylus, J. Catal. 219 (2003) 362-371.

[134] D. M. Minahan, G. B. Hoflund, J. Catal. 158 (1996) 109-115.

[135] G. B. Hoflund, D. M. Minahan, J. Catal. 162 (1996) 48-53.

[136] D. M. Minahan, G. B. Hoflund, W. S. Epling, D. W. Schoenfeld, J. Catal. 168 (1997) 393-399.

[137] K. Luo, X. Lai, C. -W. Yi, K. A. Davis, K. K. Gath, D. W. Goodman, J. Phys. Chem. B 109 (2005) 4064-4068.

[138] S. Wodiunig, J. M. Keel, T. S. E. Wilson, F. W. Zemichael, R. M. Lambert, Catal. Lett. 87 (2003) 1-5.

[139] S. W. Gaarenstroom, N. Winograd, J. Chem. Phys. 67 (1977) 3500-3506.

[140] J. R. Monnier, Appl. Catal. A 221 (2001) 73-91.

[141] B. E. Douglas, D. H. McDaniel, Concepts and Models of Inorganic Chemistry, Blaisdell Publishing, New York, 1965, p. 102, 345.

APPENDIX A:

LIST OF PUBLICATIONS

1. **W. Diao**, C.D. DiGiulio, M.T. Schaal, S. Ma, J.R. Monnier, "An investigation on the role of Re as a promoter in Ag-Cs-Re/α-Al_2O_3 high-selectivity, ethylene epoxidation catalysts", J. Catal. 322 (2015) 14-23.

2. **W. Diao**, J.M.M. Tengco, J.R. Regalbuto, J.R. Monnier, "Preparation and characterization of Pt-Ru bimetallic catalysts synthesized by electroless deposition methods", ACS Catal. 5 (2015) 5123-5134.

3. Y. Zhang, **W. Diao**, J.R. Monnier, C.T. Williams, "Pd-Ag/SiO_2 bimetallic catalysts prepared by galvanic displacement for selective hydrogenation of acetylene in excess ethylene", Catal. Sci. Technol. 5 (2015) 4123-4132.

4. Y. Zhang, **W. Diao**, C.T. Williams, J.R. Monnier, "Selective hydrogenation of acetylene in excess ethylene using Ag- and Au-Pd/SiO_2 bimetallic catalysts prepared by electroless deposition", Appl. Catal. A 469 (2014) 419-426.

5. T.R. Garrick, **W. Diao**, J.M.M. Tengco, J.R. Monnier, J.W. Weidner, "The effect of bimetallic surface composition for methanol oxidation", ECS Trans. 53 (2013) 79-84.

6. R.P. Galhenage, K. Xie, **W. Diao**, J.M.M. Tengco, G.S. Seuser, J.R. Monnier, D.A. Chen "Platinum-Ruthenium bimetallic clusters on graphite: A comparison of vapor deposition and electroless deposition methods" – Phys. Chem. Chem. Phys. DOI: 10.1039/C5CP00075K.

7. S. Cao, J.R. Monnier, C.T. Williams, **W. Diao**, J.R. Regalbuto, "Rational nanoparticle synthesis to determine the effects of size, support, and K dopant on Ru activity for levulinic acid hydrogenation to γ-valerolactone", J. Catal. 326 (2015) 69-78.

APPENDIX B:

PERMISSION TO REPRINT

Permission to Reprint Chapter 3

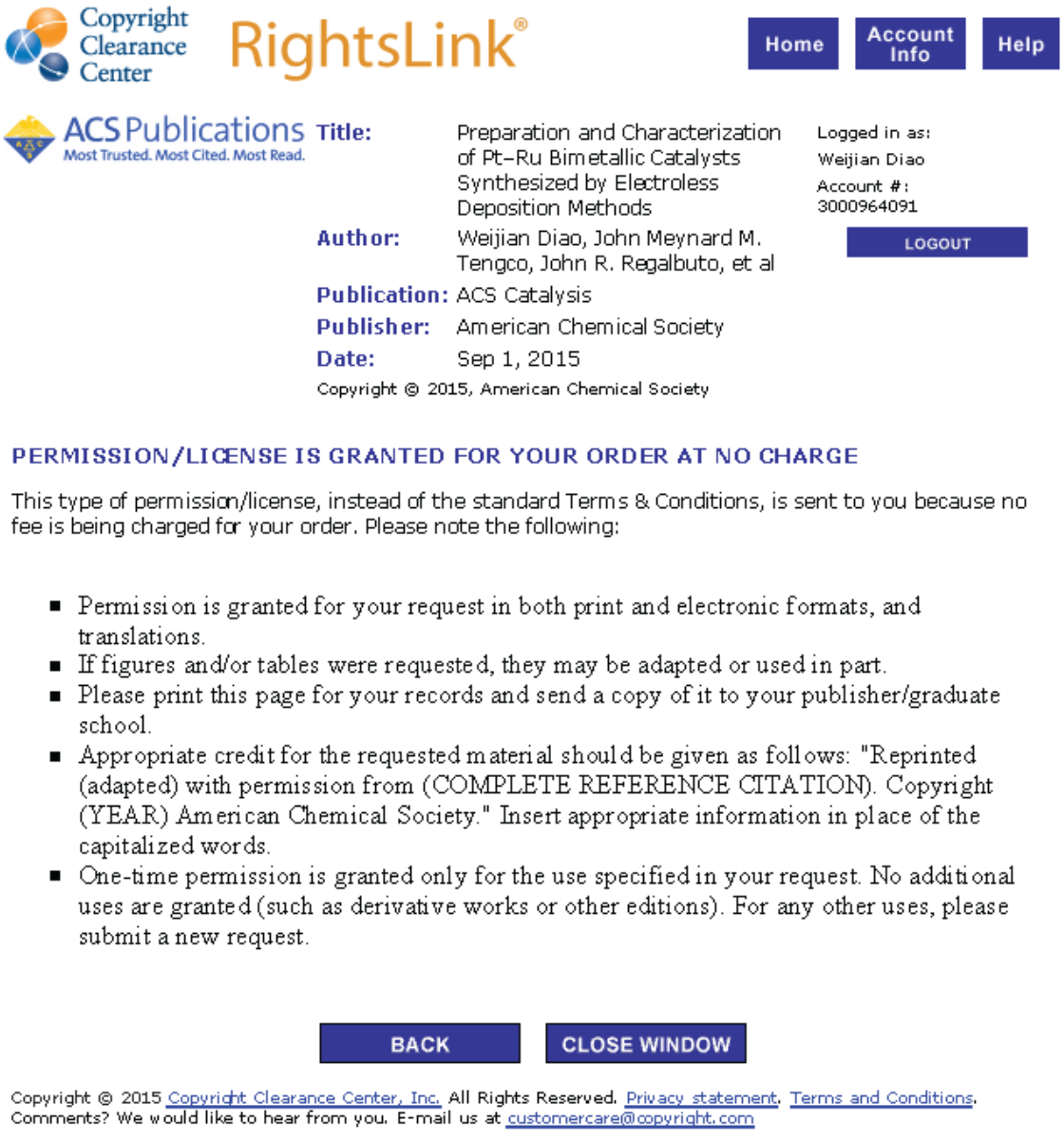

Copyright Clearance Center RightsLink®

Home | Account Info | Help

ACS Publications Most Trusted. Most Cited. Most Read.

Title: Preparation and Characterization of Pt–Ru Bimetallic Catalysts Synthesized by Electroless Deposition Methods

Author: Weijian Diao, John Meynard M. Tengco, John R. Regalbuto, et al

Publication: ACS Catalysis

Publisher: American Chemical Society

Date: Sep 1, 2015

Copyright © 2015, American Chemical Society

Logged in as: Weijian Diao
Account #: 3000964091

LOGOUT

PERMISSION/LICENSE IS GRANTED FOR YOUR ORDER AT NO CHARGE

This type of permission/license, instead of the standard Terms & Conditions, is sent to you because no fee is being charged for your order. Please note the following:

- Permission is granted for your request in both print and electronic formats, and translations.
- If figures and/or tables were requested, they may be adapted or used in part.
- Please print this page for your records and send a copy of it to your publisher/graduate school.
- Appropriate credit for the requested material should be given as follows: "Reprinted (adapted) with permission from (COMPLETE REFERENCE CITATION). Copyright (YEAR) American Chemical Society." Insert appropriate information in place of the capitalized words.
- One-time permission is granted only for the use specified in your request. No additional uses are granted (such as derivative works or other editions). For any other uses, please submit a new request.

BACK | CLOSE WINDOW

Copyright © 2015 Copyright Clearance Center, Inc. All Rights Reserved. Privacy statement. Terms and Conditions.
Comments? We would like to hear from you. E-mail us at customercare@copyright.com

Permission to Reprint Chapter 4

Dear Weijian,

As an Elsevier journal author, you retain various rights including Inclusion of the article in a thesis or dissertation (provided that this is not to be published commercially) whether in part or *in toto*; see http://www.elsevier.com/about/company-information/policies/copyright#Author%20rights for more information. As this is a retained right, no written permission is necessary provided that proper acknowledgement is given.

This extends to the online version of your dissertation and would include any version of the article including the final published version provided that it is not available as an individual download but only embedded within the dissertation itself.

If the article would be available as an individual download, only the preprint or (subject to the journal-specific embargo date) accepted manuscript version, but not the final published version, may be made available; see http://www.elsevier.com/journal-authors/sharing-your-article for more information. Information regarding embargo dates can be found here http://www.elsevier.com/__data/assets/pdf_file/0018/121293/external-embargo-list.pdf

If you need any additional assistance, please let us know.

Best Wishes,

Laura

Laura Stingelin

Permissions Helpdesk Associate

Elsevier

1600 John F. Kennedy Boulevard

Suite 1800

Philadelphia, PA 19103-2899

T: (215) 239-3867

F: (215) 239-3805

E: l.stingelin@elsevier.com